

RESEARCH ON SIDESLIP ANGLE ESTIMATION  
USING GPS AND MULTI-RATE KALMAN FILTER  
FOR ELECTRIC VEHICLE STABILITY CONTROL

(GPS とマルチレートカルマンフィルタを用いた  
電気自動車の安定化制御のための  
車体横滑り角推定に関する研究)

THESIS

Submitted to the Graduate School of Engineering of  
The University of Tokyo  
In Partial Fulfillment  
Of the Requirements  
For the Degree of  
MASTER OF ENGINEERING  
(修士学位論文)

By

NGUYEN BINH MINH  
(37-106908)

Supervisor

Professor Yoichi Hori, Ph.D.

Department of Electrical Engineering  
THE UNIVERSITY OF TOKYO  
February 2012

© Copyright by Nguyen Binh Minh 2012

All Rights Reserved

## **The Way**

Every person has a path to follow.  
It widens, narrows, climbs, and descends.  
There are times of desperate wanderings.  
But with courageous perseverance and  
personal conviction,  
the right road will be found.  
This is what brings real joy.

Konosuke Matsushita

(The Founder of Panasonic)

## Acknowledgements

First, I want to express my deeply-felt thanks to my supervisor, Prof. Hori, for providing an excellent environment for research and study. I appreciate his guidance and encouragement to me so that I could find my own way of research. I would also like to thank Prof. Hori for giving me the opportunity of becoming a PhD candidate.

I would like to thank Prof. Fujimoto for not only taking care of my experiments but also giving me critical and helpful comments on my research. I learned many things from him, especially multi-rate control theory.

I am happy listening to Dr. Oh's kind advices and instructions, not only for my research but also for my life in Japan. I appreciate Yafei for his corporate work with me on the topic of GPS. I am grateful for the help of Nam with my study on tire force sensor. I would like to thank my colleagues, Huang, Kim, Palakon, Koh, Vissuta, Koji, Beh, Minaki, Kimura ..., for the supports, advices, and friendship.

I would like to thank Panasonic Scholarship Co., Ltd., not only for their financial supports during my Master course in Japan but also for giving me a lot of activities to learn Japanese culture.

I would like to thank Japan Radio Company (JRC) for the technical supports, discussions, and advices. Without the equipment and confidential information from JRC, I could not finish my research topic on GPS.

Finally, for their emotional support and encouragement through my life, I would like to thank my family. Specially thank to my mom and my wife, two most important women in my life. They always take care of me and believe in me.

# Abstract

The main contribution of this thesis is the proposal of advanced multi-rate Kalman filter for vehicle sideslip angle estimation using GPS. This method is applied to the stability control system of electric vehicle. The other contribution is the thorough evaluation of lateral tire force sensors for sideslip angle estimation. This thesis is organized in five chapters and a special part as the followings.

Chapter 1 presents the background and motivation of the research. Electric vehicles (EVs) will be the means of transportation for human society in near future. Using in-wheel motors, EVs have become the novel motion control system. In order to maintain the stability and safety of EVs, stability control system should be designed. In this system, sideslip angle estimation is the main problem because the sideslip angle sensor is very expensive for practical applications. A number of previous researches on this topic are reviewed in chapter 1.

Chapter 2 discusses the lateral dynamics of electric vehicle in which lateral tire force characteristic is the main point. The linear bicycle model is introduced for state estimation and control design in the following chapters.

Chapter 3 proposes the application of GPS in sideslip angle estimation. The promising scenario of GPS in vehicle motion control is introduced. Then, the experiment setup of GPS receiver CCA-600 by Japan Radio Company in electric vehicle COMS is presented. The course angle of vehicle measured by GPS receiver is utilized as a measurement input for estimation using multi-rate Kalman filter. However, the conventional multi-rate Kalman filter faces with the problem of low update rate of GPS signal, the time-variant parameters, and the effect of external disturbances to electric vehicle. Therefore, the quality of multi-rate estimation is degraded during inter-samples (between two continuous updates of GPS). In order to enhance the inter-samples performance of multi-rate estimation, this chapter proposes two advanced methods. The first is the prediction of GPS course angle measurement residual for more accurate inter-samples estimation. The second is the general disturbance estimation for compensating the effect of both model error and external disturbance. Both simulations and experiments are conducted in order to evaluate the proposed methods.

Chapter 4 proposes the vehicle stability control system based on sideslip angle estimation using GPS and direct yaw moment control. LQR method is utilized for designing the yaw moment control to manage both sideslip angle and yaw rate. Both simulation and experiment tests are conducted with electric vehicle COMS.

Special part is a thorough evaluation of estimation based on tire lateral force sensors for vehicle stability control system. A new method of on-line identification of cornering stiffness without sideslip angle is proposed thanks to the lateral tire force sensors produced by NSK Ltd. Based on the difference between the left and right side tire lateral forces, sideslip angle estimation without cornering stiffness is proposed. By combining the influence of load transfer and non-linear tire force as a

disturbance term to be estimated, we can achieve an advanced configuration of sideslip angle estimation. Experiments using electric vehicle Kanon are conducted to evaluate the proposed methods. The two-input two-output controller for vehicle stability control system is also proposed by integrating yaw moment control with active steering control. The simulation tests are conducted in order to proof the higher robustness in comparison with conventional decoupling control method.

Chapter 6 gives the summary and conclusions on the works done in this thesis. The future research plan on application of GPS in electric vehicle control is also stated.

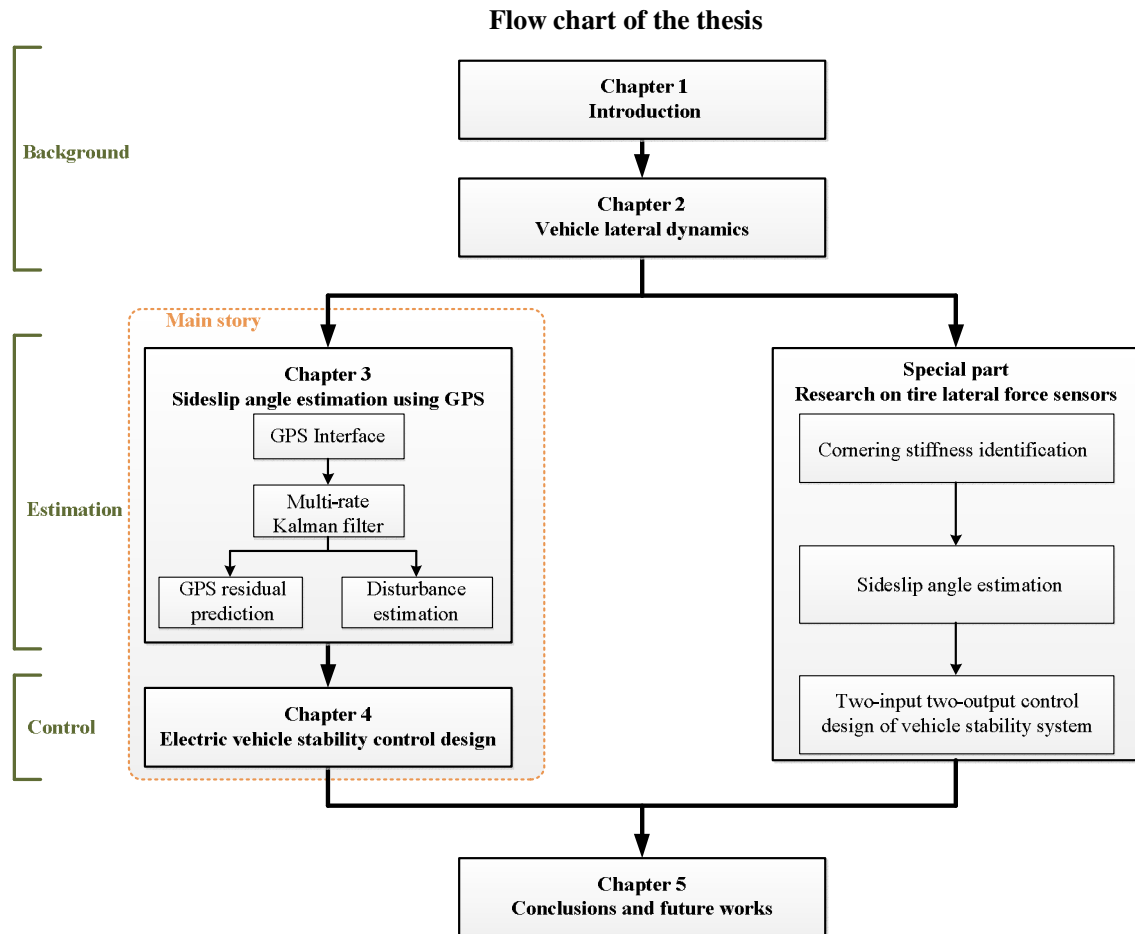


# Table of contents

<b>Acknowledgements</b> .....	i
<b>Abstract</b> .....	ii
<b>Chapter 1: Introduction</b> .....	1
1.1 Era of electric vehicles.....	1
1.2 Sideslip angle and vehicle stability control system .....	2
1.3 Review of researches on vehicle sideslip angle estimation.....	4
1.3.1 Kinematic based estimation.....	4
1.3.2 Model based estimation.....	4
1.3.3 Vision based estimation.....	5
1.3.4 GPS based estimation.....	5
1.3.5 Tire force sensor based estimation.....	5
1.4 Objectives.....	6
<b>Chapter 2: Vehicle lateral dynamics</b> .....	7
2.1 Lateral tire force characteristics.....	7
2.2 Vehicle handling models.....	8
2.3 Linear model of vehicle.....	10
2.4 Chapter summary.....	11
<b>Chapter 3: Sideslip angle estimation using GPS</b> .....	12
3.1 Introduction.....	12
3.1.1 Global positioning system.....	12
3.1.2 Scenario of GPS for vehicle motion control.....	13
3.1.3 Problems of measurement based on GPS.....	16
3.1.4 Previous researches on GPS based sideslip angle estimation.....	16
3.1.5 Japan Radio Company's GPS receiver CCA-600.....	17
3.2 Experiment Setup.....	17
3.2.1 GPS interface design.....	17
3.2.2 Experimental vehicle.....	18
3.2.3 Preliminary measurement using GPS.....	19
3.3 Single-rate and multi-rate Kalman filter.....	20

3.3.1	Single-rate Kalman filter.....	20
3.3.2	Multi-rate Kalman filter.....	22
3.4	Multi-rate Kalman filter for sideslip angle estimation using GPS.....	23
3.4.1	Estimation design.....	23
3.4.2	Preliminary results.....	25
3.4.3	Pros and cons of three-state MRKF.....	25
3.5	Inter-samples enhancement by prediction of measurement residual.....	27
3.5.1	Dynamics of single-rate estimation error.....	27
3.5.2	Prediction of measurement residual.....	27
3.5.3	Previous method on enhancement of inter-sample estimation.....	28
3.5.4	Simulation results.....	30
3.5.5	Experiment results.....	31
3.5.6	Section Conclusions.....	31
3.6	Inter-samples enhancement by disturbance estimation.....	32
3.6.1	Disturbance accommodating for robust estimation.....	32
3.6.2	Sideslip angle and disturbance estimation using multi-rate Kalman filter.....	33
3.6.3	Simulation results.....	35
3.6.4	Experiment results.....	37
3.6.5	Section conclusions.....	37
3.7	Chapter summary.....	38
 <b>Chapter 4: Electric vehicle stability control design.....</b>		<b>39</b>
4.1	Reference model for vehicle stability control.....	39
4.2	Electric vehicle stability control based on direct yaw moment control.....	40
4.2.1	General configuration.....	40
4.2.2	Feedback controller design based on linear quadratic regulator method.....	41
4.2.3	Torque distribution to in-wheel motors.....	42
4.2.4	Simulation results.....	44
4.2.5	Experiment results.....	45
4.3	Chapter summary.....	46
 <b>Special part: Research on tire lateral force sensor.....</b>		<b>47</b>
1.	Introduction.....	47
2.	Experimental vehicle.....	47
3.	Single and multi forgetting factor identification.....	49
4.	Cornering stiffness identification using tire lateral force sensors.....	50
4.1	Beta-less identification of cornering stiffness.....	50



4.2 Experimental evaluation.....	51
5. Sideslip angle estimation using tire lateral force sensors.....	53
5.1 Design of sideslip angle identification.....	53
5.2 Experimental evaluation.....	54
6. Electric vehicle stability based on two-input two-output control.....	57
6.1 Two-input two-output control configuration.....	57
6.2 Simulation evaluation of two-input two-output control configuration.....	60
7. Summary.....	61
<b>Chapter 5: Conclusions and future works.....</b>	<b>62</b>
5.1 Achievements of the thesis.....	62
5.2 Limitations of the thesis.....	62
5.3 Future works.....	63
<b>Appendix 1: Feature of GPS receiver CCA-600.....</b>	<b>65</b>
<b>Appendix 2: NMEA 0183 protocol for sending GPS data.....</b>	<b>66</b>
<b>Appendix 3: GPS coordinates to local coordinates.....</b>	<b>67</b>
<b>References.....</b>	<b>69</b>
<b>Publication list.....</b>	<b>72</b>
<b>Curriculum vitae.....</b>	<b>73</b>

# Chapter 1: Introduction

## 1.1 Era of electric vehicles

Due to the environmental protection and energy conservation, electric vehicles (EVs) have been interested by both industry and academic circles. The era of EVs started as various types of EVs have been produced by automotive companies all over the world. Along with the development of wireless power transfer, super-capacitor, and energy management, EVs will become popular in near future to replace internal combustion engine vehicles (ICEVs). Driven by electric motor, EVs has number of remarkable advantages in comparison with ICEVs:

1. EVs' motor torque response is very quick, 10-100 times faster than that of ICEVs. This property enables two degree of freedom control for EVs with motor torque as control input. High performance adhesion control of EVs was realized, such as anti skid control [1]. Generally speaking, motor torque can develop the characteristic of mechanical system like vehicles.
2. Motor torque can be calculated easily from motor current. Based on the understanding of motor torque, road condition estimation and driving force observer can be realized [2].
3. Electric motors are compact and inexpensive such that they can be installed at each wheel. Therefore, each wheel's torque can be controlled independently for vehicle stability control system [3].
4. If electric motor is used, there will be no difference between acceleration and deceleration. This means electric motor can be utilized as actuator for both traction and braking control [1].

In conclusion, EVs present a novel motion control system. Therefore, research on motion control of EVs has big contributions to both society and academic theory.

## 1.2 Sideslip angle and vehicle stability control system

Car accidents may happen due to the loss of control in critical driving situation, for instance, vehicle cornering into slippery road at high speed. In order to prevent serious accidents, vehicle stability control (VSC) based on active safety technologies, has been widely applied to assist the driver to keep vehicle on the intended path. In Audi A6 3.0, the electronic brake-force distribution (EBD) is designed to generate direct yaw moment control (DYC). 2009 BMW 750Li has the four-wheel-steering (4WS) to increase vehicle stability.

In order to design the VSC system, vehicle's actual behavior must be measured or estimated to be compared with the nominal behavior which is calculated from driver's inputs [4]. The actual directional behavior of vehicle is calculated from motion variables, such as yaw rate and sideslip angle. As can be seen in Fig. 1, yaw rate is defined as the angular velocity of vehicle body around the vertical axis.

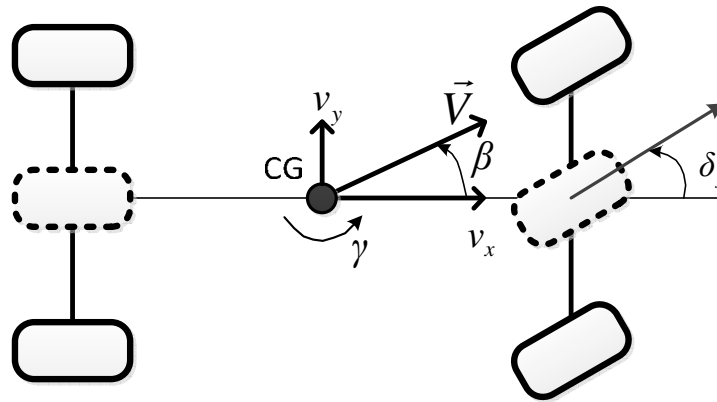


Fig 1.1 Definition of sideslip angle

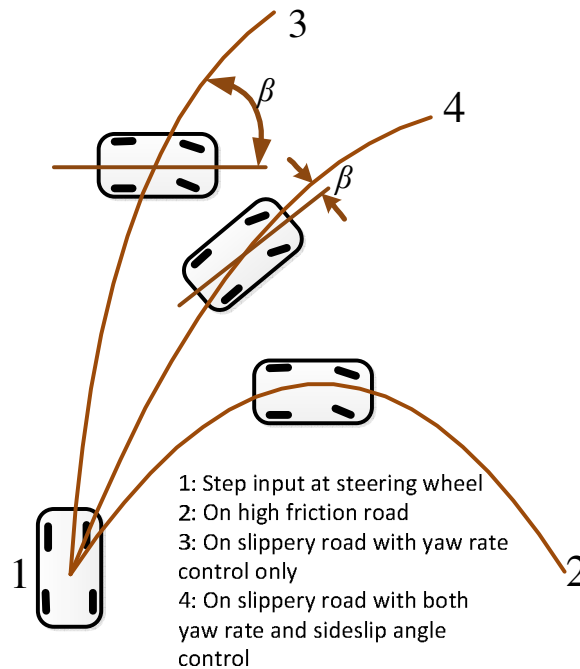


Fig 1.2 Vehicle motion with/without sideslip angle control

Sideslip angle is defined as the angle between vehicle velocity vector at the center of gravity (CG) and the longitudinal axis. Sideslip angle can be calculated by the following formula

$$\beta = \tan^{-1} \left( \frac{v_y}{v_x} \right) \quad (1.1)$$

As can be seen in Fig 1.2, on a slippery road, yaw rate control can only maintain the vehicle in desired orientation, but the vehicle sideslip angle may increase significantly [5]. As the result, the vehicle may deviate considerably from intended path. In contrast, integrated control of both yaw rate and sideslip angle results in small sideslip angle response. In other words, the stability of the vehicle is enhanced.

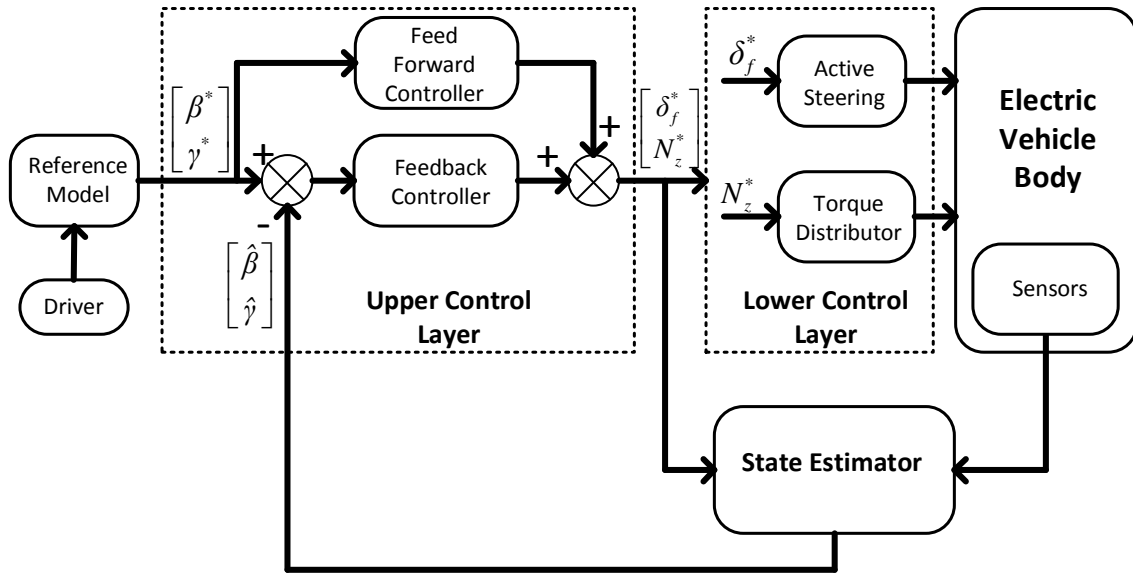


Fig 1.3 Electric vehicle stability control system



Fig 1.4 Corsys-Datron optical sensor for sideslip angle measurement

Fig 1.3 shows the general stability control system of EVs where two control inputs are the active front steering angle and the yaw moment generated by torque difference between left and right side in-wheel motors. The reference model calculates the reference of sideslip angle and yaw rate from driver's inputs. The upper control layer is the combination of a feedback and feed forward controller which generates the steering angle and yaw moment that can stabilize vehicle motion. The lower control layer includes the active steering system and the torque distributor. While vehicle's yaw rate can be measured easily from popular gyroscope sensor, current vehicles are not equipped with an ability to measure the sideslip angle directly. Corsys-Datron produced the noncontact optical sensor for accurate sideslip angle measurement [6]. However, because of its very high cost, Corsys-Datron sensor is only used for experiment, as shown in Fig 1.4. Therefore, state estimator is designed in order to provide the "virtual measurement" of sideslip angle based on the control inputs and available measurement outputs.

### 1.3 Review of researches on vehicle sideslip angle estimation

As above discussion, sideslip angle estimator plays an important role in vehicle stability control system. Sideslip angle estimation has been a hot topic in motion control of vehicle. Based on literature review, previous researches on this topic can be organized in five groups as the following.

#### 1.3.1 Kinematic based estimation

Kinematic approaches are based on the kinematic relation of yaw rate and vehicle's acceleration which is simple for estimation design [7]. The advantage of this approach is that it does not depend on the tire force characteristics of the vehicle. However, measurement from gyroscope and accelerometer are always affected by bias, electric noise, and temperature changes. Although Kalman filter can be utilized, other problems has not been solved. Firstly, the roll angle and road inclination introduce the offset to lateral acceleration sensor due to gravity component. Secondly, the influence of side wind is also not properly captured from measured acceleration.

#### 1.3.2 Model based estimation

Basically, a model based observer is designed with the assumption that tire cornering stiffness is constant to construct a linear model of vehicle dynamics. For instance, Kiencke *et al* proposed the linear Luenberger observer based on linear bicycle model [8]. Unfortunately, a running vehicle is a time variant parameter system due to the change of velocity or road condition. Therefore, a fixed linear model cannot provide accurate sideslip angle estimation. Aoki *et al* proposed the robust design of linear observer gain in [9]. The problem is, even with robust observer gain, this method is still sensitive with model error. Cong Geng *et al* improved Aoki's method by a hybrid-like observer of sideslip angle [10]. By using fuzzy logic, this method can deal with both linear and non-linear region of lateral tire force characteristics. However, the affection of external disturbance was not considered according to this method.

In [11], a non-linear model based observer of lateral velocity was proposed. The key point of this method is the construction of non-linear tire force model using the measurement of gyroscope and accelerometers. However, this method does not deal with the effect of side wind force or gravity to accelerometers. A number of non-linear observer has been published, such as in [12] and [13]. Although non-linear observer can be proofed mathematically by Lyapunov theory, the non-linear model is complicated for a practical application.

In [14], sideslip angle is estimated by combining the model based and kinematic based method. A fuzzy logic is used to determine that the system is in transient or steady state. In case of steady state, the estimated sideslip angle will rely mainly on the linear model based observer. During the transient maneuver, the kinematic based observer will dominate. This combination aims to eliminate the variation of model parameters. The limitation of the combined method comes up when the large slip angle is maintained for long duration of time, for instance, when vehicle completely exceeds the handling limit.

### 1.3.3 Vision based estimation

Not only applying in automobile robot, camera can be utilized in motion control of vehicle [15]. The principle of this approach is based on the combination of the lateral dynamics model and the vision model. Besides the measurement output from dynamics model, camera provides two redundant measurements to correct the estimated sideslip angle: the offset from the centerline at the look-ahead, and the angle between the tangent to the road and the vehicle orientation. The advantage of vision based system is that it usually requires fewer infrastructure modifications. Vision information can also be used for other purposes, such as identifying the obstacle, traffic sign, and road curvature. In other side, the low update rate of camera information is the main disadvantage of this approach. Moreover, this method requires the visibility of camera which may be unavailable when road markings are covered with leaves, snow, water, or dirt.

### 1.3.4 GPS based estimation

One antenna GPS system can provide a horizontal position accuracy of 5-10 m, and a velocity accuracy of 0.05 m/s. By using velocity measurement in absolute earth coordinates, the orientation of the vehicle velocity vector on the horizontal plane can be obtained. By placing two GPS antenna at two points along the vehicle, sideslip angle can be calculated directly [16]. Anderson *et al* combines the GPS antenna with a linear model based to estimate both sideslip angle and yaw angle [17]. The advantage of GPS based estimation is that GPS signal is available in all weather conditions. However, GPS based system is unreliable in urban environment where tall buildings can prevent access to GPS satellite signals. Moreover, the poor update rate of conventional GPS receiver (1-10 Hz) is not enough for motion control. High update rate GPS receiver can be produced but with very expensive price. GPS can be integrated with inertia navigation system (INS) to provide accurate sideslip angle. However, the high quality INS unit is extremely expensive for vehicle in the market. For example, the RT3000 system produced by Oxford Technical Solutions costs over \$50,000 [18].

### 1.3.5 Tire force sensor based estimation

The most difficult problem in sideslip angle estimation is the non-linear characteristics of tire force. In order to solve this problem, a number of projects on tire force sensor design have been conducted for years. Since 1988, at Darmstadt Technical University (Germany) the tire force sensor based on tire tread deformation had been studied [19]. At Helsinki University of Technology (Finland), the optical tire sensor was produced [20]. The core of this sensor is a two dimensional position sensitive detector (PSD) that utilizes photodiode surface resistance. The PSD is located on the rim and can detect the movement of a light emitting diode (LED) that is installed in the inner of the tire. The intensity of the LED is not constant versus angular displacement due to the change of tire force. In industry, there are several productions of lateral tire force sensor, such as bearing load sensor unit by SKF group [21]. In [22], by utilizing lateral tire force sensor, a Kalman filter is designed for sideslip angle estimation.

## **1.4 Objectives**

Application: This thesis aims to propose advanced method of sideslip angle estimation for electric vehicle stability control system by using low cost GPS receiver.

Theory: This thesis aims to develop the general multi-rate Kalman filter theory which can be applied not only for sideslip angle estimation, but also for other vehicle states, and even for other control systems.

## Chapter 2: Vehicle lateral dynamics

### 2.1 Lateral tire force characteristics

The tire is the main component of vehicle which interacts with the road. Therefore, lateral tire force has an important role in research on vehicle dynamics control. In this section, the relation between lateral tire force and tire slip angle is examined. As shown in Fig 2.1, since the tire slip angle appears, the lateral force will exert on the tire at the contact patch. As a result, the tire will be deformed. When the tire slip angle is small, the force distribution is triangular with more force at the rear part. The lateral force is proportional to the sideslip angle. The cornering stiffness can be defined by the following equation:

$$F_y = C\alpha \quad (2.1)$$

Where  $F_y$  is the lateral tire force,  $\alpha$  is the tire slip angle, and  $C$  is the tire cornering stiffness.

When tire slip angle becomes larger and larger, the lateral tire force will increase. Eventually, at a certain large tire slip angle, the lateral tire force will saturate due to the friction limit [23]. The friction limit circle in Fig 2.2 shows that the total of lateral and longitudinal tire force is limited by the vertical component multiplied by the road friction coefficient. The rear part of the contact patch will saturate first. This phenomenon explains the characteristics of lateral tire force in Fig 2.3. When tire slip angle is small, tire force is at linear region with a certain cornering stiffness. In contrast, at large tire slip angle, the tire force falls into non-linear region. When the road friction coefficient decreases, the maximum lateral tire force will reduce. During the operation of vehicle, load transfer due to both longitudinal and lateral acceleration results in the change of vertical force at each tire.

The above discussion shows that a linear model is not always suitable for capturing the tire force in real time. Various models have been proposed in order to model the relation between tire force and tire slip angle. For instance, in [23], an empirical second order model is chosen as:

$$F_y = \begin{cases} C\alpha - \frac{(C\alpha)^2}{4\mu F_z} & \text{when } \alpha < \frac{F_z}{C} \\ \mu F_z & \text{when } \alpha \geq \frac{F_z}{C} \end{cases} \quad (2.2)$$

Where  $F_z$  the vertical force, and  $\mu$  is the road friction coefficient. In this thesis, the second order model in (2.2) is used in order to construct the simulation model using MATLAB/SIMULINK.

In [24], by using “magic formula”, a more complex model is constructed for tire modeling:

$$F_y = D \sin \left[ C \arctan \left\{ B\alpha - E \left( B\alpha - \arctan(B\alpha) \right) \right\} \right] \quad (2.3)$$

Where  $B$  is the stiffness factor,  $C$  is the shape factor,  $D$  is the peak factor, and  $E$  is the curvature factor. By adjusting such stiffness factors, the force expression can be modified flexibly to fit the experimental results.



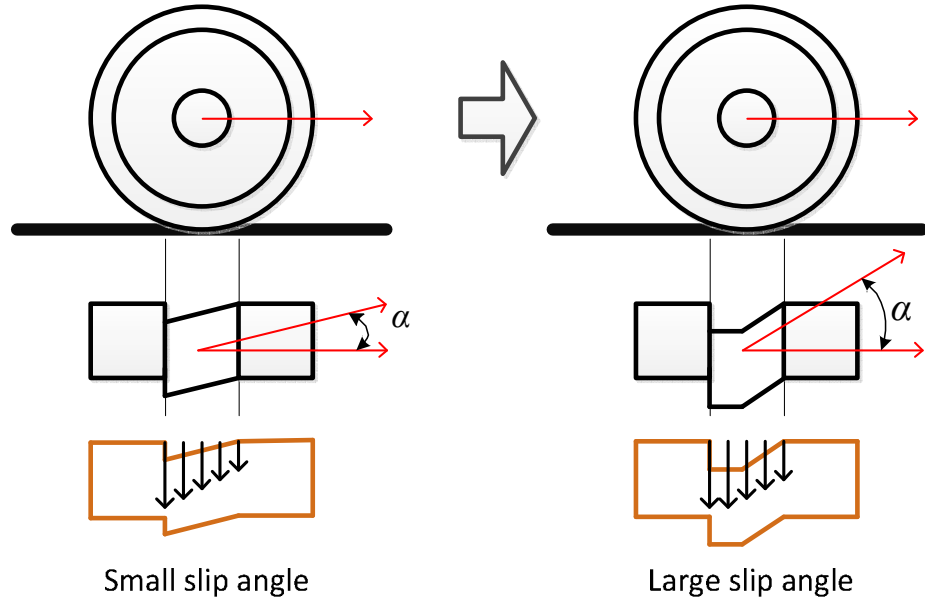


Fig 2.1 Tire deformation at different slip angle

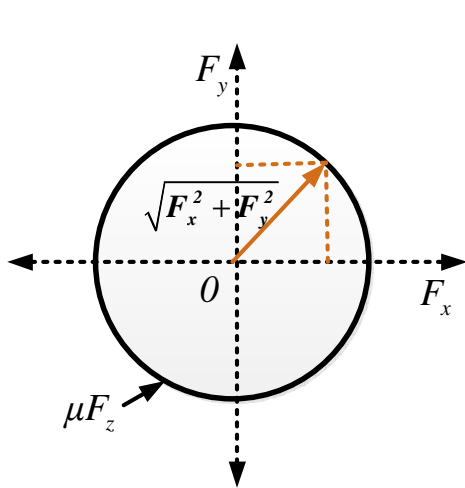


Fig 2.2 Friction limit circle

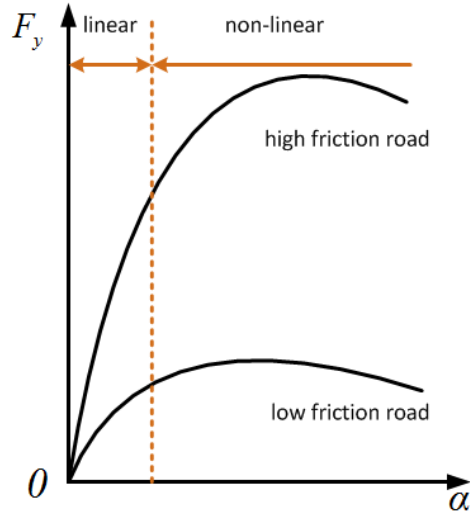


Fig 2.3 Lateral tire force characteristics

## 2.2 Vehicle handling models

In this thesis, electric vehicles with active front steering are used for experiments. Therefore, a front steer vehicle model is constructed as shown in Fig 2.4. In the following equations,  $\beta$  is the sideslip angle;  $\gamma$  is the yaw rate;  $a_x$  and  $a_y$  are the longitudinal and lateral acceleration;  $v_x$  is the longitudinal velocity;  $v_y$  is the lateral velocity;  $V$  is the velocity vector;  $\delta_f$  is the front steering angle;  $l_f, l_r, d_f$ , and  $d_r$  are the dimensions of the vehicle;  $h$  is the distance from center of gravity to the ground;  $g$  is the gravity of Earth;  $m$  is the mass of vehicle;  $I_z$  is the yaw moment of inertia; and  $N_z$  is the yaw moment generated by the difference between the left and right side driving forces.

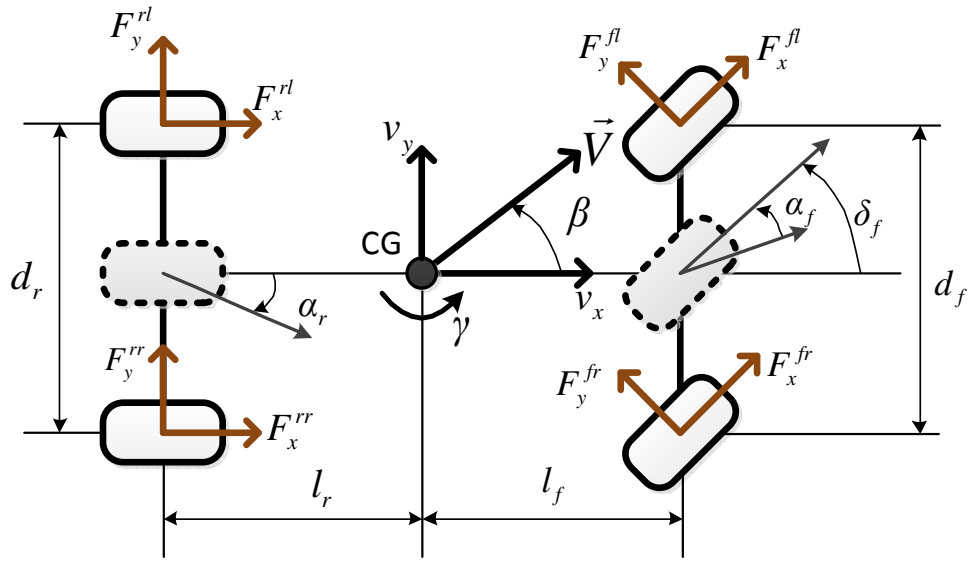


Fig 2.4 Front steer vehicle model

Using vehicle model in Fig 2.4 and based on linear tire model, the calculation of lateral tire force from sideslip angle can be expressed as the following:

$$F_y^{fl} = -C_f \left( \frac{v_x \beta + l_f \gamma}{v_x - \frac{d_f}{2} \gamma} - \delta_f \right) \quad (2.4)$$

$$F_y^{fr} = -C_f \left( \frac{v_x \beta + l_f \gamma}{v_x + \frac{d_f}{2} \gamma} - \delta_f \right) \quad (2.5)$$

$$F_y^{rl} = -C_r \left( \frac{v_x \beta - l_r \gamma}{v_x - \frac{d_r}{2} \gamma} \right) \quad (2.6)$$

$$F_y^{rr} = -C_r \left( \frac{v_x \beta - l_r \gamma}{v_x + \frac{d_r}{2} \gamma} \right) \quad (2.7)$$

The vertical tire force can be calculated from measurements of longitudinal and lateral acceleration sensor as follows:

$$F_z^{fl} = \frac{m(l_r g - h a_x)}{2(l_f + l_r)} - \frac{h m a_y}{d_f} \quad (2.8)$$

$$F_z^{fr} = \frac{m(l_r g - ha_x)}{2(l_f + l_r)} + \frac{hma_y}{d_f} \quad (2.9)$$

$$F_z^{rl} = \frac{m(l_f g + ha_x)}{2(l_f + l_r)} - \frac{hma_y}{d_r} \quad (2.10)$$

$$F_z^{rr} = \frac{m(l_f g + ha_x)}{2(l_f + l_r)} + \frac{hma_y}{d_r} \quad (2.11)$$

The lateral force equation and yaw moment equation can be expressed as follows:

$$F_y^{fl} + F_y^{fr} + F_y^{rl} + F_y^{rr} = mv_x(\dot{\beta} + \gamma) \quad (2.12)$$

$$(F_y^{fl} + F_y^{fr})l_f - (F_y^{rl} + F_y^{rr})l_r + N_z = I_z \dot{\gamma} \quad (2.13)$$

### 2.3 Linear model of vehicle

In order to design the controller or estimator for vehicle stability control system, the linear bicycle model is widely used. This model is constructed under the following assumptions: 1) Tire slip angle is small such that lateral tire force is at linear region. 2) Vehicle is symmetric about the fore-and-aft center line. 3) Load transfer is neglected. 4) Vehicle velocity is approximately constant.

Based on the above assumptions, the motion of the 4 wheel vehicle model in Fig 2.4 can be represented by the 2 wheel model (bicycle model) placed at the fore-and-aft center line as shown in Fig 2.5. The general front and rear lateral tire force can be expressed as follows:

$$F_{yf} = -2C_f \alpha_f \quad (2.14)$$

$$F_{yr} = -2C_r \alpha_r \quad (2.15)$$

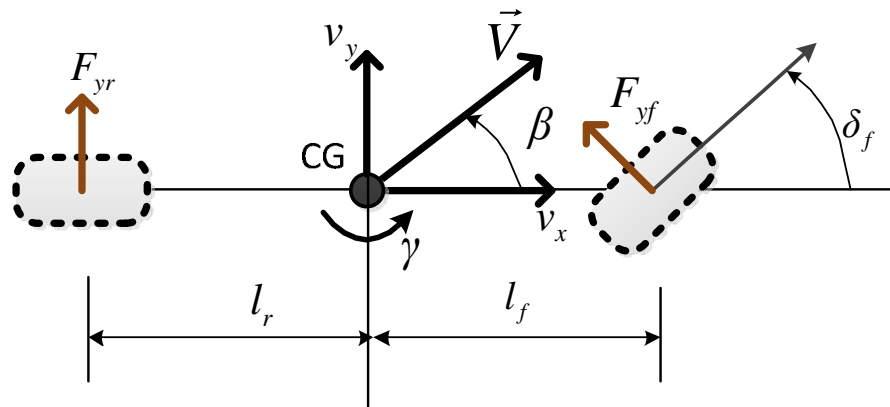


Fig 2.5 Linear bicycle model

The front and rear tire slip angle can be expressed as:

$$\alpha_f = \delta_f - \frac{l_f}{v_x} \dot{\gamma} - \beta \quad (2.16)$$

$$\alpha_r = \frac{l_r}{v_x} \dot{\gamma} - \beta \quad (2.17)$$

The lateral force equation and the yaw moment equation can be rewritten as:

$$F_{yf} + F_{yr} = m v_x (\dot{\beta} + \dot{\gamma}) \quad (2.18)$$

$$F_{yf} l_f - F_{yr} l_r + N_z = I_z \dot{\gamma} \quad (2.19)$$

Using the above equations, the two-degree-of-freedom model of vehicle can be described in state space form as follows:

$$\dot{X} = AX + BU \quad (2.20)$$

$$X = [\beta \quad \dot{\gamma}]^T \quad (2.21)$$

$$U = [\delta_f \quad N_z]^T \quad (2.22)$$

$$A = \begin{bmatrix} a_{11} & a_{12} \\ a_{21} & a_{22} \end{bmatrix} = \begin{bmatrix} \frac{-2(C_f + C_r)}{m v_x} & -1 - \frac{2(C_f l_f - C_r l_r)}{m v_x^2} \\ \frac{-2(C_f l_f - C_r l_r)}{I_z} & \frac{-2(C_f l_f^2 + C_r l_r^2)}{I_z v_x} \end{bmatrix} \quad (2.23)$$

$$B = \begin{bmatrix} b_{11} & b_{12} \\ b_{21} & b_{22} \end{bmatrix} = \begin{bmatrix} \frac{2C_f}{m v_x} & 0 \\ \frac{2C_f l_f}{I_z} & \frac{1}{I_z} \end{bmatrix} \quad (2.24)$$

## 2.4 Chapter summary

This chapter discusses the lateral tire force characteristic which is the most important problem in sideslip angle estimation. Dynamics equations of vehicle lateral motion are established based on both four wheel model and two wheel model.

## Chapter 3: Sideslip angle estimation using GPS

In this chapter, the application of GPS in sideslip angle estimation is presented. Firstly, GPS is introduced following with its promising scenario in vehicle motion control. Previous researches are analyzed to show the problems required to be solved. The experiment setup of GPS receiver in electric vehicle is then described. Multi-rate Kalman filter is applied to overcome the low update rate of GPS. Then, two enhancements are proposed in this chapter in order to develop the accuracy of multi-rate Kalman filter. The first is inter-samples estimation with prediction of measurement residual. The second is the integration of disturbance estimation with sideslip angle estimation using multi-rate Kalman filter.

### 3.1 Introduction

#### 3.1.1 Global positioning system

Global positioning system (GPS) is a space-based satellite navigation system that provides location and time information in anywhere on or near the Earth. It was created by U.S. Department of Defense since 1978. Fully operation of GPS was achieved in 1994 with 24 satellites (Fig 3.1). GPS was originally designed for military purposes, but can be freely accessed now a day.

As the satellites orbit, they continuously transmit radio signals towards the Earth at the speed of light. The GPS receiver receives such signals to calculate its distance to each satellite. The fundamental frequency of radio signal from satellites is 10.23 MHz. This frequency carries two timing signals L1 and L2 at 1575.42 MHz and 1227.60 MHz, respectively [25]. The L1 frequency contains two codes, the Coarse Acquisition (C/A) and the Precision (P) code while the L2 frequency contains only P code. In GPS receiver, the L1 and L2 codes are decoupled to distinguish between satellites and calculate the ranging time of the broadcasts. In total, there are five pieces of data that a GPS receiver can receive for measurement, as shown in Fig 3.2. Based on the distances from visible satellites to GPS receiver, triangular is used to compute the receiver's latitude, longitude, elevation, and time. At least four visible satellites are required for accurate positioning. The more satellites a GPS receiver can see at any given time, the more information it can process, and thus the greater the precision can be achieved.

GPS became popular in human being's society. It has been widely applied in navigation of flight, boat, and ground vehicle. An application can be seen in Fig 3.3 which is a photo of a personal navigation for driver in Japan. The real time position of vehicle is displayed on digital map. This can help the driver to understand the current position and find the road. Google and Toyota have used GPS for autonomous car (driver-less car). Not only applying for vehicle, GPS is also installed in smart-phone for finding the road.

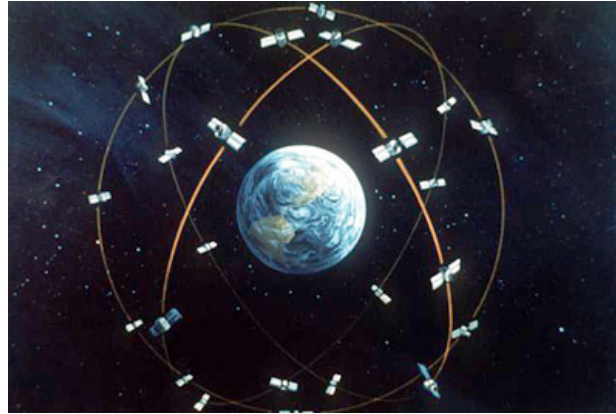
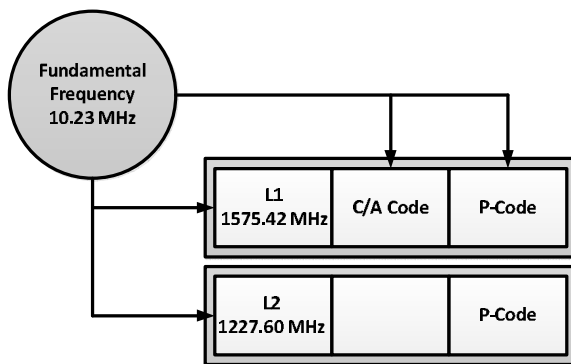
Fig 3.1 GPS constellation (<http://technicalhut.blogspot.com>)

Fig 3.2 GPS signal frequencies



Fig 3.3 Car navigation using GPS

### 3.1.2 Scenario of GPS for vehicle motion control

The development of GPS technology allows us to access GPS signal everywhere on the Earth with high accuracy of GPS based measurement. The principle is to use signals from augmentation sources placed in a fix position on or near the Earth. If the augmentation sources are reference station on Earth, we have the local based augmentation system (LBAS). In contrast, space based augmentation system (SBAS) uses other augmentation satellites which rotate with the Earth and are always in a fixed location above the Earth, unlike GPS satellites which revolve around the Earth. This technology has been widely developed all over the world. It is named wide area augmentation system (WAAS) in United States, and European geostationary overlay system (EGNOS) in Europe. Indian has the GPS aided GEO augmented navigation system (GAGAN) while China has the Chinese satellite navigation augmentation system (SNAS). Now a day, centimeter-level accuracy of GPS positioning can be achieved with high quality real time kinematic GPS [26]. The accuracy of velocity and attitude measurement based on GPS can be 5 cm/s and 0.25 degree, respectively.

In Japan, a promising scenario of GPS application can be viewed. National projects have been conducted in order to establish Japan's own GPS. The Quasi-zenith satellite system (QZSS) has been

designed by Japan Space Association (JAXA) to provide high elevation satellites over Japan to overcome problems with navigation in urban canyons, as shown in Fig 3.4. The first QZSS satellite was launched in September 2010 [27]. The MTSAT satellite-based augmentation system (MSAS) has been developed by Japan Civil Aviation Bureau (JCAB). Two MTSAT satellites were successfully launched in 2007. The MSAS is described in Fig 3.5 with two master control stations (MCS) located in Kobe and Hitachiota. As the Japan's plan, till the year of 2015, Japan can fulfill its own GPS with the accuracy of ten times higher than current system by United States.

The development of GPS technology reveals that GPS can be applied for not only navigation. The high accuracy of velocity and attitude measurement based on GPS can be utilized for estimation and control of vehicle. Fig 3.6 shows the planar vehicle model where course angle  $c$  is the angle between vehicle direction and the North, and  $\psi$  is the yaw angle which is the Euler angle about vertical axis. The following equation expresses the important relation between sideslip angle and course angle that will be utilized in this thesis:

$$c = \beta + \psi \tag{3.1}$$

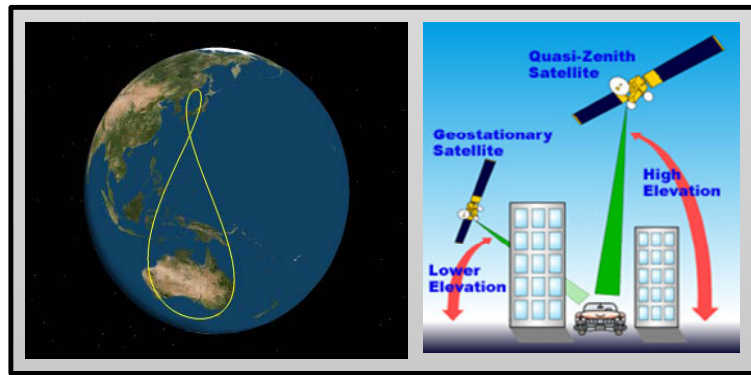


Fig 3.4 QZSS ground track and its high elevation

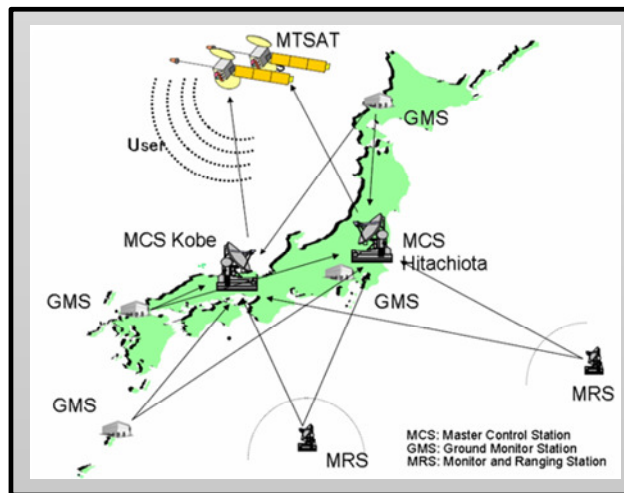


Fig 3.5 Japan's MSAS (end of 2007)

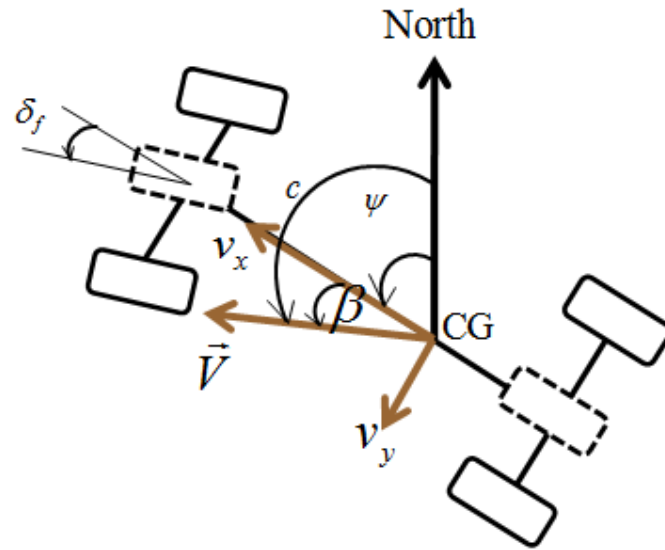


Fig 3.6 Planar vehicle model

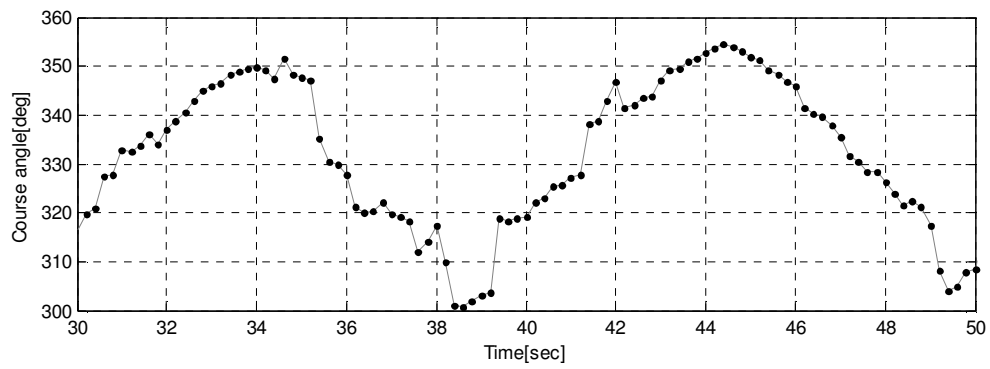


Fig 3.7 Vehicle's course angle measured by 5Hz GPS receiver

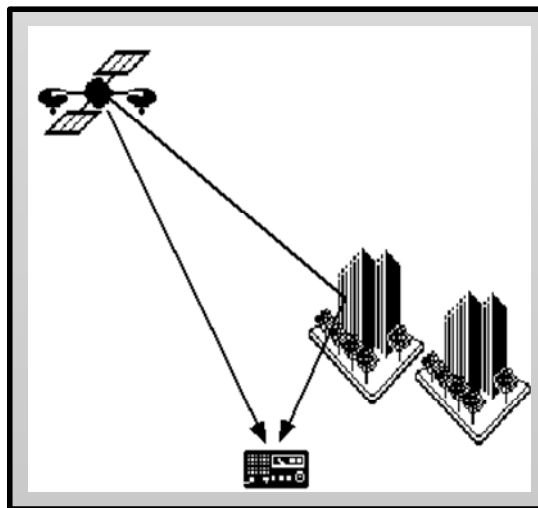


Fig 3.8 GPS signal reflection



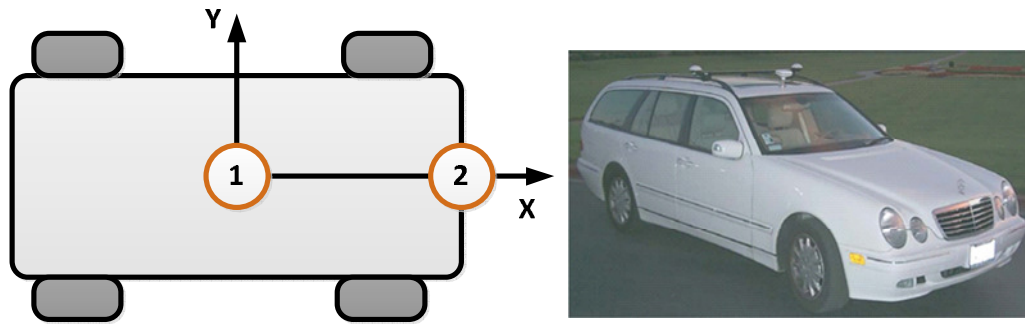


Fig 3.9 Dual GPS antenna system for sideslip angle measurement at Stanford University



Fig 3.10 CCA-600

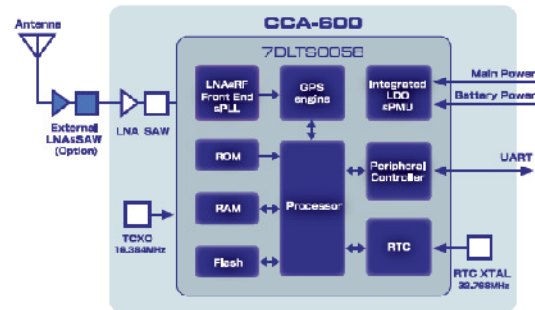


Fig 3.11 Electronic circuit design of CCA-600

### 3.1.3 Problems of measurement based on GPS

The biggest problem of measurement based on GPS is the poor update rate of GPS receiver. Conventional GPS receiver in smart phone or personal navigation equipment can provide update information at 1 Hz which means one time per second. Fig 3.7 shows the vehicle course angle measurement at 5 Hz which means only five updates per second. High update rate GPS receiver (up to 50 Hz) can be produced but with very high cost which may be not suitable for practical application. However, motion control of vehicle requires the signal update rate at 1 kHz or more.

The second problem is GPS signal is not always stable. Delay may be introduced to measurement based on GPS due to the reflection in urban area with tall buildings, as shown in Fig 3.8. Moreover, the accuracy of measurement depends on the number of visible satellites. If the total of visible satellites is less than four, measurement is unreliable.

### 3.1.4 Previous researches on GPS based sideslip angle estimation

From literature review, at Stanford University, Ryu used a dual GPS antenna system for directly calculation of sideslip angle [16]. The placement of dual antenna system can be seen in Fig 3.9. At Auburn University, Anderson integrated one GPS receiver with gyroscope sensor for sideslip angle estimation using Kalman filter [17]. However, the following problems have not been solved.

- 1) Application of multi-rate theory: Because course angle is provided by GPS at low rate while other sensors like gyroscope can be measured at high rate, multi-rate control theory should be applied.
- 2) Robust estimation of sideslip angle: As discussion in chapter 1, vehicle is a time variant parameter

systems. The velocity can change during driving operation. Due to road friction variation, the tire cornering stiffness is not a constant.

- 3) Consideration of external disturbance: Strong external disturbances may attack the vehicle lateral system, such as lateral wind force or gravity when vehicle is running on bank road. Due to the effect of external disturbance, the accuracy of sideslip angle estimation may be degraded.
- 4) Compensation of GPS signal delay: The GPS based measurement delay may happen due to signal reflection. Therefore, this delay should be taken to be accounted in estimation model.
- 5) Adaptation to quality of GPS measurement: The accuracy of GPS based measurement may change due to the number of visible satellites and signal strength. This means that an auto tuning Kalman filter is reasonable to be studied.
- 6) Control evaluation: The sideslip angle estimation in previous researches was not integrated with a sideslip angle controller for real-time verification.

This thesis aims to develop the sideslip angle estimation using GPS by considering problem 1, 2, 3, and 6.

### **3.1.5 Japan Radio Company's GPS receiver CCA-600**

The GPS receiver CCA-600 at our lab is supported by Japan Radio Co., Ltd. (JRC). Designed based on single chip ASIC, this is a small size, low power consumption GPS receiver with accurate measurement of velocity and course angle. In open sky condition, CCA-600 has the azimuth accuracy of 0.14 degree RMS which is better than the GPS receiver at Stanford University (azimuth accuracy of 0.25 degree RMS). The update rate of CCA-600 is 5 Hz which means five measurement updates per second. Other features of CCA-600 can be seen in Appendix 1. CCA-600 can output data using NMEA 0183 protocol through serial port at baud rate 38,400 bps. A photo of CCA-600 can be seen in Fig 3.10 while Fig 3.11 shows the general circuit design.

## **3.2 Experiment setup**

### **3.2.1 GPS interface design**

In order to transfer the data from CCA-600 to the experimental electric vehicle, GPS interface software is designed. As shown in Fig 3.12, the laptop is used for real time GPS signal processing. It receives the NMEA messages from CCA-600 through serial port. In the laptop, GPS interface software decodes the NMEA messages. Then, decoded data are sent to EV's controller through LAN cable by user datagram protocol (UDP). The first version of GPS interface software is designed using MATLAB 2010. The second version is designed using C language in Linux operating system. The interface software includes three following modules:

- 1) Module I/O: This module controls the serial communication by setting the baud rate, serial port number, and working frequency. UDP communication is established by setting the IP address of the vehicle's controller. Data received from CCA-600 can be recorded in real-time.
- 2) Module data analysis: This module decodes the NMEA sentences for required data, such as

velocity, course angle, position in latitude and longitude, local time, number of visible satellites... The vehicle in GPS coordinates (Latitude, Longitude, Height) can be converted into local planar coordinates (East, North, Up). The structure of NMEA messages and coordinates transformation equations can be seen in Appendix 2 and 3, respectively.

- 3) Module data display: The decoded data such as velocity or position can be display in real-time or off-line mode. This module can also generate keyhole markup language (KML) file which contains position information. Google Earth map can be called from interface software to display the trace of position presented in KML file.

### 3.2.2 Experimental vehicle

A one seat micro EV named “Super-capacitor COMS1” is used for research on application of GPS in sideslip angle estimation (Fig 3.13). Two in-wheel motors are equipped in the rear wheels. Other sensors are steering angle sensor, longitudinal and lateral acceleration sensor, and gyroscope for yaw rate measurement. In order to measure the sideslip angle sensor to evaluate the sideslip angle estimation, a Corrsys-Datron optical sensor is installed in the front of the vehicle. Using the lateral and longitudinal velocity measured by this optical sensor, sideslip angle at the center of gravity can be achieved easily. A Linux PC is used as the controller of COMS1 with the sampling time of 1 millisecond. The drive train specification and parameters of the experimental EV are shown in Table 4.1 and Table 4.2, respectively.

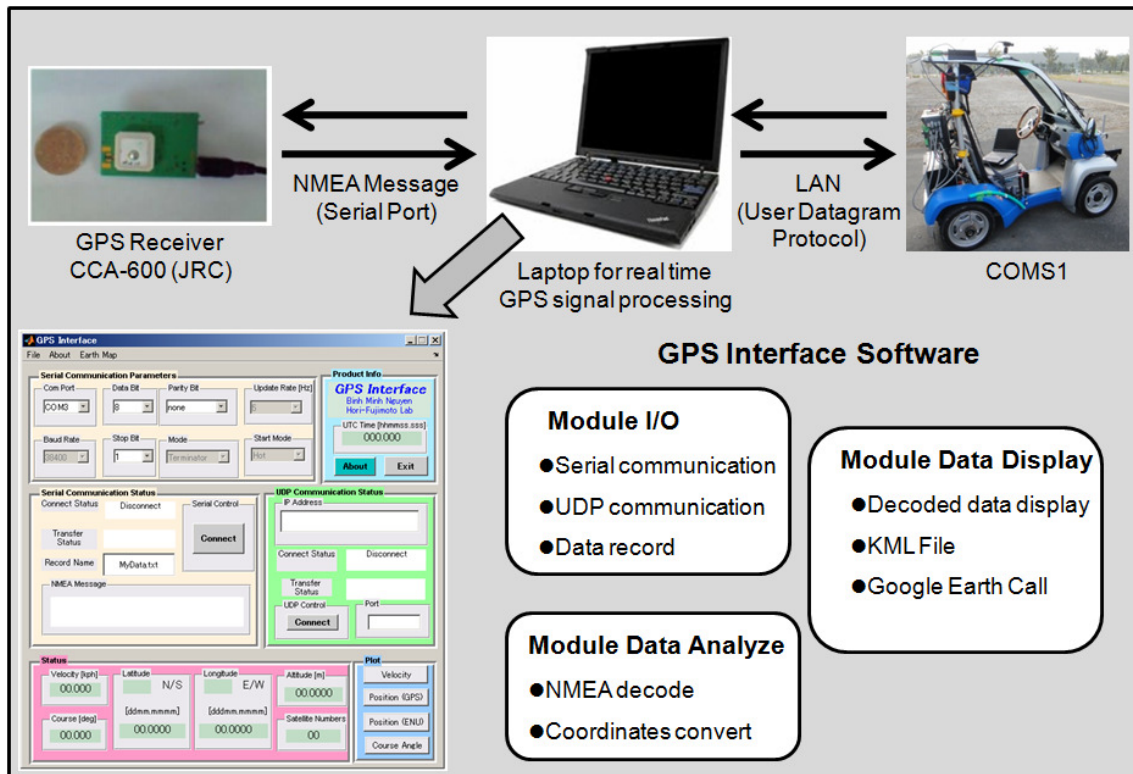


Fig 3.12 Configuration of GPS interface

Table 3.1 Drive train specification of COMS1

Motor	
Category	PSM
Phase/Pole	3/12
Rating power/Max	0.29 kW/2 kW
Max torque	100 Nm
Max velocity	50 km/h
Inverter	
Power switch	MOSFET
Control method	PWM vector control
Energy storage	
Type	Electric double layer capacitor
Energy	210V/173Wh/29.3F

Table 3.2 Parameters of COMS1

Name	Description	Value
$m$	Total mass	378 kg
$m_s$	Sprung mass	332 kg
$m_u$	Unsprung mass	46 kg
$l_f$	Distance from CG to front axle	0.8 m
$l_r$	Distance from CG to rear axle	0.4 m
$d_f$	Tread at front axle	0.840 m
$d_r$	Tread at rear axle	0.815 m
$h$	Height of CG	0.4 m
$C_f$	Front tire cornering stiffness	10,000 N/rad
$C_r$	Rear tire cornering stiffness	10,000 N/rad
$I_z$	Yaw moment of inertia	44.4 Nm/(rad/s <sup>2</sup> )

### 3.2.3 Preliminary measurement using GPS

In order to verify the GPS interface software and experiment setup, preliminary experiments are conducted. The result of a lane-change test is shown in Fig 3.14: (a) vehicle trace on Google Earth map, (b) vehicle position on local planar coordinates, (c) vehicle velocity, and (d) vehicle course angle.

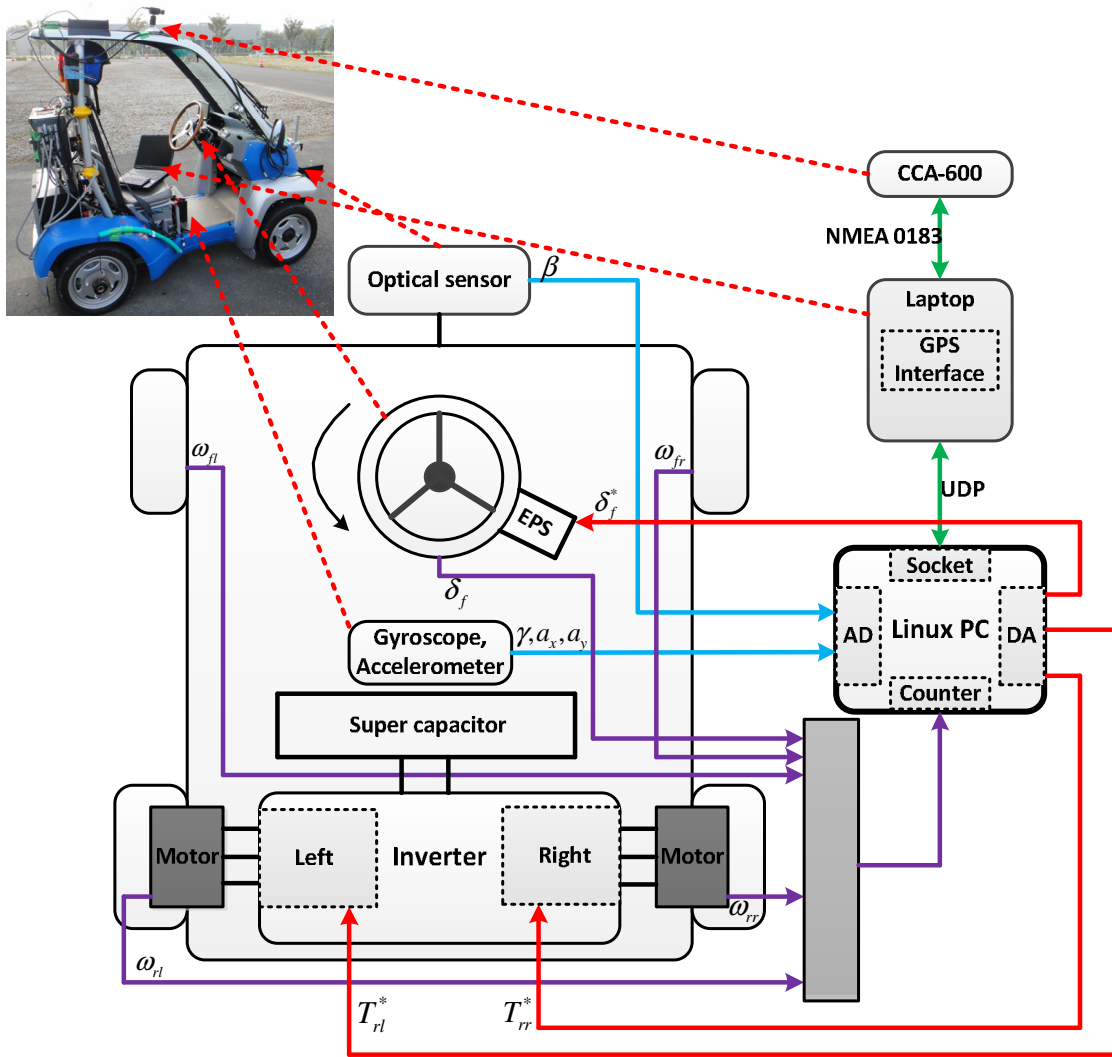


Fig 3.13 Experiment setup of electric vehicle COMS1

### 3.3 Single-rate and multi-rate Kalman filter

#### 3.3.1 Single-rate Kalman filter

Invented by R. E. Kalman in 1960, Kalman filter has been a useful algorithm for state estimation [41]. A continuous system is expressed in (3.2) with the state  $x$ , the control input  $u$ , output measurement  $y$ , process noise  $w$ , and measurement noise  $v$ . Single-rate Kalman filter is designed based on the assumption that all the sampling times of output measurements and holding times of control inputs are the same as  $T_c$ . The discrete system can be established as (3.3) using the discrete transformation in (3.4) where  $k$  is the time index.

$$\begin{cases} \dot{x} = Ax + Bu + w \\ y = Cx + v \end{cases} \quad (3.2)$$

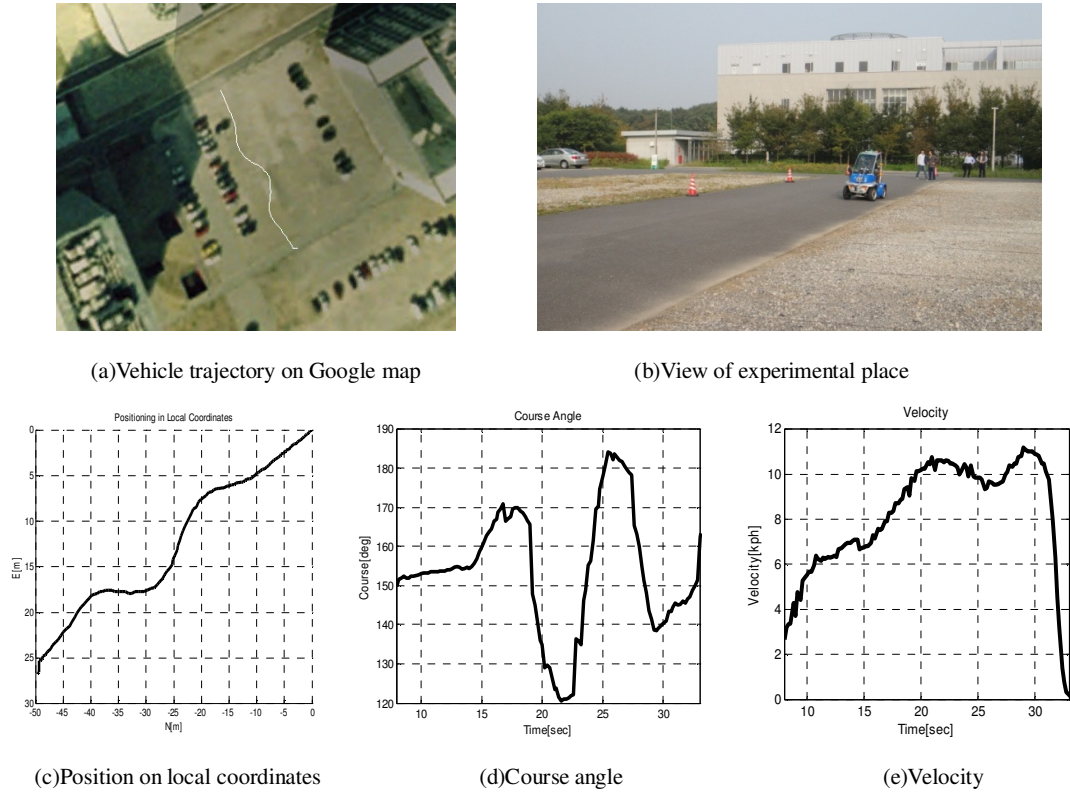


Fig 3.14 Preliminary experiment results using GPS interface

$$\begin{cases} x_{k+1} = A_d x_k + B_d u_k + w_k \\ y_k = C_d x_k + v_k \end{cases} \quad (3.3)$$

$$\begin{cases} A_d = e^{A T_c} \\ B_d = \int_0^{T_c} e^{A \tau} d\tau B \\ C_d = C \end{cases} \quad (3.4)$$

In fact, every real control system is affected by noises. For instance, the measurement of yaw rate by gyroscope or acceleration by accelerometer always contains noises. We assume that  $w$  and  $v$  occur in a random process and their average values are zero. We also further assume that no correlation exists between  $w$  and  $v$ . That is, at any time,  $w$  and  $v$  are independent random variables. Then the process noise covariance  $Q_w$  and measurement noise covariance  $Q_v$  are defined as:

$$\begin{cases} Q_w = E(w_k w_k^T) \\ Q_v = E(v_k v_k^T) \end{cases} \quad (3.5)$$

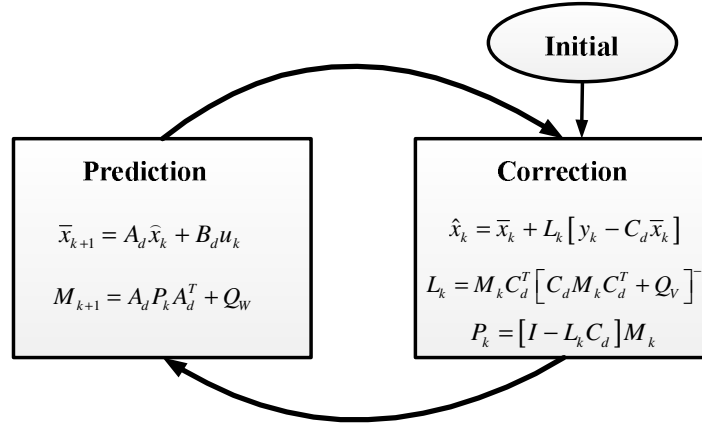


Fig 3.15 Single-rate Kalman filter algorithm

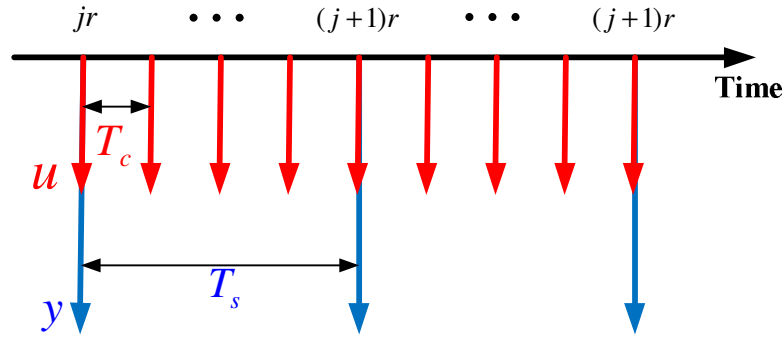


Fig 3.16 Two sampling times in a control system

Single-rate Kalman filter is designed with two stages, prediction and correction, as shown in Fig 3.15. At any estimation step  $k$ ,  $\bar{x}_k$  is the predicted state,  $\hat{x}_k$  is the corrected state,  $L_k$  is Kalman gain, and  $\varepsilon_k = y_k - C_d \bar{x}_k$  is the measurement residual.

Prediction:

$$\bar{x}_{k+1} = A_d \bar{x}_k + B_d u_k \quad (3.6)$$

$$M_{k+1} = A_d P_k A_d^T + Q_W \quad (3.7)$$

Correction:

$$\hat{x}_k = \bar{x}_k + L_k [y_k - C_d \bar{x}_k] \quad (3.8)$$

$$L_k = M_k C_d^T [C_d M_k C_d^T + Q_V]^{-1} \quad (3.9)$$

$$P_k = [I - L_k C_d] M_k \quad (3.10)$$

### 3.3.2 Multi-rate Kalman filter

In a control system, there are holding period of control signal and sampling period of measurement from sensor. If such sampling times are different, we have a multi-rate control system which had been studied by a lot of researchers, such as M. Tomizuka in [28], [29] or H. Fujimoto in

[30]. In this thesis, a case of dual rate control system is examined. We assume that there are two sampling times,  $T_c$  of control period, and  $T_s$  of output measurement. We also assume that output measurement sampling is longer than the control period, as shown in Fig 3.16. The multi-rate ratio  $r$  is defined as:

$$r = T_s / T_c \quad (3.11)$$

Multi-rate Kalman filter is designed in order to provide state estimation every  $T_c$ . The multi-rate Kalman filter algorithm is almost the same single-rate case, except the correction stage. If the measurement update is available, the state is corrected as single-rate Kalman filter. If the measurement update is unavailable, the state is only predicted. The predictions between two measurement updates are called inter-sample predictions. With  $j$  is the integer, the correction stage of multi-rate Kalman filter can be as:

$$\begin{cases} k = jr: \hat{x}_k = \bar{x}_k + L_k [y_k - C\bar{x}_k] \\ k \neq jr: \hat{x}_k = \bar{x}_k \end{cases} \quad (3.12)$$

### 3.4 Multi-rate Kalman filter for sideslip angle estimation using GPS

#### 3.4.1 Estimation design

In chapter 2, the lateral dynamics model of vehicle is establish based with two states: sideslip angle  $\beta$  and yaw rate  $\gamma$ . By introducing the yaw angle  $\psi$  as the third state, yaw rate and course angle from GPS receiver as output measurement, the following dynamics equation is constructed:

$$\begin{cases} \dot{x} = Ax + Bu + w \\ y = Cx + v \end{cases} \quad (3.13)$$

Where

$$x = [\beta \quad \gamma \quad \psi]^T, u = [\delta_f \quad N_z]^T, y = [\gamma \quad c]^T \quad (3.14)$$

$$A = \begin{bmatrix} a_{11} & a_{12} & 0 \\ a_{21} & a_{22} & 0 \\ 0 & 1 & 0 \end{bmatrix}, B = \begin{bmatrix} b_{11} & b_{12} \\ b_{21} & b_{22} \\ 0 & 0 \end{bmatrix}, C = \begin{bmatrix} 0 & 1 & 0 \\ 1 & 0 & 1 \end{bmatrix} \quad (3.15)$$

In this system, yaw rate measurement is sampled at the sampling time the same as the control period  $T_c = 1 \text{ ms}$ , while course angle is sampled at longer period  $T_s = rT_c = 200 \text{ ms}$ . The discrete system is established using (3.4) with the basic sampling time  $T_c = 1 \text{ ms}$ .

The measurement noise covariance matrix is defined as:

$$Q_v = \begin{bmatrix} \sigma_{\gamma\_gyro}^2 & 0 \\ 0 & \sigma_{c\_GPS}^2 \end{bmatrix} \quad (3.16)$$

Where  $\sigma_{\gamma\_gyro}$  and  $\sigma_{c\_GPS}$  denotes the variance of yaw rate noise and course angle noise, respectively.

$Q_v$  is chosen such that measurement of course angle is more reliable than measurement of yaw rate. If



$Q_w$  is selected to large, the Kalman gain will decrease, thus, the estimation fails to update the propagated disturbance term based on measurements. The system has two inputs, the steering angle and yaw moment. Assume they introduce the process noises which are represented by the variance  $\sigma_{\delta_f}$  and  $\sigma_{N_z}$ . The process noise covariance matrix can be calculated as:

$$Q_w = T_c \begin{bmatrix} b_{11} & b_{12} \\ b_{21} & b_{22} \\ 0 & 0 \end{bmatrix} \begin{bmatrix} \sigma_{\delta_f}^2 & 0 \\ 0 & \sigma_{N_z}^2 \end{bmatrix} \begin{bmatrix} b_{11} & b_{12} \\ b_{21} & b_{22} \\ 0 & 0 \end{bmatrix}^T \quad (3.17)$$

$Q_w$  is another tuning factor of estimation. Small  $Q_w$  results in unstable estimation. On the other hand, large  $Q_w$  compels the estimation to completely rely upon the measurement, and therefore, the noise associated with the measurement is directly transmitted into the estimated values.

When GPS measurement update is available, estimation of sideslip angle is corrected by both measurement residual of yaw rate and course angle:

$$\hat{\beta}_k = \bar{\beta}_k + L_k^{\beta\gamma} (\gamma_k - \bar{\gamma}_k) + L_k^{\beta c} (c_k - \bar{c}_k) \quad (3.18)$$

When GPS measurement update is unavailable, estimation of sideslip angle is corrected by only measurement of yaw rate. During such inter-samples, the matrix C is switched to  $\begin{bmatrix} 0 & 1 & 0 \\ 0 & 0 & 0 \end{bmatrix}$ .

$$\hat{\beta}_k = \bar{\beta}_k + L_k^{\beta\gamma} (\gamma_k - \bar{\gamma}_k) \quad (3.19)$$

Where  $L_k^{\beta\gamma}$  and  $L_k^{\beta c}$  are two components of the matrix of Kalman gain calculated by (3.9).

$$L_k = \begin{bmatrix} L_k^{\beta\gamma} & L_k^{\beta c} \\ L_k^{\gamma\gamma} & L_k^{\gamma c} \\ L_k^{w\gamma} & L_k^{wc} \end{bmatrix} \quad (3.20)$$

The above sideslip angle estimation is called three-state multi-rate Kalman filter (three-state MRKF) in this thesis.

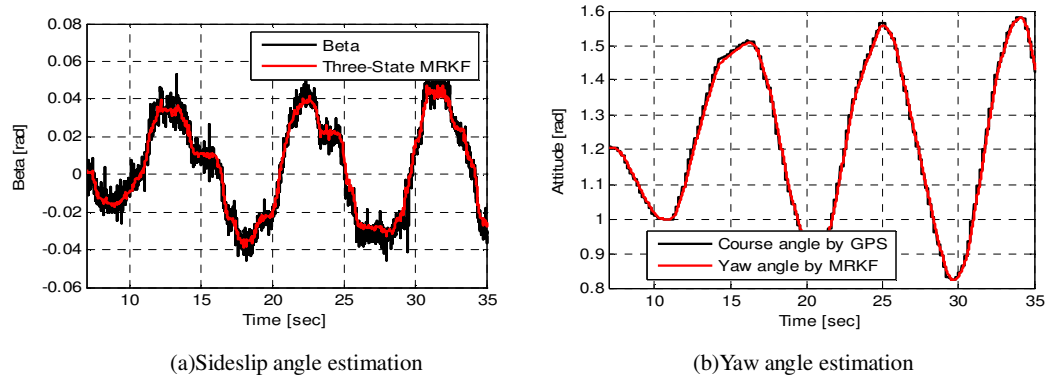


Fig 3.17 Estimation result of three-state MRKF

### 3.4.2 Preliminary results

A lane-change test is conducted and experiment results of three-state MRKF are shown in Fig 3.17. In this experiment, the vehicle runs on high friction road and the cornering stiffness is set as the true value. In Fig 3.17 (a), the black line is the true sideslip angle measured by optical sensor. The result show that the estimated value (the red line) matches very well with the true value. In Fig 3.17 (b), the black line is course angle from GPS receiver which is sampled every 200 millisecond. By using three-state MRKF, the estimated yaw angle can be provided every 1 millisecond.

However, the preliminary results do not show the advantages of sideslip angle estimation using three-state MRKF, for example, when the estimation model errors happen. In the following section, the advantages and problems of three-state MRKF will be discussed by both simulations and experiments.

### 3.4.3 Pros and cons of three-state MRKF

Firstly, a two-state Kalman filter (two-state KF) is designed in order to compare with three-state MRKF. Two states are sideslip angle and yaw rate while only one measurement is yaw rate by gyroscope. The model of two-state system is expressed by the following equations:

$$\begin{cases} \dot{x} = Ax + Bu + w \\ y = Cx + v \end{cases} \quad (3.21)$$

Where

$$x = [\beta \ \dot{\gamma}]^T, u = [\delta_f \ N_z]^T, y = \dot{\gamma} \quad (3.22)$$

$$A = \begin{bmatrix} a_{11} & a_{12} \\ a_{21} & a_{22} \end{bmatrix}, B = \begin{bmatrix} b_{11} & b_{12} \\ b_{21} & b_{22} \end{bmatrix}, C = [0 \ 1] \quad (3.23)$$

As discussing before, while running, vehicle velocity can change and tire cornering stiffness may vary from the nominal value of the estimation model. Therefore, the following simulation condition is set:

- Time variant parameter: vehicle velocity is accelerated from 20 kph to 30 kph.
- Model error: The tire cornering stiffness of vehicle model are set as

$$C_f^V = 10000, C_r^V = 10000 [N / rad] \text{ while the tire cornering stiffness of the estimation model is set as}$$

$$C_f^M = 6000, C_r^M = 6000 [N / rad].$$

A case of lane-change test is conducted with both two-state KF and three-state MRKF. Simulation results are shown in Fig 3.18. The black curve is the true sideslip angle. Under model error condition, sideslip angle estimated by two-state KF cannot match with true value. In contrast, when an update of course angle is available, the estimation error of three-state MRKF can be minimized. This is the advantage of three-state MRKF with GPS in comparison with two-state KF with only yaw rate measurement. In other words, the redundant measurement from GPS receiver can develop the sideslip

angle estimation. However, during inter-samples, when there is no new update of GPS course angle, the estimation error increases due to model error. During inter-samples, estimated values are corrected by only yaw rate measurement. The increase of estimation error during inter-samples is actually the problem of sideslip angle estimation based on GPS. For comparison, three-state MRKF is verified with two update rate, 5 Hz (yellow line) and 20 Hz (violet line). Simulation results in Fig 3.18 suggest that higher rate GPS signal results in smaller estimation error. This is because with higher rate GPS receiver, there are more updates of course angle measurement.

Lane-change experiments are conducted, and the results are shown in Fig 3.19. Course angle from 5 Hz GPS receiver is sampled every 200 millisecond. Vehicle runs on high friction road which means  $C_f^V = 10000, C_r^V = 10000[N/rad]$ . However, the cornering stiffness of the estimation model is set as  $C_f^M = 6000, C_r^M = 6000[N/rad]$ , in order to make the model error condition. The experiment results have the same phenomenon as the simulation results: When the new course angle measurement is updated, estimation error of three-state MRKF is minimized. However, between two course angle measurement updates, the estimation error increases. This is the problem of multi-rate estimation which will be solved in the following section.

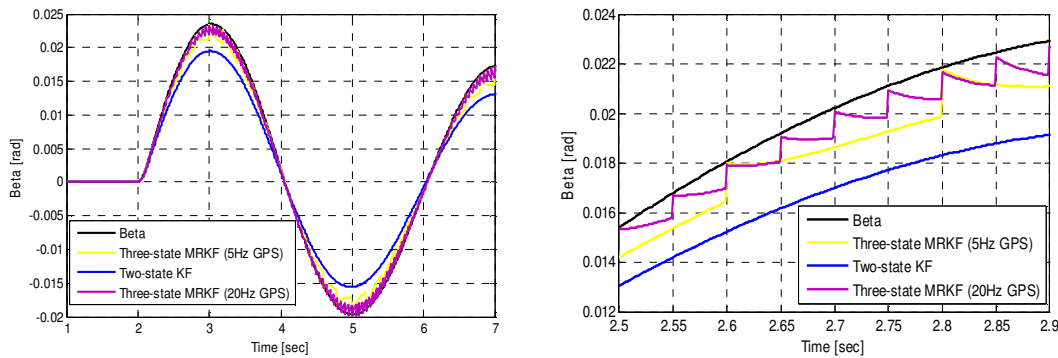


Fig 3.18 Lane-change test with model error (Simulation)

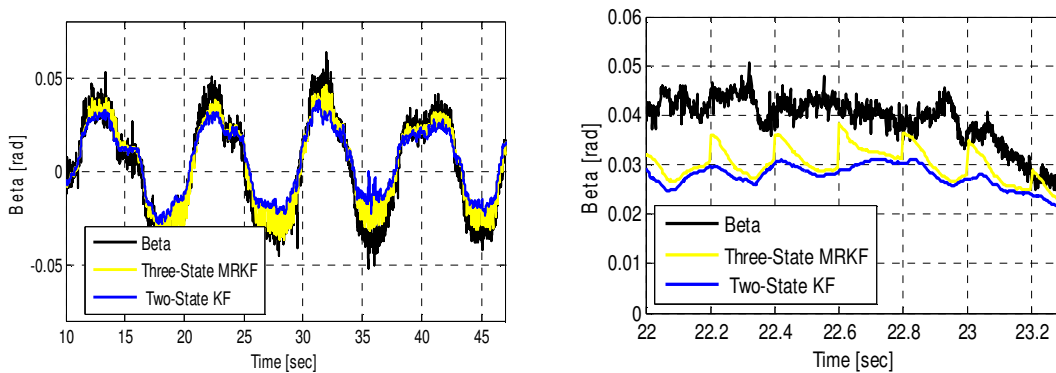


Fig 3.19 Lane-change test with model error (Experiment)

### 3.5 Inter-samples enhancement by prediction of measurement residual

#### 3.5.1 Dynamics of single-rate estimation error

Firstly, we examine the dynamics of single-rate estimation error. At estimation step  $(k+1)$ , the prediction and correction equation can be expressed as:

$$\bar{x}_{k+1} = A_k \hat{x}_k + B_k u_k \quad (3.24)$$

$$\hat{x}_{k+1} = \bar{x}_{k+1} + L_{k+1} (y_{k+1} - C\bar{x}_{k+1}) \quad (3.25)$$

The estimation error can be calculated as:

$$\begin{aligned} e_{k+1} &= x_{k+1} - \hat{x}_{k+1} = A_k x_k + B_k u_k - (A_k \hat{x}_k + B_k u_k) - L_{k+1} C A_k (x_k - \hat{x}_k) \\ \Rightarrow e_{k+1} &= (I - L_{k+1} C) A_k e_k \end{aligned} \quad (3.26)$$

The relation between measurement residual and estimation error can be calculated as:

$$\begin{aligned} \varepsilon_{k+1} &= y_{k+1} - C\bar{x}_{k+1} = C(A_k x_k + B_k u_k) - C(A_k \hat{x}_k + B_k u_k) \\ \Rightarrow \varepsilon_{k+1} &= C A_k e_k \end{aligned} \quad (3.27)$$

At estimation step  $(k+2)$ , the measurement residual and estimation error is expressed as:

$$\varepsilon_{k+2} = C A_{k+1} e_{k+1} \quad (3.28)$$

#### 3.5.2 Prediction of measurement residual

The idea of measurement residual prediction is explained in Fig 3.20. A general case is examined such that the output measurement is sampled at every  $T_s = rT_c$ , while the control period is  $T_c$ . In case of multi-rate Kalman filter, estimated value is corrected only when measurement input is updated. Between two output measurement update, the estimated value is only predicted. This explains why the estimation error increases during inter-samples as shown in the previous section. In order to enhance the inter-samples estimation, we propose to use the real measurement residual to predict the measurement residual during inter-samples till the next real measurement residual coming. The predictive measurement residual is used to correct the estimated value during inter-samples. By this way, multi-rate estimation works like single-rate estimation, hence, the quality of multi-rate estimation is enhanced.

Assume that the measurement update is available at step  $(k+1)$ , but not available at step  $(k+2)$ , from (3.26), (3.27), and (3.28), we introduce the predictive measurement residual at step  $(k+2)$ :

$$\tilde{\varepsilon}_{k+2} = C A_{k+1} (I - L_{k+1} C) A_k G_{k+1} \varepsilon_{k+1} \quad (3.29)$$

Due to the fact that the single-rate is fast enough (1 kHz), the estimation error of step  $(k)$  and  $(k+1)$  are almost the same. We can assume that:

$$G_{k+1} \varepsilon_{k+1} = \varepsilon_{k+1} \quad (3.30)$$

From (3.26), (3.27), and (3.30), we get:

$$G_{k+1} C A_k e_k = (I - L_{k+1} C) A_k e_k \quad (3.31)$$

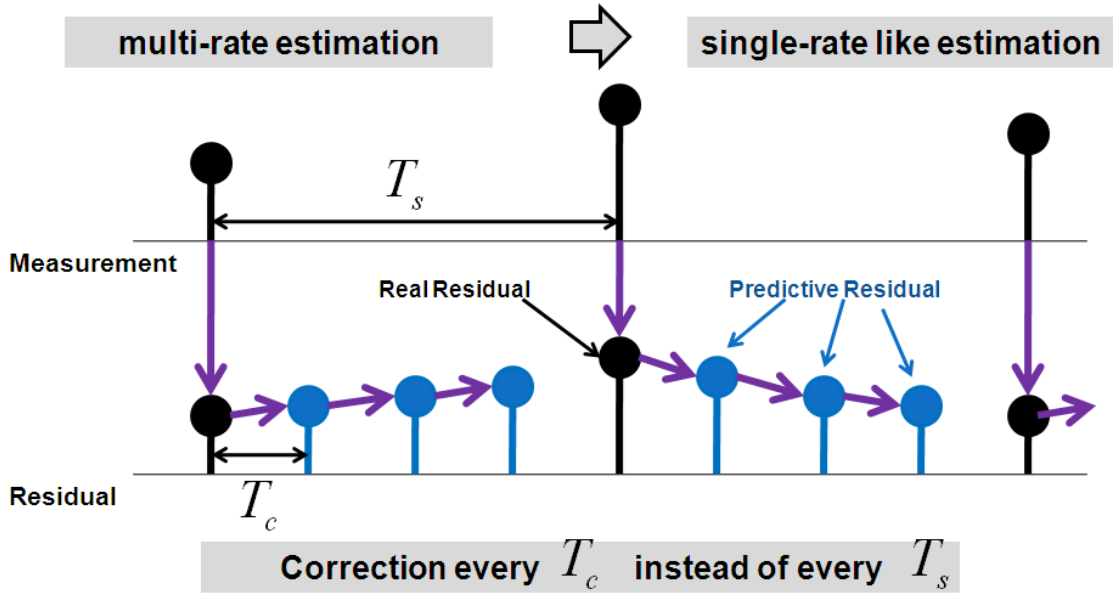


Fig 3.20 Idea of measurement residual prediction

Finally, matrix  $G$  can be calculated as:

$$G_{k+1} = C^T (CC^T)^{-1} - L_{k+1} \quad (3.32)$$

From (3.29) and (3.32), we can predict the measurement residual at step  $(k+2)$  based on real measurement residual at step  $(k+1)$ :

$$\tilde{\epsilon}_{k+2} = CA_{k+1} (I - L_{k+1}C) A_k \left[ C^T (CC^T)^{-1} - L_{k+1} \right] \epsilon_{k+1} \quad (3.33)$$

(3.33) can be applied in predicting of inter-sample measurement residuals, such that the measurement residual at any inter-sample step can be calculated from the previous. The summary of inter-sample prediction is shown in Table 3.3.

### 3.5.3 Previous method on enhancement of inter-sample estimation

From literature review, enhancement of inter-sample estimation was proposed by T. Hara and M. Tomizuka in [29]. This is the “measurement residual holding” method which is applied for multi-rate observer in hard disk drive control system. The method can be presented as followings:

At step  $(k = jr)$ , the measurement update is available, hence, the measurement residual  $\epsilon_{jr} = y_{jr} - C\bar{x}_{jr}$  is used to correct the estimated state:

$$\hat{x}_{jr} = \bar{x}_{jr} + L_0 [y_{jr} - C\bar{x}_{jr}] \quad (3.34)$$

During inter-samples, from step  $(k = jr + 1)$  to step  $(k = jr + r - 1)$ , there is no measurement update, but the measurement residual at step  $(k = jr)$  is held to correct the estimated values.

$$\hat{x}_{jr+i} = \bar{x}_{jr+i} + L_i [y_{jr} - C\bar{x}_{jr}] \quad |i = (1, \dots, r-1) \quad (3.35)$$

Table 3.3 Prediction of inter-sample measurement residuals

Step	State correction	Measurement residual
$k = jr$	$\hat{x}_{jr} = \bar{x}_{jr} + L_{jr} \epsilon_{jr}$	$\epsilon_{jr}$
$k = jr + 1$	$\hat{x}_{jr+1} = \bar{x}_{jr+1} + L_{jr+1} \tilde{\epsilon}_{jr+1}$	$\tilde{\epsilon}_{jr+1} = CA_{jr} (I - L_{jr} C) A_{jr-1} G_{jr} \epsilon_{jr}$
$k = jr + 2$	$\hat{x}_{jr+2} = \bar{x}_{jr+2} + L_{jr+2} \tilde{\epsilon}_{jr+2}$	$\tilde{\epsilon}_{jr+2} = CA_{jr+1} (I - L_{jr+1} C) A_{jr} G_{jr+1} \tilde{\epsilon}_{jr+1}$
$\vdots$	$\vdots$	$\vdots$
$k = jr + r - 1$	$\hat{x}_{jr+r-1} = \bar{x}_{jr+r-1} + L_{jr+r-1} \tilde{\epsilon}_{jr+r-1}$	$\tilde{\epsilon}_{jr+r-1} = CA_{jr+r-2} (I - L_{jr+r-2} C) A_{jr+r-3} G_{jr+r-2} \tilde{\epsilon}_{jr+r-2}$

Table 3.4 List of estimation methods for comparison

No.	Estimation method	Description
1	Two-state KF	Single-rate Kalman filter with only yaw rate measurement
2	Three-state MRKF	Conventional multi-rate Kalman filter with yaw rate and course angle measurement
3	Three-state MROb	Multi-rate observer with the holding of course angle measurement residual
4	Enhanced three-state MRKF	Proposed multi-rate Kalman filter with prediction of course angle measurement residual

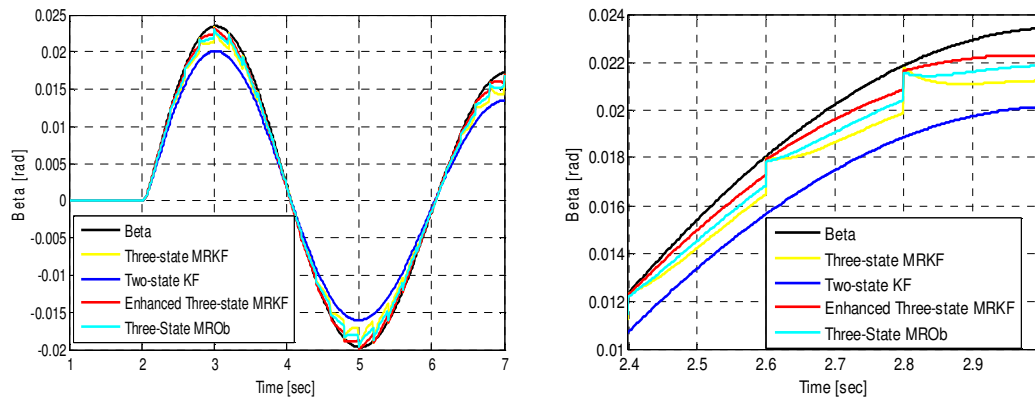


Fig 3.21 Lane-change test with model error (simulation)

In (3.34) and (3.35), the observer gain is designed as:

$$L_0 = L_1 = \dots = L_{r-1} = \left( \sum_{i=1}^r A_d^i \right)^{-1} A_d^r L_{sr} \quad (3.36)$$

Where  $L_{sr}$  is the observer gain matrix of single-rate observer designed by pole placement.

The multi-rate ratio of hard disk drive system (2-10) is smaller than the multi-rate ratio of vehicle system (50-200 for 5-20 Hz GPS receiver). Moreover, the working condition of vehicle frequently changes, such as road condition or external disturbance. For this reason, instead of linear observer, we propose the Kalman filter which is the optimal linear estimator in sense that no other linear filter can give a smaller variance on the estimation error [31]. Our proposed method will be compared with the multi-rate linear observer in the followings.

### 3.5.4 Simulation results

Four estimation methods are performed for comparison, as can be seen in Table 3.4. Vehicle velocity is accelerated from 20 kph to 30 kph. The tire cornering stiffness of vehicle model are set as  $C_f^V = 10000, C_r^V = 10000 [N/rad]$  while the tire cornering stiffness of the estimation model is set as  $C_f^M = 6000, C_r^M = 6000 [N/rad]$ . The three-state MROb is designed with nominal parameters:

$v_{xn} = 20kph, C_{fn} = 6000, C_{rn} = 6000 [N/rad]$ . A case of simulation, lane-change tests is conducted and the results are shown in Fig 3.21. In order to compare four methods, the root-mean-square-deviation (RMSD) of estimated sideslip angle from true value is calculated as in (3.37).

$$RMSD = \sqrt{\frac{\sum_{i=1}^N (\theta_i - \hat{\theta}_i)^2}{N}} \quad (3.37)$$

Where  $N$  is the number of estimation step,  $\theta_i$  is the real value, and  $\hat{\theta}_i$  is the estimated value.

Table 3.5 Root-mean-square deviation of sideslip angle estimation (simulation)

Estimation method	RMSD [rad]
Two-state KF	0.0028
Three-state MRKF	0.0015
Three-state MROb	0.0011
Enhanced three-state MRKF	0.0008

Table 3.6 Root-mean-square deviation of sideslip angle estimation (experiment)

Estimation method	RMSD [rad]
Two-state KF	0.0102
Three-state MRKF	0.0086
Three-state MROb	0.0046
Enhanced three-state MRKF	0.0036

The RMSD calculation shows that the proposed enhanced three-state MRKF has the best performance during inter-samples. Although three-state MROb designed by Hara and Tomizuka's method can enhance the inter-samples, however, it has bigger error than the proposed method during inter-samples.

### 3.5.5 Experiment results

The results of lane-change test are shown in Fig 3.22. Vehicle runs on high friction road such that it has the real cornering stiffness  $C_f^V = 10000, C_r^V = 10000 [N/rad]$ . However, the cornering stiffness of the estimation model is set as  $C_f^M = 6000, C_r^M = 6000 [N/rad]$ , in order to make the model error condition. RMSD of each estimation method is calculated for comparison, and is organized in Table 3.6. The RMSD calculation shows that three-state MRKF is better than two-state KF. Three-state MROb can enhance the sideslip angle estimation, but the enhanced three-state MRKF has the best performance. Fig 3.22 (f) shows the inter-sample performance of four methods. It is clear that the enhanced three-state MRKF (the red) has the best convergence to the true sideslip angle (the black).

### 3.5.6 Section Conclusions

Based on the simulations and experiments, we conclude that:

- Multi-rate Kalman filter with course angle measurement can be applied for sideslip angle estimation and has better performance than single-rate method.
- The prediction of course angle measurement residual can enhance the inter-sample of multi-rate estimation. The enhanced multi-rate Kalman filter with predictive measurement residual shows the better performance than multi-rate observer with measurement residual holding under model error and time-variant parameter condition.



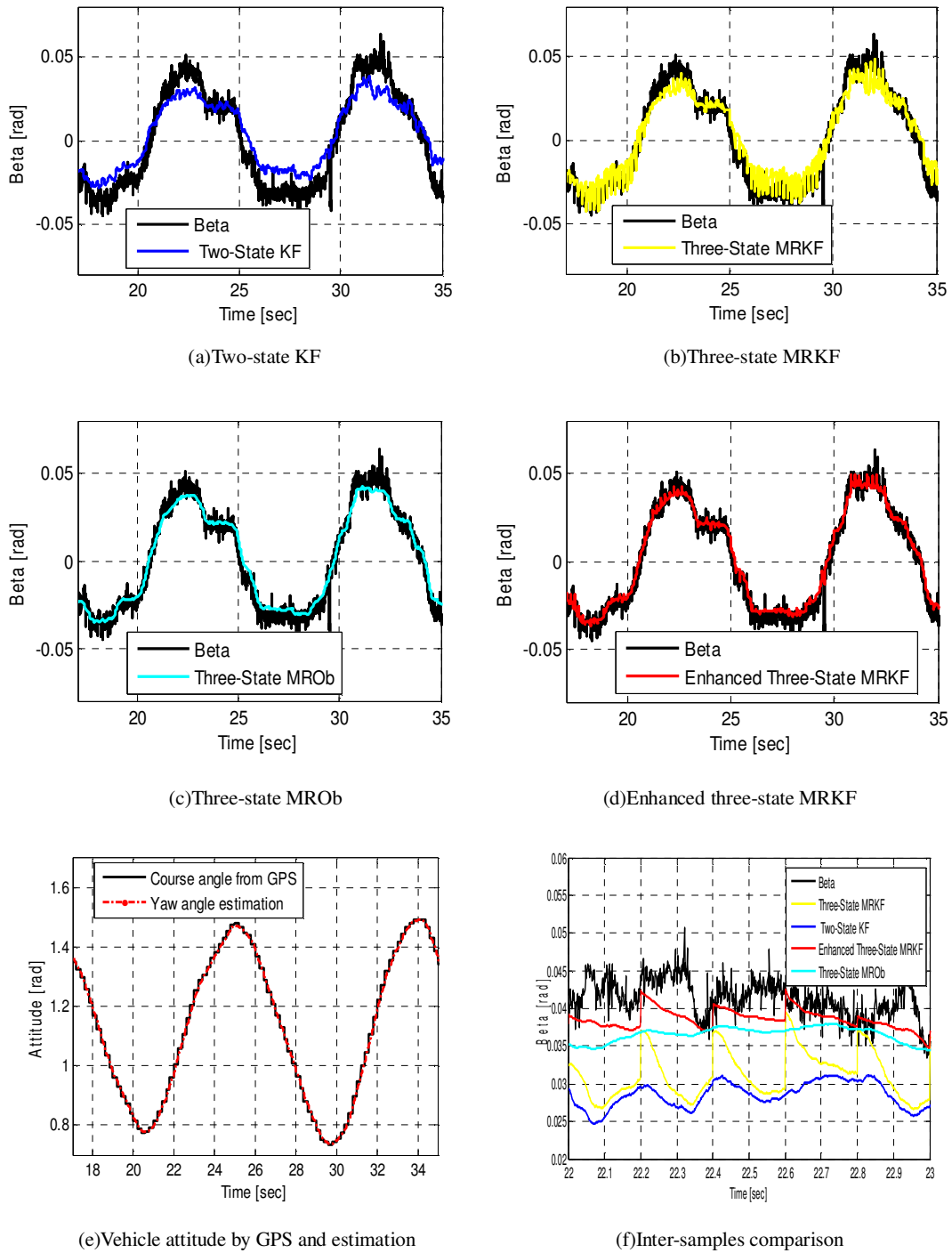


Fig 3.22 Lane-change test with model error (experiment)

### 3.6 Inter-samples enhancement by disturbance estimation

#### 3.6.1 Disturbance accommodating for robust estimation

Disturbance observer was introduced in [42] for improving the robustness of the control system

by compensating the influence of disturbance, model variation, and noises. Disturbance accommodating control was firstly introduced in [43] in which the external disturbances are considered as extended states. In [44], both external disturbances and model uncertainty are lumped into a disturbance term. By this way, disturbance attenuation is effectively achieved in control of helicopter. The main idea of disturbance accommodating is explained as followings:

Consider a system with model uncertainty and unknown input disturbance  $W_d$ . Here we assume that the uncertainty is only associated with the dynamics of disturbance term.

$$\begin{cases} \dot{X} = (A_n + \Delta A)X + (B_n + \Delta B)U + B_d W_d \\ Y = CX \end{cases} \quad (3.38)$$

The dynamics of external term can be written as:

$$\dot{W}_d = \Gamma_1(X, U, W_d) \quad (3.39)$$

The external disturbance and model uncertainty can be lumped into a disturbance term:

$$D_d = \Delta AX + \Delta BU + B_d W_d \quad (3.40)$$

The dynamics equation of disturbance term can be written as:

$$\dot{D}_d = \Delta A \dot{X} + \Delta B \dot{U} + B_d \Gamma_1(X, U, W_d) = \Gamma_2(X, D_d, U) \quad (3.41)$$

We usually do not know the precise dynamics of the disturbance term. For simplicity, one method of modeling the disturbance term can be expressed as following:

$$\dot{D}_d = A_D D_d \quad (3.42)$$

In (3.42),  $A_D$  is Hurwitz:

Construct the new state vector  $Z = [X \ D_d]^T$ , the dynamics equation of new model with disturbance accommodating is expressed as:

$$\dot{Z} = \begin{bmatrix} A_n & I \\ 0 & A_D \end{bmatrix} Z + \begin{bmatrix} B_n \\ 0 \end{bmatrix} U \quad (3.43)$$

$$Y = [C \ 0]Z \quad (3.44)$$

The disturbance can be estimated and compensated by considering the new system expressed in (3.43) and (3.44).

### 3.6.2 Sideslip angle and disturbance estimation using multi-rate Kalman filter

As we known, the vehicle is a time-variant parameter system. During operation, the tire cornering stiffness may change such that model error may be introduced to estimation model. During inter-samples, when there is no course angle measurement update, the model error is counted step by step and the estimation error is increased. Moreover, the strong external disturbance, such as wind force may attack vehicle and degrade the estimation performance. In electric vehicle, when the road

condition on left and right side are different, anti-slip controller may give different torque commands to the left and right in-wheel motor. Due to this reason, the yaw moment disturbance may happen and can reduce the correction of sideslip angle estimation.

Assume that the estimation model is designed with the nominal tire cornering stiffness  $C_{fn}, C_m$ . If the road condition changes, unknown model error is introduced and the real tire cornering stiffness can be written as  $C_{fn} + \Delta C_f, C_m + \Delta C_r$ . We also assume that the disturbance force  $F_d$  and disturbance yaw moment  $N_d$  happens to the vehicle system. The dynamics equation of lateral motion in (2.20) can be re-expressed as:

$$\begin{aligned} \begin{bmatrix} \dot{\beta} \\ \dot{\gamma} \end{bmatrix} &= \begin{bmatrix} \frac{-2[(C_{fn} + \Delta C_f) + (C_m + \Delta C_r)]}{mv_x} & -1 - \frac{2[(C_{fn} + \Delta C_f)l_f - (C_m + \Delta C_r)l_r]}{mv_x^2} \\ \frac{-2[(C_{fn} + \Delta C_f)l_f - (C_m + \Delta C_r)l_r]}{I_z} & \frac{-2[(C_{fn} + \Delta C_f)l_f^2 + (C_m + \Delta C_r)l_r^2]}{I_z v_x} \end{bmatrix} \begin{bmatrix} \beta \\ \gamma \end{bmatrix} \\ &+ \begin{bmatrix} \frac{2(C_{fn} + \Delta C_f)}{mv_x} & 0 \\ \frac{2(C_{fn} + \Delta C_f)l_f}{I_z} & \frac{1}{I_z} \end{bmatrix} \begin{bmatrix} \delta_f \\ N_z \end{bmatrix} + \begin{bmatrix} \frac{1}{mv_x} & 0 \\ 0 & \frac{1}{I_z} \end{bmatrix} \begin{bmatrix} F_d \\ N_d \end{bmatrix} \end{aligned} \quad (3.45)$$

If we consider all the model error, disturbance force, and disturbance yaw moment are general disturbance, we can define two general disturbances:

$$d_1 = \frac{-2(\Delta C_f + \Delta C_r)}{mv_x} \beta + \frac{-2(\Delta C_f l_f - \Delta C_r l_r)}{mv_x^2} \gamma + \frac{2\Delta C_f}{mv_x} \delta_f + \frac{1}{mv_x} F_d \quad (3.46)$$

$$d_2 = \frac{-2(\Delta C_f l_f - \Delta C_r l_r)}{I_z} \beta + \frac{-2(\Delta C_f l_f^2 + \Delta C_r l_r^2)}{I_z v_x} \gamma + \frac{2\Delta C_f l_f}{I_z} \delta_f + \frac{1}{I_z} N_d \quad (3.47)$$

The idea of disturbance estimation is utilized in this thesis for robust multi-rate Kalman filter. By introducing new state vector  $h = [\beta \ \gamma \ \psi \ d_1 \ d_2]^T$ , the new system for estimation design is established as following:

$$\begin{cases} \dot{h} = Kh + Gu + w \\ y = Mh + v \end{cases} \quad (3.48)$$

$$K = \begin{bmatrix} \frac{-2(C_{fn} + C_m)}{mv_x} & -1 - \frac{2(C_{fn}l_f - C_m l_r)}{mv_x^2} & 0 & 1 & 0 \\ \frac{-2(C_{fn}l_f - C_m l_r)}{I_z} & \frac{-2(C_{fn}l_f^2 + C_m l_r^2)}{I_z v_x} & 0 & 0 & 1 \\ 0 & 1 & 0 & 0 & 0 \\ 0 & 0 & 0 & 0 & 0 \\ 0 & 0 & 0 & 0 & 0 \end{bmatrix} \quad (3.49)$$

$$G = \begin{bmatrix} \frac{2C_{fn}}{mv_x} & 0 \\ \frac{2C_{fn}l_f}{I_z} & \frac{1}{I_z} \\ 0 & 0 \\ 0 & 0 \\ 0 & 0 \end{bmatrix} \quad (3.50)$$

$$M = \begin{bmatrix} 0 & 1 & 0 & 0 & 0 \\ 1 & 0 & 1 & 0 & 0 \end{bmatrix} \quad (3.51)$$

Here we assume that: 1) the change of the disturbances with time is slow. 2) sideslip angle and yaw rate are controlled so that they converge to the steady values. Therefore, the derivative of the general disturbances in (3.41) is assumed to be zero.

Using (3.48), a five-state multi-rate Kalman filter can be designed with the measurement of yaw rate and course angle from GPS receiver. This method is named five-state MRKF in this thesis. The configuration of five-state MRKF is shown in Fig 3.23.

### 3.6.3 Simulation results

In order to evaluate the proposed five-state MRKF, the following condition is set for simulation:

- Vehicle runs at the speed of 20 kph and starts cornering at 2 second.
- Model error: The tire cornering stiffness of vehicle model are set as

$$C_f^V = 10000, C_r^V = 10000 [N / rad] \text{ while the tire cornering stiffness of the estimation model is set as}$$

$$C_f^M = 7000, C_r^M = 7000 [N / rad].$$

- External disturbance: Lateral wind force  $F_{dw} = 100N$  attacks the vehicle from 3second. Assume that the distance from aerodynamics center to center of gravity is  $l_w = 0.1m$ , a disturbance yaw moment  $N_{dw} = \frac{l_w}{I_z} F_{dw}$  is generated and gives effect to the yaw motion of vehicle.

Two-state KF and three-state MRKF are also performed for comparison. Simulation results are shown in Fig 3.24. Before the attacking of lateral wind force, three-state MRKF (the yellow line) has small estimation error during inter-samples. However, under the lateral wind, the estimation error

during inter-samples increases considerably. In contrast, five-state MRKF (the red line) can minimize the estimation error during inter-samples even with model error and external disturbances. Both five-state MRKF and three-state MRKF are better than two-state KF (the blue line). The estimation of general disturbances is shown in Fig 3.24 (c) and (d). RMSD of each estimation method is calculated and organized in Table 3.7 in which five-state MRKF has the smallest RMSD value.

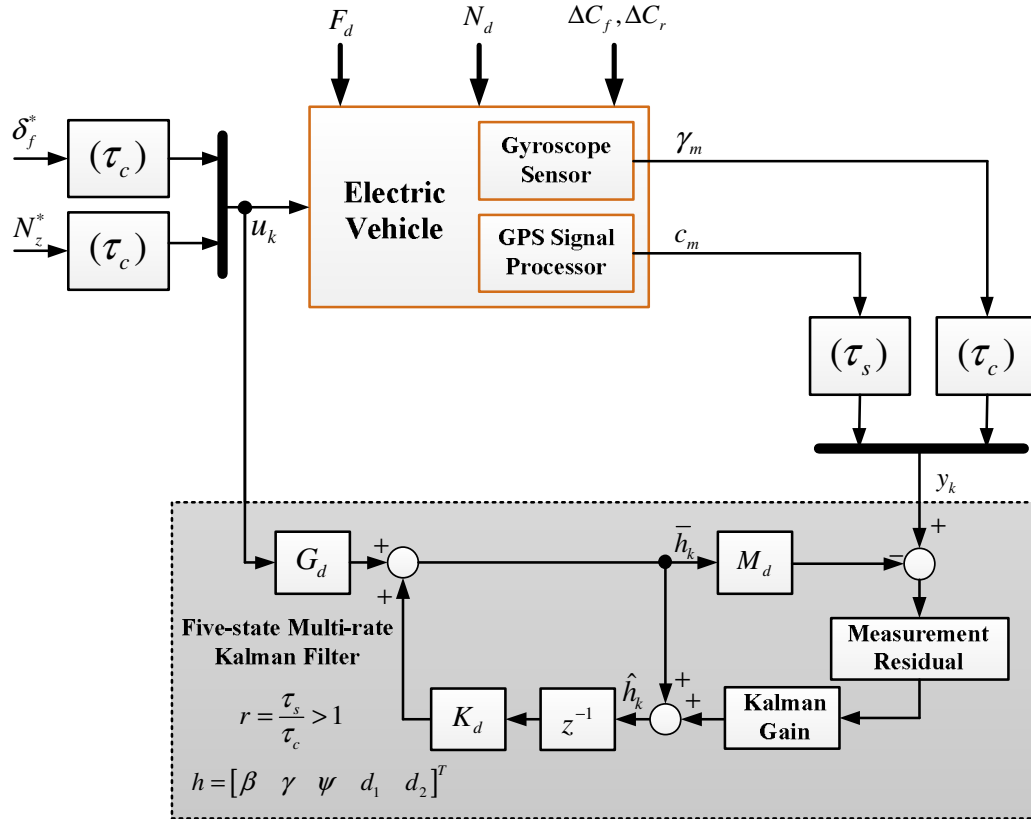


Fig 3.23 Configuration of five-state multi-rate Kalman filter

Table 3.7 Root-mean-square deviation of sideslip angle estimation (simulation)

Estimation method	RMSD [rad]
Two-state KF	0.0018
Three-state MRKF	0.0013
Five-state MRKF	0.0002

Table 3.8 Root-mean-square deviation of sideslip angle estimation (experiment)

Estimation method	RMSD [rad]
Two-state KF	0.0112
Three-state MRKF	0.0087
Five-state MRKF	0.0041

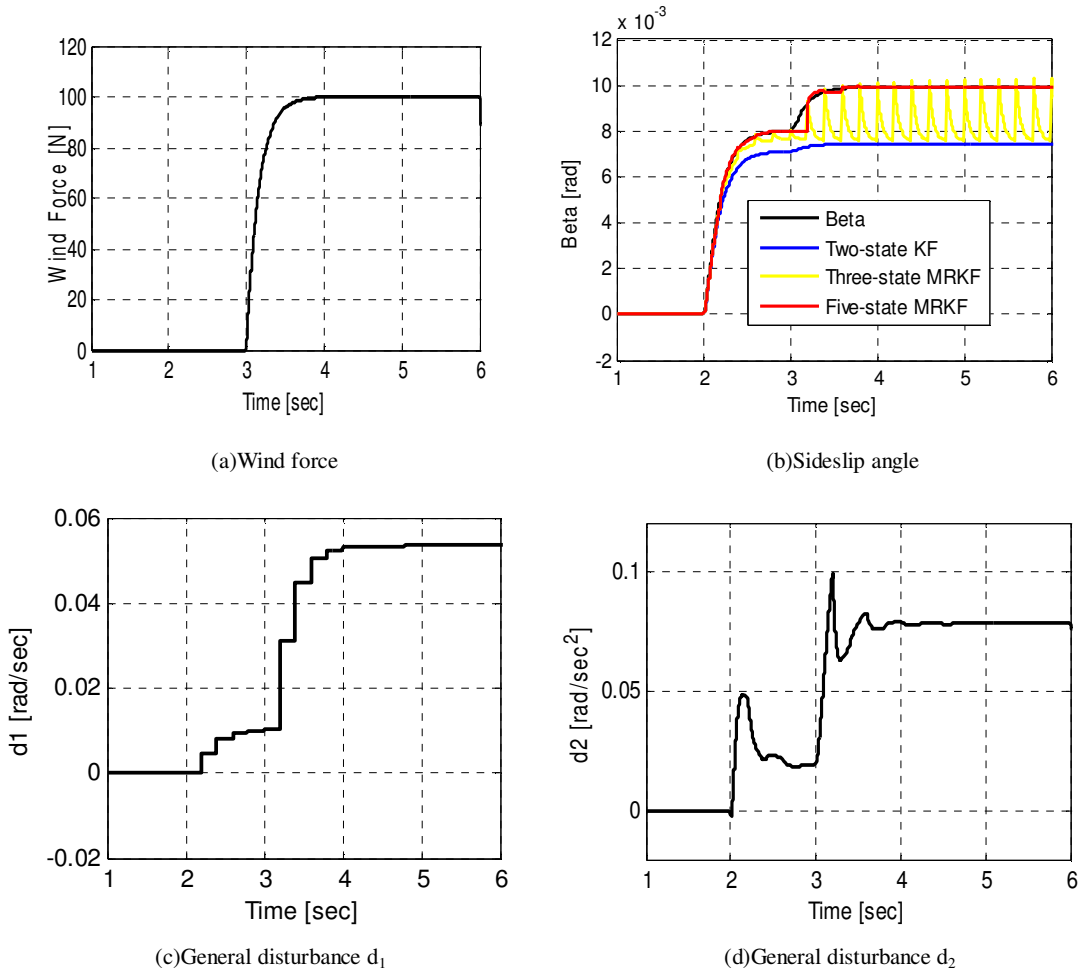


Fig 3.24 Simulation results of five-state MRKF (cornering test)

### 3.6.4 Experiment results

Experiment is conducted with the same model error condition as simulations in previous sub-section. During experiment, the effect of the external disturbances, such as wind force and disturbance yaw moment, is unknown. Results of cornering test are shown in Fig 3.25. In comparison with two-state KF and three-state MRKF, five-state MRKF has the best estimation performance because the estimation error during inter-samples is compensated. The estimation of general disturbances is shown in Fig 3.25 (c) and (d). RMSD of each estimation method is calculated and organized in Table 3.8 in which five-state MRKF has the smallest RMSD value.

### 3.6.5 Section conclusions

Based on both simulation and experiment results, we propose that by general disturbance estimation, the performance of multi-rate Kalman filter for sideslip angle estimation using GPS is developed.

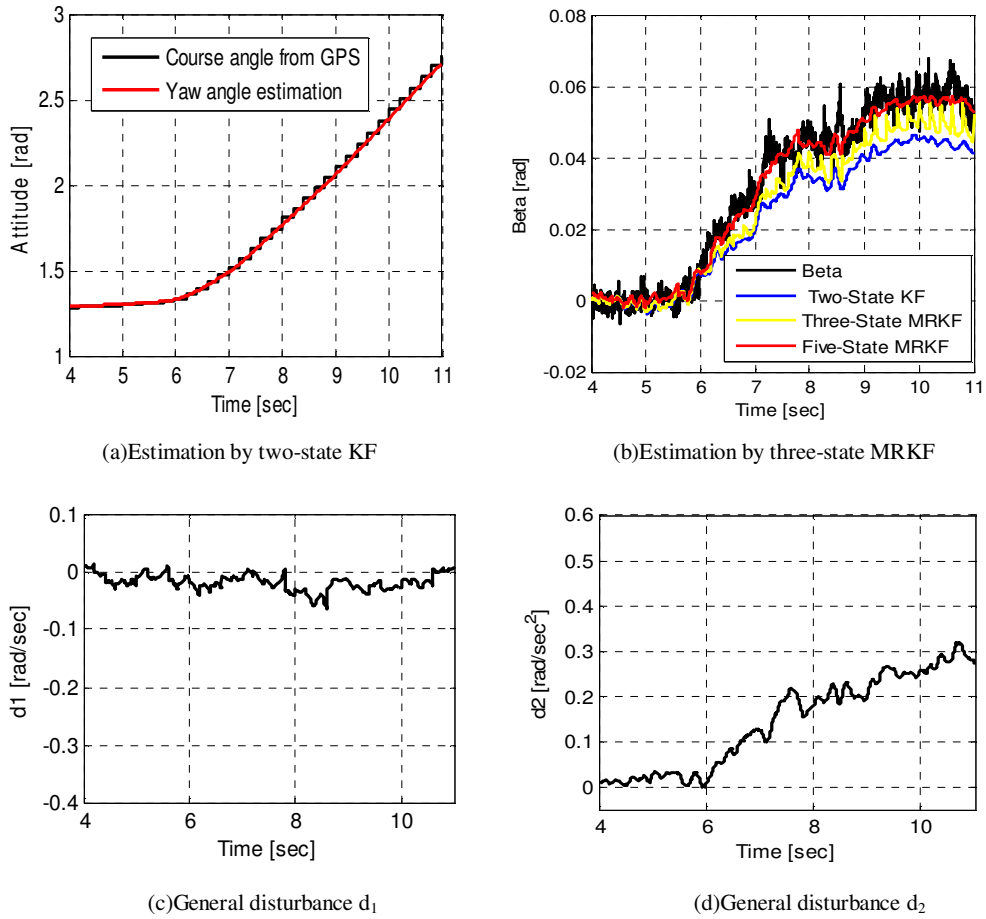


Fig 3.25 Experiment results of five-state MRKF (cornering test)

### 3.7 Chapter summary

In this chapter, the scenario of GPS for vehicle state estimation is analyzed. GPS has the advantage such that it provides another redundant measurement for vehicle control system: the course angle. The problem of GPS based estimation for vehicle control is the low update rate of GPS signal and the unknown disturbances as well as model error.

We have applied the new GPS receiver CCA-600 produced by Japan Radio Company in small electric vehicle COMS. The GPS interface software is designed for real time processing of GPS signal and sending measurement data from CCA-600 to COMS's controller. In order to overcome the low update rate of GPS signal, the prediction of course angle measurement residual is proposed. The general disturbances are combined with other estimation states in five-state multi-rate Kalman filter. By this way, we can compensate the effect of both model error and external disturbances to sideslip angle estimation. Both simulations and experiments are conducted in order to evaluate the proposed methods.

## Chapter 4: Electric vehicle stability control design

In this chapter, sideslip angle estimation using GPS which is designed in the previous chapter is applied in vehicle stability control system. Yaw moment generated by the different torque of left and right side in-wheel motors is utilized for stabilizing electric vehicle motion.

### 4.1 Reference model for vehicle stability control

As presented in chapter 2, the lateral motion of vehicle can be expressed by the following matrix equation:

$$\begin{bmatrix} \dot{\beta} \\ \dot{\gamma} \end{bmatrix} = \begin{bmatrix} a_{11} & a_{12} \\ a_{21} & a_{22} \end{bmatrix} \begin{bmatrix} \beta \\ \gamma \end{bmatrix} + \begin{bmatrix} b_{11} & b_{12} \\ b_{21} & b_{22} \end{bmatrix} \begin{bmatrix} \delta_f \\ N_z \end{bmatrix} \quad (4.1)$$

From (4.1), the transformation from steering angle and yaw moment to sideslip angle and yaw rate can be expressed as the following second-order transfer functions:

$$\begin{bmatrix} \beta \\ \gamma \end{bmatrix} = \begin{bmatrix} G_{11} & G_{12} \\ G_{21} & G_{22} \end{bmatrix} \begin{bmatrix} \delta_f \\ N_z \end{bmatrix} \quad (4.2)$$

$$G_{11} = \frac{b_{11}s + b_{21}a_{12} - b_{11}a_{22}}{(s - a_{11})(s - a_{22}) - a_{12}a_{21}} \quad (4.3)$$

$$G_{12} = \frac{b_{22}a_{12}}{(s - a_{11})(s - a_{22}) - a_{12}a_{21}} \quad (4.4)$$

$$G_{21} = \frac{b_{21}s + b_{11}a_{21} - b_{21}a_{11}}{(s - a_{11})(s - a_{22}) - a_{12}a_{21}} \quad (4.5)$$

$$G_{22} = \frac{b_{22}s - b_{21}a_{11}}{(s - a_{11})(s - a_{22}) - a_{12}a_{21}} \quad (4.6)$$

For simplicity, the steady-state response of sideslip angle and yaw rate from driver's steering angle input can be used as references for vehicle stability control system:

$$\beta^* = \frac{K_\beta}{1 + \tau_\beta s} \delta_f \quad (4.7)$$

$$\gamma^* = \frac{K_\gamma}{1 + \tau_\gamma s} \delta_f \quad (4.8)$$

The steady state gains of sideslip angle and yaw rate are calculated by the following equations. Such gains depend on the nominal parameters of vehicle and are updated in real time with vehicle velocity.

$$K_\beta = \frac{\left[ \frac{1 - \frac{m}{2(l_f + l_r)^2} \frac{l_f}{C_r l_r} v_x^2}{1 - \frac{m}{2(l_f + l_r)^2} \frac{C_f l_f - C_r l_r}{C_f C_r} v_x^2} \right] \frac{l_r}{(l_f + l_r)}}{\quad} \quad (4.9)$$



$$K_\gamma = \left[ \frac{1}{1 - \frac{m}{2(l_f + l_r)^2} \frac{C_f l_f - C_r l_r}{C_f C_r} v_x^2} \right] \frac{v_x}{(l_f + l_r)} \quad (4.10)$$

The reference gain of sideslip angle and yaw rate will increase as the velocity increases. At high speed, this is unsafe for the driver. Therefore, the reference value of yaw rate and sideslip angle should be limited as followings:

$$|\beta^*| \leq \beta_{\max}^* \quad (4.11)$$

$$|\dot{\gamma}^*| \leq \frac{\mu g}{v_x} \quad (4.12)$$

Where  $\mu$  is the road friction coefficient,  $g$  is the gravity, and  $v_x$  is the vehicle velocity.

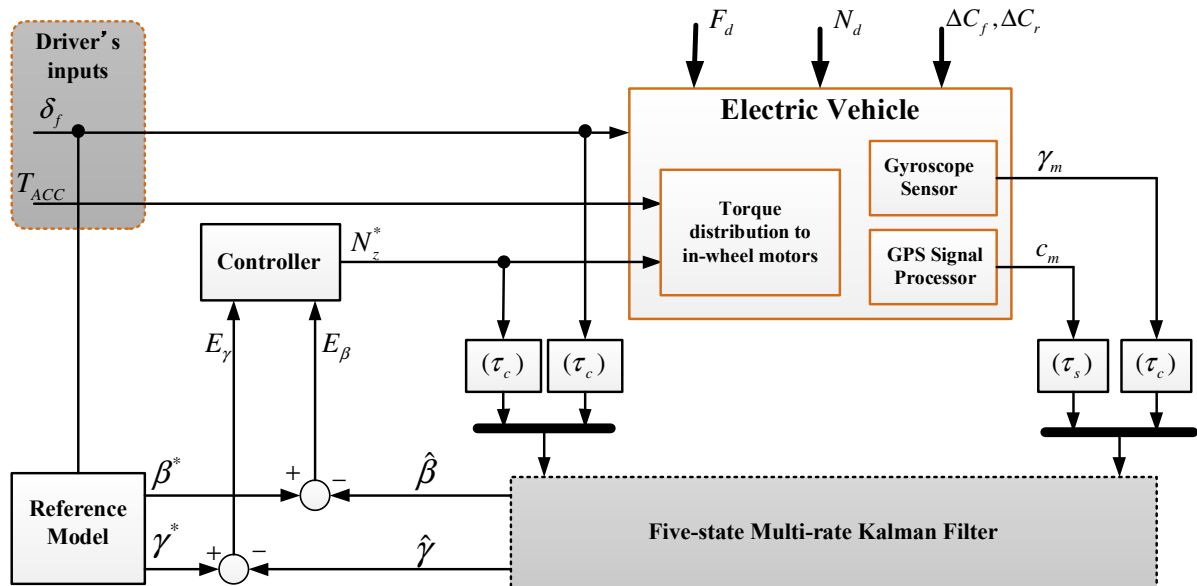


Fig 4.1 Vehicle stability control system based on direct yaw moment control and multi-rate Kalman filter

## 4.2 Electric vehicle stability control based on direct yaw moment control

### 4.2.1 General configuration

The configuration of electric vehicle stability control system based direct yaw moment control is shown in Fig 4.1. The measurement of yaw rate and course angle from GPS receiver is used as measurements for sideslip angle estimation. In this system, five-state multi-rate Kalman filter which is

designed in the chapter 3 is utilized. Reference signals are generated from driver's steering angle input. From the differences between estimated values and reference values, the feedback controller generates the yaw moment for stabilizing vehicle motion. Torque command of the rear left and rear right in wheel motor is calculated from yaw moment control signal. This is a multi-rate control system because the course angle is sampled every 200 millisecond, while the control period of yaw moment is every 1 millisecond.

#### 4.2.2 Feedback controller design based on linear quadratic regulator method

Considering yaw moment as control input, the state equation of the system can be obtained as:

$$\dot{X} = AX + B_N N_z^* + B_\delta \delta_f \quad (4.13)$$

$$X = [\beta \quad \gamma]^T \quad (4.14)$$

$$A = \begin{bmatrix} \frac{-2(C_f + C_r)}{mv_x} & -1 - \frac{2(C_f l_f - C_r l_r)}{mv_x^2} \\ \frac{-2(C_f l_f - C_r l_r)}{I_z} & \frac{-2(C_f l_f^2 + C_r l_r^2)}{I_z v_x} \end{bmatrix} \quad (4.15)$$

$$B_N = \begin{bmatrix} 0 \\ \frac{1}{I_z} \end{bmatrix} \quad (4.16)$$

$$B_\delta = \begin{bmatrix} \frac{2C_f}{mv_x} \\ \frac{2C_f l_f}{I_z} \end{bmatrix} \quad (4.17)$$

Let  $E$  be the tracking error between the reference and the estimated state.

$$E = X^* - \hat{X} = [E_\beta \quad E_\gamma]^T [\beta^* - \hat{\beta} \quad \gamma^* - \hat{\gamma}]^T \quad (4.18)$$

The reference model can be represented as:

$$\dot{X}^* = A^* X^* + B^* \delta_f \quad (4.19)$$

$$A^* = \begin{bmatrix} \frac{-1}{\tau_\beta} & 0 \\ 0 & \frac{-1}{\tau_\gamma} \end{bmatrix} \quad (4.20)$$

$$B^* = \begin{bmatrix} \frac{K_\beta}{\tau_\beta} \\ \frac{K_\gamma}{\tau_\gamma} \end{bmatrix} \quad (4.21)$$

From (4.13), (4.18), and (4.19), the dynamics equation of tracking error is obtained as:

$$\dot{E} = AE + B_N N_z^* + (A - A^*) X^* + (B_\delta - B^*) \delta_f \quad (4.22)$$

Considering the third and the fourth term of (4.20) as disturbance  $W_d$ , the dynamics of tracking error can be written as:

$$\dot{E} = AE + B_N N_z^* + W_d \quad (4.23)$$

In order to minimize the tracking error, linear quadratic regulator (LQR) method [32] is applied to design the feedback gain. The yaw moment control is generated as:

$$N_z^* = g_\beta E_\beta + g_\gamma E_\gamma = g_\beta (\beta^* - \hat{\beta}) + g_\gamma (\gamma^* - \hat{\gamma}) \quad (4.24)$$

The feedback gains  $g_\beta$  and  $g_\gamma$  are determined by minimizing the cost function J as shown in the following equation:

$$J = \frac{1}{2} \int_0^\infty \left[ q_\beta (\beta^* - \hat{\beta})^2 + q_\gamma (\gamma^* - \hat{\gamma})^2 + q_N (N_z^*)^2 \right] dt \quad (4.25)$$

In (4.25), the weighting factors  $q_\beta, q_\gamma$ , and  $q_N$  are chosen by the size of state and control input limitation. Because there is only yaw moment for controlling two states, there is a “trade-off” between sideslip angle control and yaw rate control. Under low friction road, sideslip angle is very sensitive to the stability of vehicle. Therefore, sideslip angle is given bigger weight factor at low friction road. In contrast, at high friction road, yaw rate is given bigger weight factor.

### 4.2.3 Torque distribution to in-wheel motors

Electric vehicle COMS has two rear in-wheel motors. The torque command to rear in-wheel motors are calculated by the following equation:

$$\begin{bmatrix} T_{rl}^* \\ T_{rr}^* \end{bmatrix} = R_w \begin{bmatrix} \frac{1}{2} & \frac{-1}{d_r} \\ \frac{1}{2} & \frac{1}{d_r} \end{bmatrix} \begin{bmatrix} T_{ACC} \\ R_w N_z^* \end{bmatrix} \quad (4.26)$$

Where  $R_w$  is the radius of wheel, and  $T_{ACC}$  is the acceleration command given by the driver.

In order to prevent the wheel slip which may be very serious on low friction road, model following control (MFC) is apply for controlling the wheel torque command [33]. The configuration of wheel torque control by MFC is shown in Fig 4.2.  $J_n$  is the zero-slip nominal model which is designed as:

$$J_n = J_w + mR_w^2 \quad (4.27)$$

In the above equation,  $J_w$  is the moment of inertia of the wheel. By using the control

configuration in Fig 4.2, when wheel slip occurs, wheel torque command will be reduced in order to induce re-adhesion. Therefore, the stability of vehicle motion is enhanced. On low friction road ( $\mu = 0.2$ ), the driver accelerates the vehicle with very high and fast torque command. In case of without control, the wheel velocity becomes very high which means slip occurs (Fig 4.3). If MFC is applied, the motor torque is decreased if it reaches the limitation. As a result, the wheel velocity is reduced considerably (Fig 4.4).

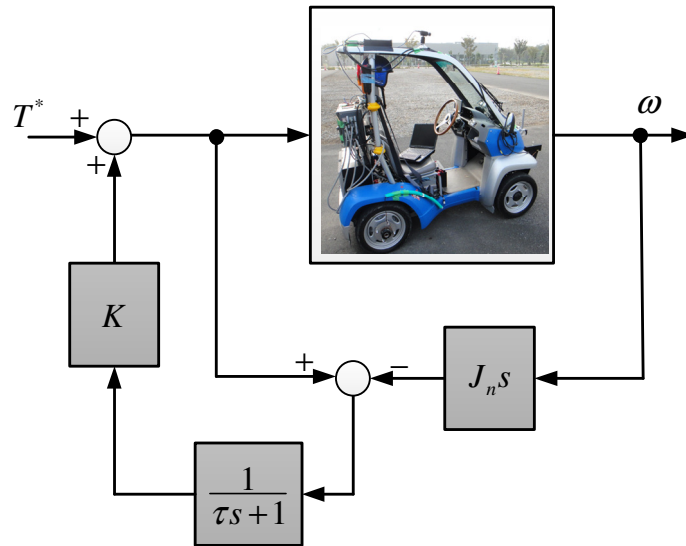


Fig 4.2 MFC of in-wheel motor's torque for slip prevention

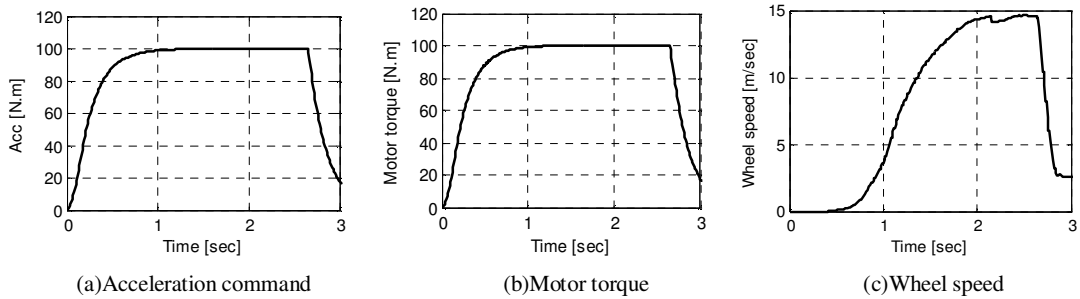


Fig 4.3 Experiment results on low friction road (without MFC)

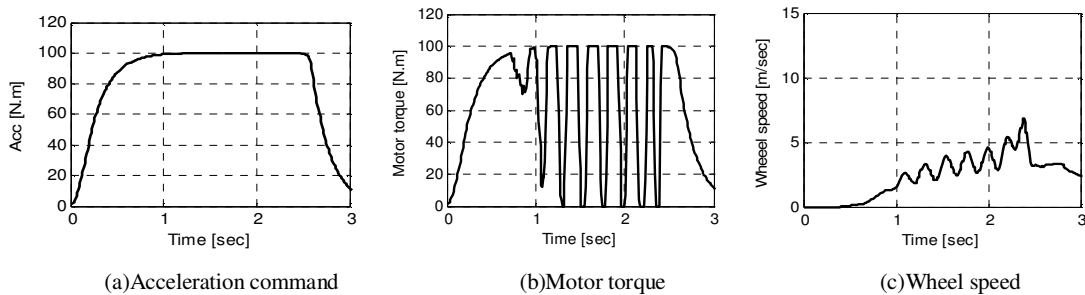
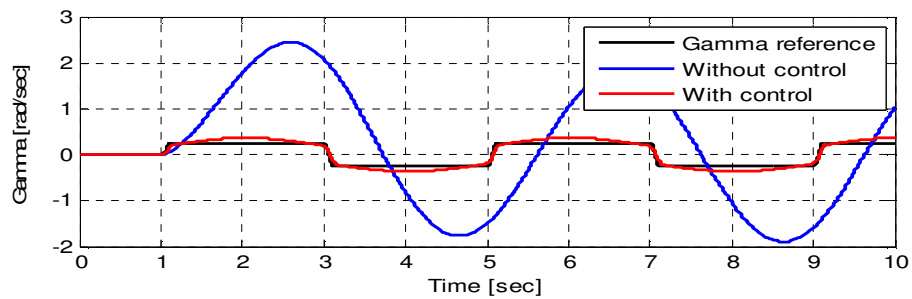


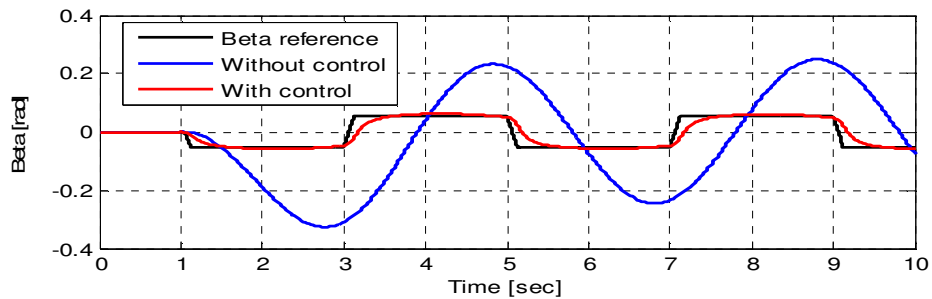
Fig 4.4 Experiment results of MFC on low friction road

#### 4.2.4 Simulation results

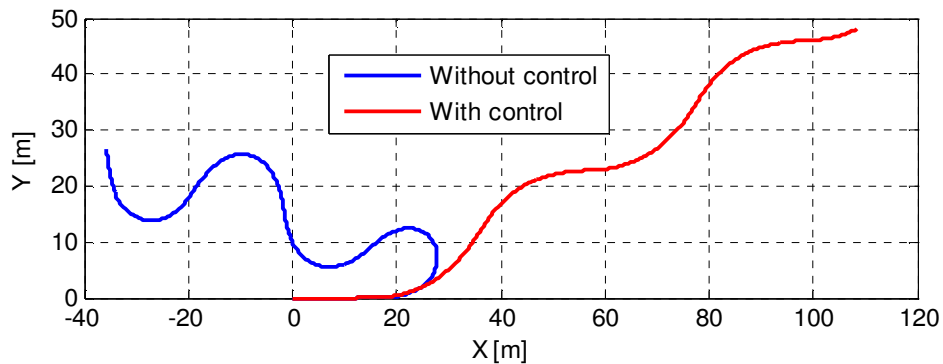
Electric vehicle COMS is designed to run at the maximum speed of 50 kph. At high speed, during the lane-changing or cornering, if sideslip angle is not controlled, vehicle may lose its stability. On low friction road ( $\mu=0.3$ ), vehicle runs at 48 kph and starts lane-changing from 1 second. Simulation results are shown in Fig 4.5. In case of without control, the vehicle motion is unstable as the yaw rate and sideslip angle response comes to a big value. As a result, the vehicle cannot follow the desired path. In case the stability control system is applied, the yaw rate and sideslip angle response is closed to the reference value. In this case, the vehicle can follow the desired path of lane-change. This simulation test proves that by using yaw moment control based sideslip angle estimation, the stability and safety of vehicle motion is maintained.



(a) Yaw rate response



(b) Sideslip angle response



(d) Vehicle trajectory

Fig 4.5 Simulation results of vehicle stability control on low friction road

### 4.2.5 Experiment results

Cornering test is conducted on high friction road at the speed of 20 kph in two cases, the first is without any control and the second case is with direct yaw moment control. As can be seen in Fig 4.6, the response of yaw rate cannot track with the reference value. The response of sideslip angle is even bigger than the reference value. In contrast, when the yaw moment control is applied (Fig 4.7), the yaw rate and sideslip angle can follow the desired values. Because only yaw moment is used for controlling two states, perfect tracking to the desired values cannot be achieved. However, the errors between the responses and desired values are reduced remarkably. The experiment results show the effect of the control method and the enhancement of vehicle stability.

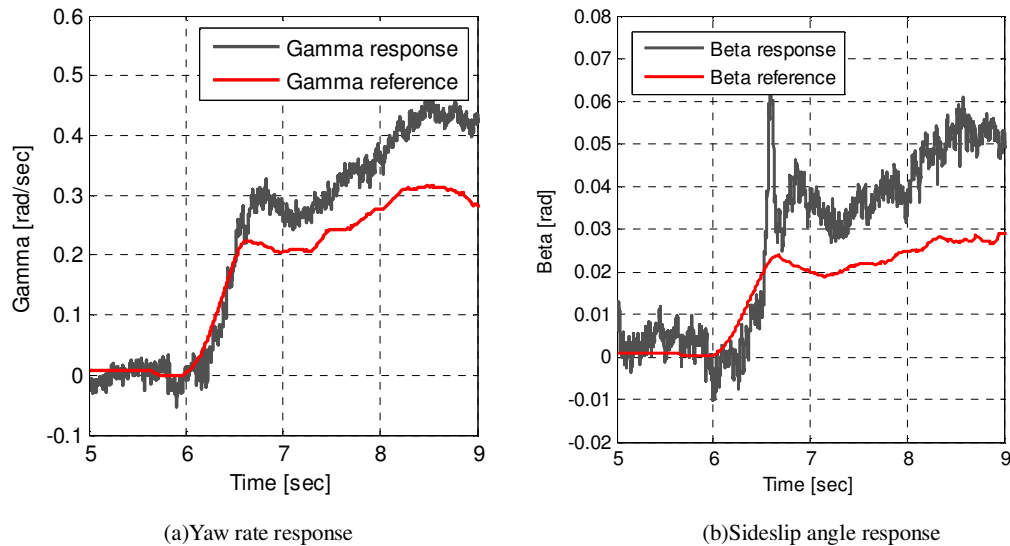


Fig 4.6 Experiment results of without control case

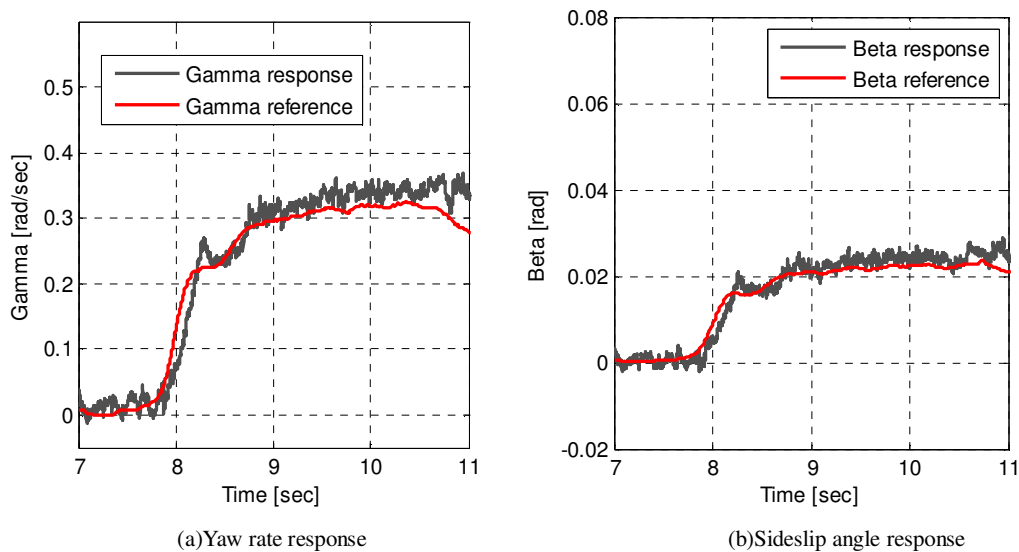


Fig 4.7 Experiment results of with control case

### **4.3 Chapter summary**

In this chapter, the vehicle stability control system by direct yaw moment control and sideslip angle estimation using GPS is proposed. Simulations and experiments are conducted to evaluate the proposed configuration. Due to the limitation of experiment space and safety condition at the campus, we have not conducted experiment at critical driving condition such as low friction road and high speed. Even though, experiments can show the effect of the control system in somehow

## **Special part: Research on tire lateral force sensor**

### **1. Introduction**

The special part presents the research on application of lateral tire force sensors in estimation of tire cornering stiffness and sideslip angle. The novel multi sensing hub unit bearing developed by NSK Ltd. can be installed at each wheel to provide the measurement of lateral tire force sensor. The multi-forgetting factor method in [39] is applied for identification design. Electric vehicle Kanon is used as experimental vehicle in the special part.

Firstly, considering the difference between left and right side lateral tire forces, on-line identification of tire cornering stiffness without sideslip angle is designed. In [34], the lateral tire force sensors were used for an advanced method of sideslip angle estimation without cornering stiffness. The idea is to utilize the difference between the left and right side lateral tire force to construct the identification of sideslip angle by least square algorithm. However, the authors of [34] did not consider the load transfer which has effect to lateral tire force characteristics. The authors also used the linear equation in (2.4) and (2.5) to design the identification. In fact, as analyzing in chapter 2, the tire characteristics contain both linear and non-linear region. In order to overcome such limitations of the original idea, the empirical second order model in (2.2) is chosen for estimation design. Moreover, the influence of load transfer and nonlinear part of tire lateral force can be compensated by considering them as a disturbance term to be estimated.

Finally, the special part proposes the two-input two-output (TITO) control of electric vehicle stability system. Two inputs are selected as the front steering angle and yaw moment generated by in-wheel motors. Simulations are conducted in order to verify the high robustness of the proposed method in comparison with conventional decoupling control.

### **2. Experimental vehicle**

The experimental electric vehicle Kanon is a four-in-wheel motored vehicle which is powered by the lithium-iron type batteries. In order to measure the tire lateral force, at each wheel, multi sensing hub unit bearing developed by NSK Ltd. is attached. Fig. 1 shows the photo of experimental vehicle and tire lateral force sensor. AutoBox DS1103 is used as the controller to collect sensor measurement for cornering stiffness identification. The optical sensor produced by Corrsys-Datron is used to measure sideslip angle. Several parameters of the experimental vehicle can be seen in Table 1. The measurement of the front left and front right lateral tire forces are shown in Fig. 2 for two experiment modes: cornering test and lane-change test.

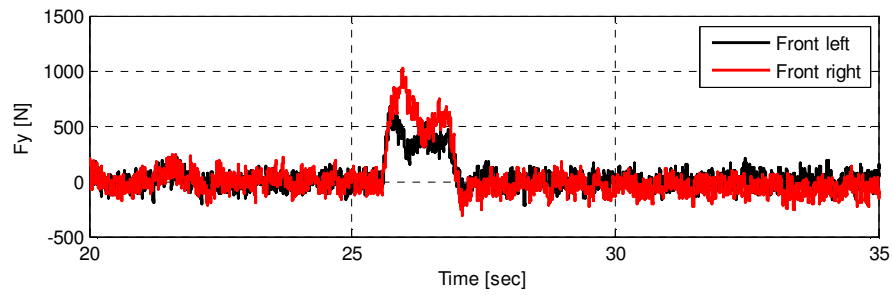




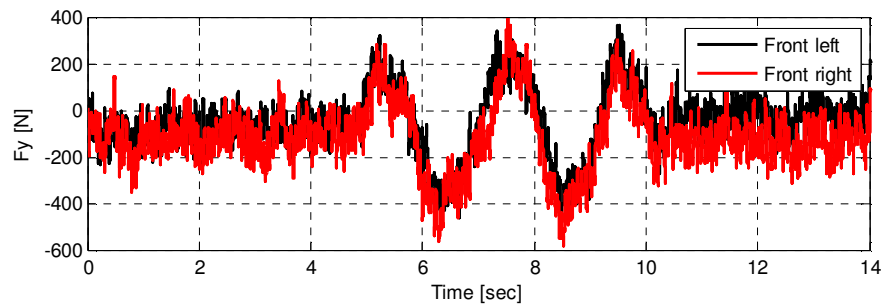
Fig. 1 Experimental electric vehicle Kanon and tire lateral force sensor

Table 1: Parameters of electric vehicle Kanon.

Parameter	Value
Total mass of vehicle	$m = 875 \text{ kg}$
Yaw moment of inertia	$I_z = 617 \text{ Nm/(rad/s}^2\text{)}$
Distance from CG to front axle	$l_f = 1.013\text{m}$
Distance from CG to rear axle	$l_r = 0.702\text{m}$
Front cornering stiffness (Asphalt)	$C_f = 11000 \text{ N/rad}$
Rear cornering stiffness (Asphalt)	$C_r = 32000 \text{ N/rad}$



(a)Cornering test



(b)Lane-change test

Fig. 2 Tire lateral force measurement

### 3. Single and multi forgetting factor identification

Recursive least square (RLS) is a well-known method for identification design [38]. The key of this method is the decision of the forgetting factor  $0 < \lambda \leq 1$ . It operates as a weight which diminishes for the old data. The cost function with forgetting factor is expressed as following in which older data is gradually discarded in favor or more recent information.

$$V(\hat{\theta}, k) = \frac{1}{2} \sum_{i=1}^k \lambda^{k-i} [y(i) - \varphi^T(i) \hat{\theta}(k)]^2 \quad (1)$$

The single forgetting factor identification equations are design with the update of covariance matrix  $P(k)$  and the identification gain  $L(k)$ :

$$\hat{\theta}(k) = \hat{\theta}(k-1) + L(k) [y(k) - \varphi^T(k) \hat{\theta}(k-1)] \quad (2)$$

$$P(k) = [I - L(k) \varphi^T(k)] P(k-1) \frac{1}{\lambda} \quad (3)$$

$$L(k) = P(k-1) \varphi(k) [\lambda + \varphi^T(k) P(k-1) \varphi(k)]^{-1} \quad (4)$$

There are cases of identification such that the incoming information is not uniformly distributed in the parameter space, or the convergence rate of each parameter is different to the other. In such cases, single forgetting factor RLS may be unsuitable. Therefore, multi-forgetting factor method was proposed and well applied in identification of vehicle mass and road grade [39]. Here, considering the case that there are two parameters but only one equation is known for identification. If two forgetting factor is used, we will have more degrees of freedom for turning the estimator:

$$\begin{bmatrix} \hat{\theta}_1(k) \\ \hat{\theta}_2(k) \end{bmatrix} = \begin{bmatrix} 1 & L_1(k) \varphi_2(k) \\ L_2(k) \varphi_1(k) & 1 \end{bmatrix}^{-1} \begin{bmatrix} \hat{\theta}_1(k-1) + L_1(k) [y(k) - \varphi_1(k) \hat{\theta}_1(k-1)] \\ \hat{\theta}_2(k-1) + L_2(k) [y(k) - \varphi_2(k) \hat{\theta}_2(k-1)] \end{bmatrix} \quad (5)$$

$$L_1(k) = P_1(k-1) \varphi_1(k) [\lambda_1 + \varphi_1^T(k) P_1(k-1) \varphi_1(k)]^{-1} \quad (6)$$

$$P_1(k) = [I - L_1(k) \varphi_1^T(k)] P_1(k-1) \frac{1}{\lambda_1} \quad (7)$$

$$L_2(k) = P_2(k-1) \varphi_2(k) [\lambda_2 + \varphi_2^T(k) P_2(k-1) \varphi_2(k)]^{-1} \quad (8)$$

$$P_2(k) = [I - L_2(k) \varphi_2^T(k)] P_2(k-1) \frac{1}{\lambda_2} \quad (9)$$

The equations (5) to (9) can be reorganized with the new identification gain:

$$L(k) = \frac{1}{1 + \frac{P_1(k) \varphi_1(k)^2}{\lambda_1} + \frac{P_2(k) \varphi_2(k)^2}{\lambda_2}} \begin{bmatrix} \frac{P_1(k) \varphi_1(k)}{\lambda_1} \\ \frac{P_2(k) \varphi_2(k)}{\lambda_2} \end{bmatrix} \quad (10)$$

#### 4. Cornering stiffness identification using tire lateral force sensors

Based on the discussion in chapter 2, cornering stiffness is one parameter which can change according to tire slip angle and road condition. It is very important to understand the cornering stiffness in order to construct the linear bicycle model and. Based on the understanding of cornering stiffness, we can analyze the performance of vehicle dynamics [37]. Moreover, on-line identification of cornering stiffness is applicable for vehicle control system, such as exactly estimation of sideslip angle [14] or improving the active steering control [35].

If sideslip angle is measured, cornering stiffness can be estimated directly. However, as mentioned in chapter 1, sideslip angle sensor is very expensive to be used as a practical method. Therefore, identification of cornering stiffness is required for vehicle control system. A method of cornering stiffness identification was proposed by Fujimoto *et al* [36]. As shown in Fig. 3, the cornering stiffness identification works simultaneously with a linear observer of sideslip angle.

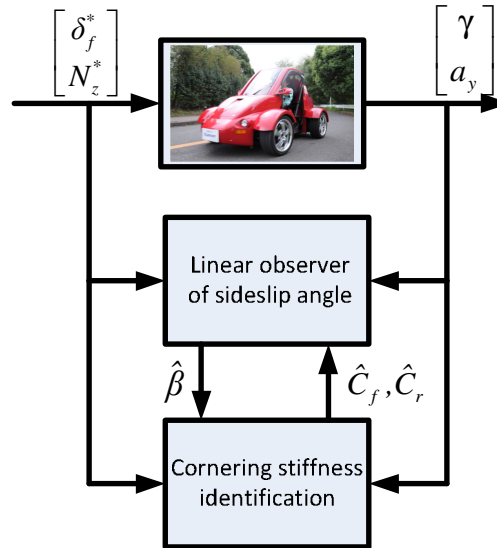


Fig. 3 On-line identification of cornering stiffness by “with-beta” method

The design of robust observer gain matrix of linear observer in Fig. 3 is presented in [9] by pole placement. The identification gets estimated value of sideslip angle, and gives back the identified value of front and rear cornering stiffness. In this thesis, this method is named “with-beta”. The closed loop between observer and identification make up the complicated structure of with beta method. Moreover, the followings are disadvantages of with-beta method: 1) Sideslip angle observer needs convergence time to true value. This will introduce a delay to cornering stiffness identification. 2) The accuracy of identification depends on the accuracy of observer, and vice versa.

##### 4.1 Beta-less identification of cornering stiffness

Using the measurement of tire lateral force, this thesis introduces a new method of cornering stiffness identification without the estimation or measurement of sideslip angle. Firstly, we define two parameters:

$$\begin{bmatrix} X_1 \\ X_2 \end{bmatrix} = \begin{bmatrix} C_f \\ C_r \\ C_f \end{bmatrix} \quad (11)$$

Based on (2.4), (2.5), (2.6), and (2.7)  $X_1$  and  $X_2$  can be identified using the following equations:

$$F_y^{fl} + F_y^{fr} = (F_y^{rl} + F_y^{rr})X_1 + 2\left(\delta_f - \frac{l_f + l_r}{v_x}\gamma\right)X_2 \quad (12)$$

$$\left(v_x + \frac{d_f}{2}\gamma\right)F_y^{fr} - \left(v_x - \frac{d_f}{2}\gamma\right)F_y^{fl} = d_f\gamma\delta_f X_2 \quad (13)$$

Combining (12) and (13), identification equation is constructed as follows:

$$y(t) = \varphi^T(t)X(t) \quad (14)$$

Where

$$y(t) = \begin{bmatrix} F_y^{fl} + F_y^{fr} \\ \left(v_x + \frac{d_f}{2}\gamma\right)F_y^{fr} - \left(v_x - \frac{d_f}{2}\gamma\right)F_y^{fl} \end{bmatrix} \quad (15)$$

$$\varphi^T(t) = \begin{bmatrix} F_y^{rl} + F_y^{rr} & 2\left(\delta_f - \frac{l_f + l_r}{v_x}\gamma\right) \\ 0 & d_f\gamma\delta_f \end{bmatrix} \quad (16)$$

$$X = \begin{bmatrix} X_1 \\ X_2 \end{bmatrix} \quad (17)$$

Cornering stiffness can be achieved from the identification of  $X_1$  and  $X_2$ . Here we notice that the parameter  $X_1$  is almost stable because it is the ratio of the front and rear cornering stiffness. In contrast, the parameter  $X_2$  may frequently change due to the road condition variation. Therefore, we apply the multi-forgetting factor method for identification. The forgetting factor  $\lambda_1$  is set closed to 1 while  $\lambda_2$  is set as a smaller value. This mean the old and new information are treated almost equally for  $X_1$ .

## 4.2 Experimental verification

Using measurement of tire lateral force and tire slip angle (calculated from sideslip angle measurement), the tire cornering stiffness of electric vehicle Kanon on asphalt road are obtained and shown in Table 1. Both “with-beta” and “beta-less” identification are conducted for comparison. In experiment, assume that the cornering stiffness is unknown. In order to verify the convergence of each estimation method to the real cornering stiffness, the initial value is set closed to zero. The results of cornering test are shown in Fig. 4 in which part (b) and (c) show the measurement of front and rear tire cornering stiffness. Part (d) shows the estimation of sideslip angle by the configuration in Fig. 3. It is clear that the estimation of sideslip angle has off-set in comparison with the true value measured by optical sensor. As the result, the with-beta method cannot converge to the true value of cornering stiffness, as can be seen in part (e) and (f). In contrast, the beta-less method can converge to the true

value of cornering stiffness with much smaller variation. Based on the experiment results, we propose that beta-less identification by using tire force sensor is an effective method for real time identification of cornering stiffness.

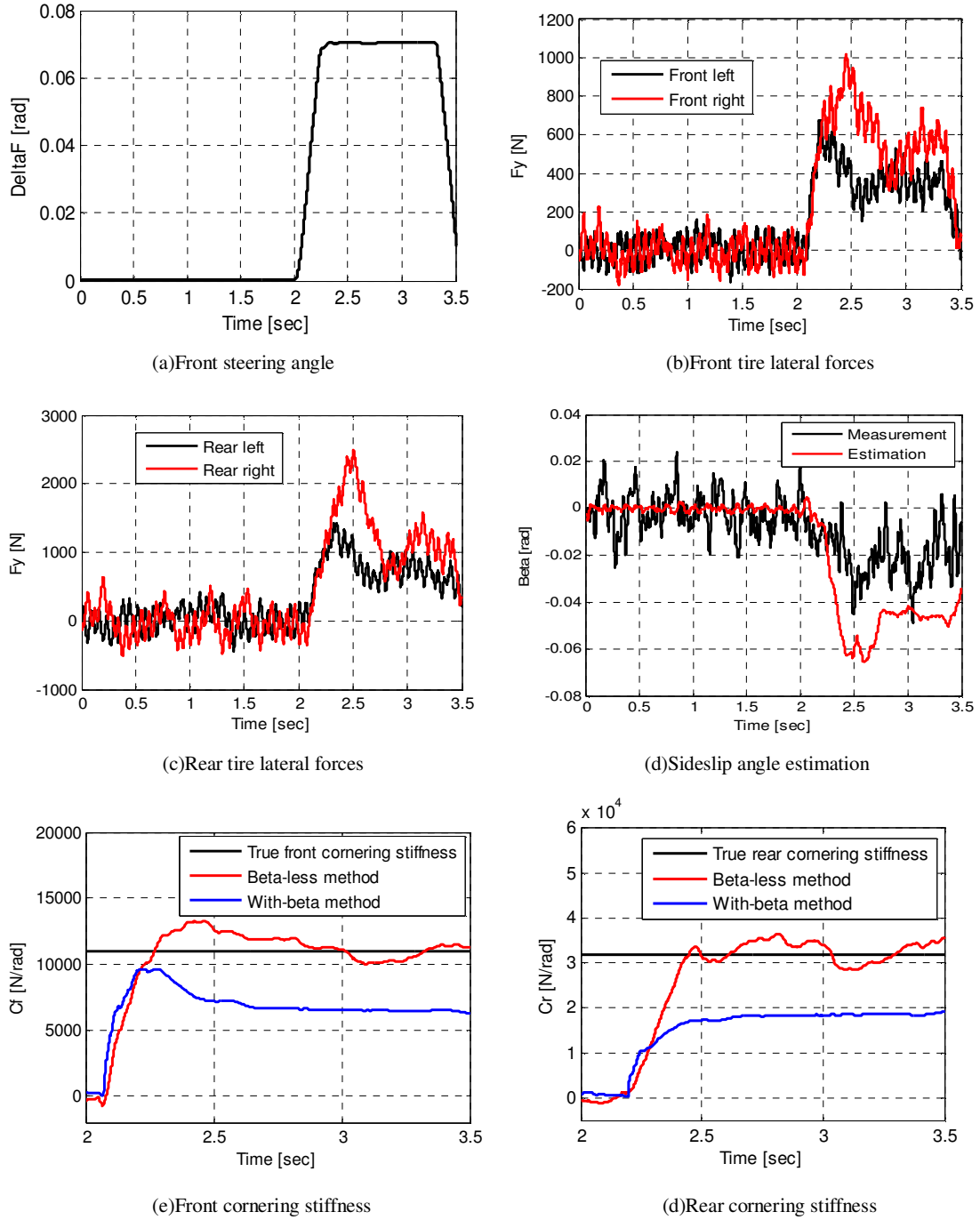


Fig. 4 Experiment results of cornering stiffness identification

## 5. Sideslip angle estimation using tire lateral force sensors

### 5.1 Design of sideslip angle identification

In order to model the non-linear characteristic of tire lateral force, the following model is often applied:

$$\begin{cases} F_y = F_y^1 [1 + f(F_y^1, \mu F_z)] \\ F_y^1 = C\alpha \end{cases} \quad (18)$$

Where  $F_y^1$  is the first order term, and  $f(F_y^1, \mu F_z)$  is the higher order function which captures the load transfer and the limitation of tire force due to road friction coefficient. For instance, in [ ], Abe proposes the two order model of tire lateral force:

$$\begin{cases} F_y = F_y^1 - \frac{(F_y^1)^2}{4\mu F_z} \\ F_y^1 = C\alpha \end{cases} \quad (19)$$

If we consider the nonlinear part of tire lateral force is the unknown disturbance term  $D = \frac{(F_y^1)^2}{4\mu F_z}$  can, we can write down the following equation:

$$F_y - D = C\alpha \quad (20)$$

The front left and front right tire lateral force can be expressed as:

$$\begin{cases} F_y^{fl} - D^{fl} = -C_f \left( \frac{V\beta + l_f \gamma}{v_x - \frac{d_f}{2} \gamma} - \delta_f \right) \\ F_y^{fr} - D^{fr} = -C_f \left( \frac{V\beta + l_f \gamma}{v_x + \frac{d_f}{2} \gamma} - \delta_f \right) \end{cases} \quad (21)$$

From (21), sideslip angle can be calculated without cornering stiffness:

$$\beta = \beta_1 + \beta_2 \quad (22)$$

$$\beta_1 = \frac{\delta_f \left[ (F_y^{fl} - D^{fl}) \left( v_x - d_f \frac{\gamma}{2} \right) - (F_y^{fr} - D^{fr}) \left( v_x + d_f \frac{\gamma}{2} \right) \right]}{v_x \left[ (F_y^{fl} - D^{fl}) - (F_y^{fr} - D^{fr}) \right]} \quad (23)$$

$$\beta_2 = -\frac{l_f \gamma}{v_x} \quad (24)$$

Two RLS identifications are designed for  $\hat{\beta}_1$  and  $\hat{\beta}_2$ .  $\hat{\beta}_2$  can be identified easily using single

forgetting factor method based on the measurement of yaw rate and vehicle velocity. In case of  $\hat{\beta}_1$  identification, the following identification is proposed:

$$y = [\varphi_1 \quad \varphi_2] \begin{bmatrix} \theta_1 \\ \theta_2 \end{bmatrix} \quad (25)$$

$$y = \delta_f \left[ F_y^{fl} \left( v_x - d_f \frac{\gamma}{2} \right) - F_y^{fr} \left( v_x + d_f \frac{\gamma}{2} \right) \right] \quad (26)$$

$$\varphi_1 = v_x (F_y^{fl} - F_y^{fr}) \quad (27)$$

$$\varphi_2 = v_x \quad (28)$$

$$\theta_1 = \beta_1 \quad (29)$$

$$\theta_2 = (D^{fr} - D^{fl}) \beta_1 + \delta_f \left[ D^{fl} \left( 1 - d_f \frac{\gamma}{2v_x} \right) - D^{fr} \left( 1 + d_f \frac{\gamma}{2v_x} \right) \right] \quad (30)$$

As shown in (30), all the disturbance term is combined in the parameter  $\theta_2$ . If the lateral acceleration is small, the disturbance term and the parameter  $\theta_2$  are also small. In this case, almost the information is distributed to the parameter  $\theta_1$ . In contrast, at high lateral acceleration, the disturbance term and the parameter  $\theta_2$  will increase. Therefore, the following adaptive law is applied for multi-forgetting factor identification:

- The forgetting factor is chosen such that  $\lambda_1 < \lambda_2$ , this mean more information is distributed to  $\theta_1$ .
- If lateral acceleration is small ( $a_y < a_y^*$ ):  $\lambda_2$  is set as a big value ( $\lambda_2 \approx 1$ ).
- If lateral acceleration is large ( $a_y \geq a_y^*$ ):  $\lambda_2$  is reduced to a smaller value.

In this research,  $a_y^* = 0.3g$  (30% of gravity) is chosen for experiment.

Two identifications are designed for two local of lateral acceleration (small and large). Based on the measurement of lateral acceleration, two models are weighted, and the sideslip angle can be estimated by the following equation:

$$\hat{\beta}_1 = \hat{\beta}_{1l} w_l + \hat{\beta}_{1n} w_n \quad (31)$$

The configuration of sideslip angle estimation using tire lateral force sensors is shown in Fig. 5. Local model 1 will dominate the identification of at small lateral acceleration. In contrast, at large lateral acceleration, local model 2 is weighted much more.

## 5.2 Experimental verification

Experiments are conducted with electric vehicle Kanon and multi sensing hub units for measurement of tire lateral forces. Two cases of experiment, lane-change test and cornering test are demonstrated as followings. The linear observer in [9] is also performed for comparison.

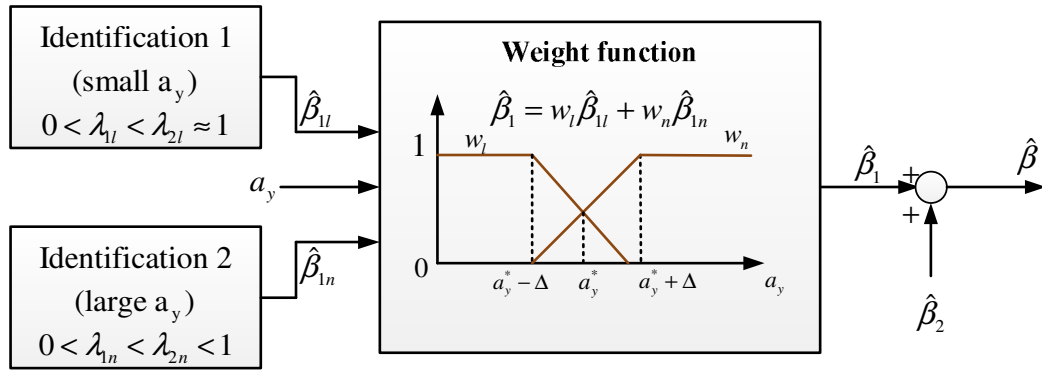
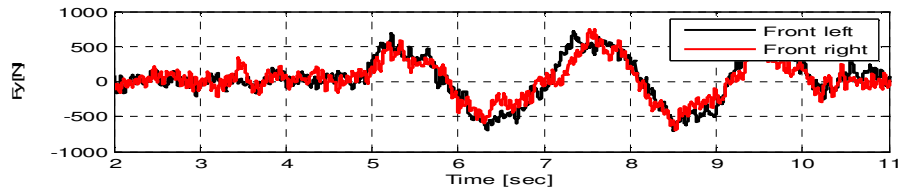
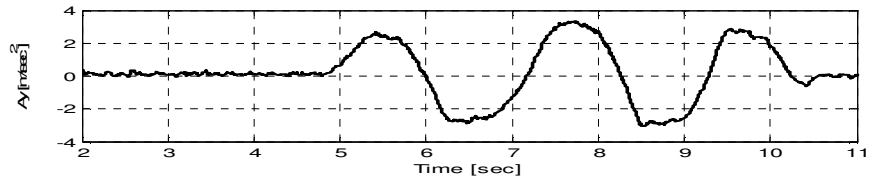


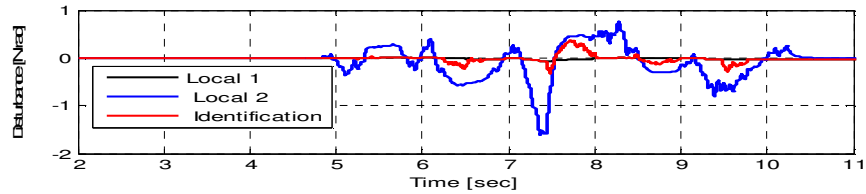
Fig. 5 Configuration of sideslip angle identification using tire lateral force sensors



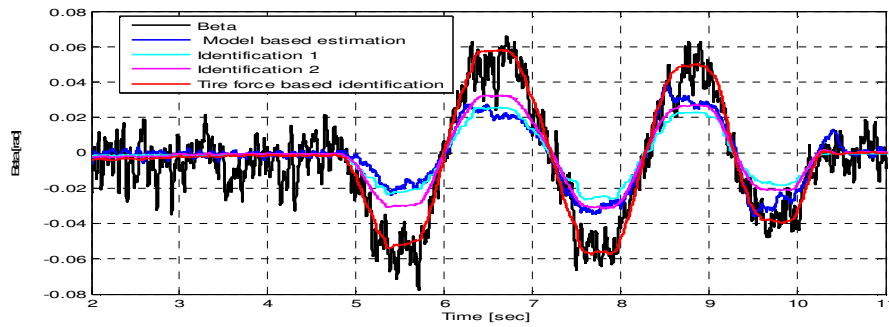
(a) Tire lateral force measurement



(b) Lateral acceleration



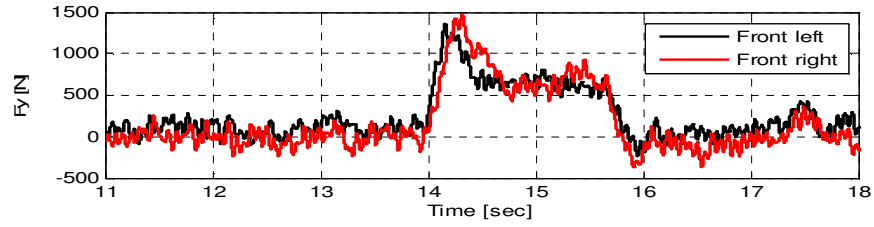
(c) Disturbance term  $\theta_2$



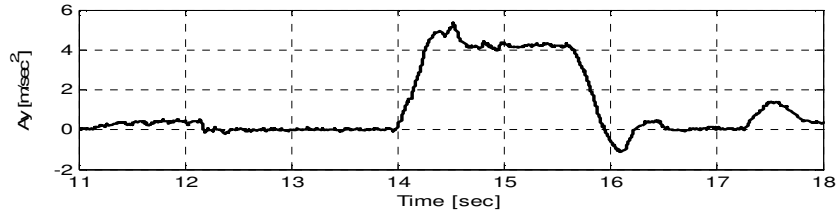
(d) Sideslip angle estimation

Fig. 6 Experiment results of lane-change test

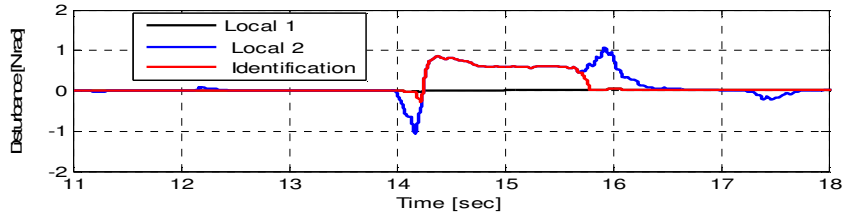




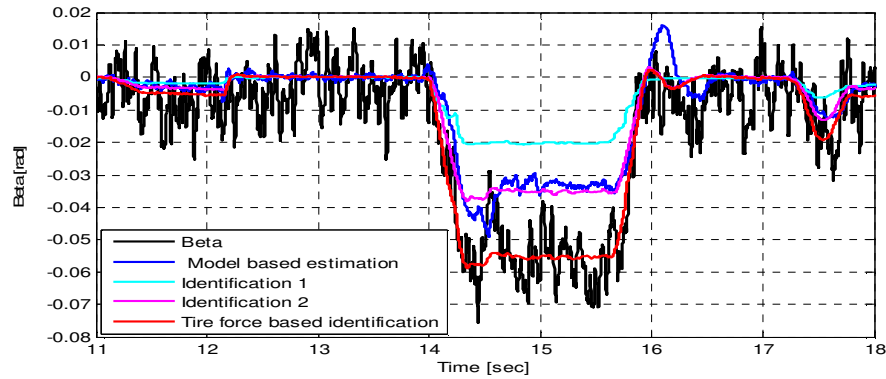
(a) Tire lateral force measurement



(b) Lateral acceleration



(c) Disturbance term  $\theta_2$



(d) Sideslip angle estimation

Fig. 7 Experiment results of cornering test

Experiment results of lane-change test are shown in Fig. 6. The measurement of the front left and front right tire lateral forces and lateral acceleration are shown in Fig. 6 (a) and (b), respectively. The identification of disturbance term is shown in Fig. 6 (c). In Fig. 6 (d), the black line is the measurement of sideslip angle by optical sensor produced by Corrsys-Datron. The red line is the identification of sideslip angle by the proposed method. This is the combination of two estimated values obtained from identification 1 and 2. The blue line is the sideslip angle by linear observer. Here,

a big model error is introduced to the linear observer. The cornering stiffness of the model based linear observer is reduced 50% of its true value in Table 1. As a result, the linear observer cannot match with real value of sideslip angle. In contrast, the proposed method does not rely on cornering stiffness. Moreover, by introducing the disturbance term to be estimated, the load transfer or the non-linear tire force due to friction limit circle can be compensated. The proposed method has the remarkable estimation accuracy in comparison with the linear observer method.

The other case of cornering-test is shown in Fig. 7. A model error of 50% value of real cornering stiffness is also introduced to the linear observer. As the lane-change test, the proposed method can match the real sideslip angle from sensor while the linear observer has a large “off-set”. Based on the experiment results, we propose the sideslip angle estimation using tire lateral force sensor for vehicle stability control system.

## 6. Electric vehicle stability based on two-input two-output control

### 6.1 Two-input two-output control configuration

In the previous section, only yaw moment is selected for stabilizing lateral motion of electric vehicle. However, this one-input two-output control system faces with the problem that is the trade-off between two controlled states. In order to enhance the stability of electric vehicle, another control input is introduced: the active steering. The active steering system driven by electric motor can adjust the steering angle input by driver. The photo of active steering system is shown in Fig. 8.

Decoupling method is usually applied for two-input two-output (TITO) control system [40]. The decoupling control configuration applied for electric vehicle stability system is shown in Fig. 9. In which, sideslip angle is controlled by front steering angle while yaw rate is controlled by yaw moment generated by in-wheel motors. The decoupling terms  $D_{11}$  and  $D_{22}$  are chosen as 1, while  $D_{12}$  and  $D_{21}$  are calculated by the following equation:

$$\begin{cases} D_{12}G_{11} + G_{12} = 0 \\ D_{21}G_{22} + G_{21} = 0 \end{cases} \Leftrightarrow \begin{cases} D_{12} = -\frac{G_{12}}{G_{11}} = -\frac{b_{22}a_{12}}{b_{11}s + b_{21}a_{12} - b_{11}a_{22}} \\ D_{21} = -\frac{G_{21}}{G_{22}} = -\frac{b_{21}s + b_{11}a_{21} - b_{21}a_{11}}{b_2s - b_2a_{11}} \end{cases} \quad (32)$$

Assume that the decoupling terms follow the parameter variation of the real vehicle; we draw the step response of the decoupling terms at different vehicle velocity and different road condition. The model of electric vehicle Kanon is chosen for examining in this section. Fig. 10 shows that  $D_{21}$  is very stable to the change of vehicle velocity. The step response of  $D_{21}$  changes not too much under road friction variation. In contrast, in Fig. 11, the step response of  $D_{12}$  considerably changes due to the variation of both vehicle velocity and road friction. In fact, constant nominal parameters are chosen to design the controller including the decoupling terms. The step response analysis shows that the fixed decoupling term  $D_{21}$  is more robust than  $D_{12}$ . This means, if we utilized the decoupling control system in Fig. 9, yaw rate control channel is much more robust than sideslip angle control channel.

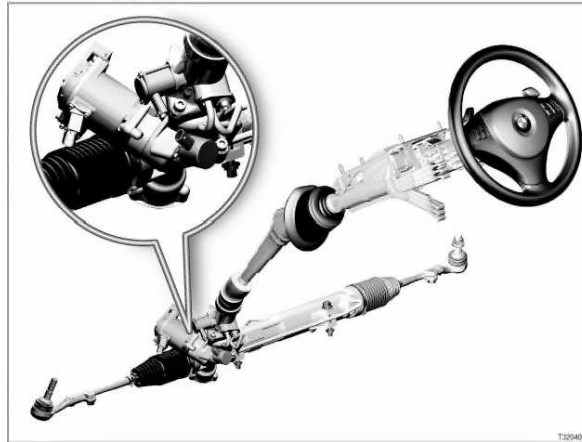


Fig. 8 Active steering system produced by BMW

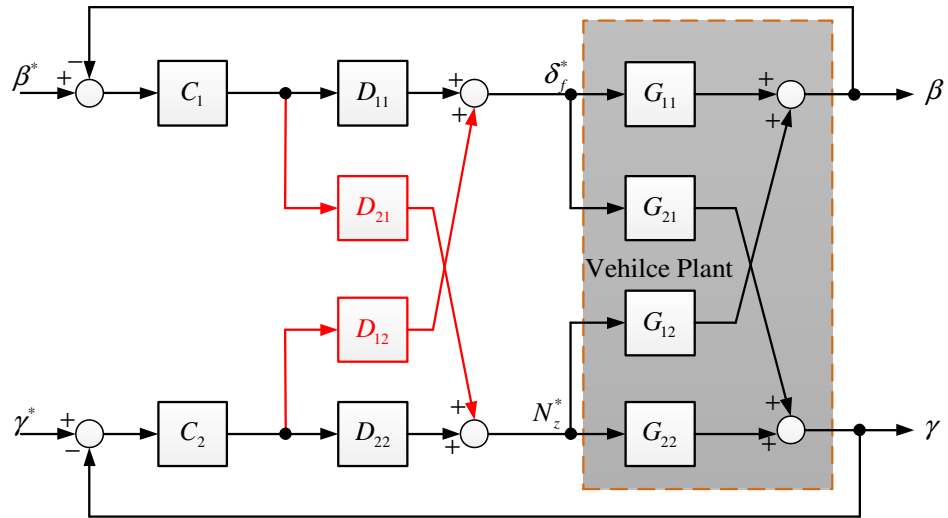
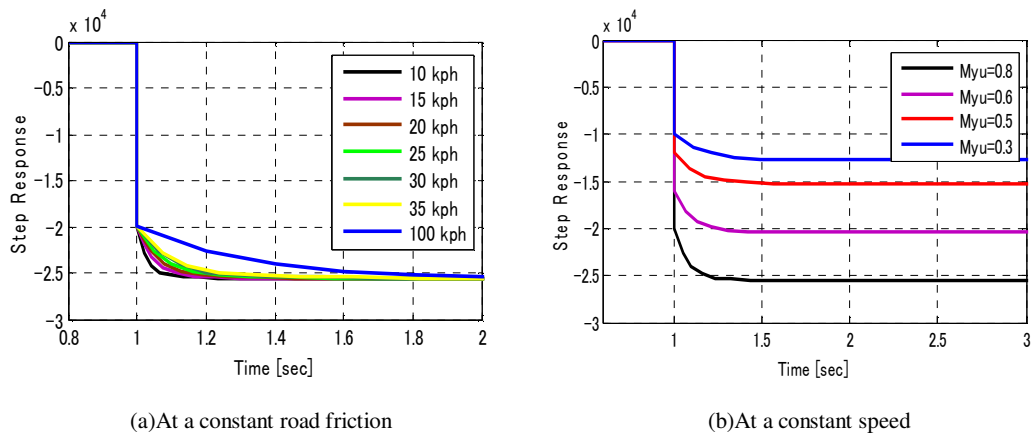


Fig. 9 Decoupling control system



(a) At a constant road friction

(b) At a constant speed

Fig. 10 Step response of decoupling term  $D_{21}$

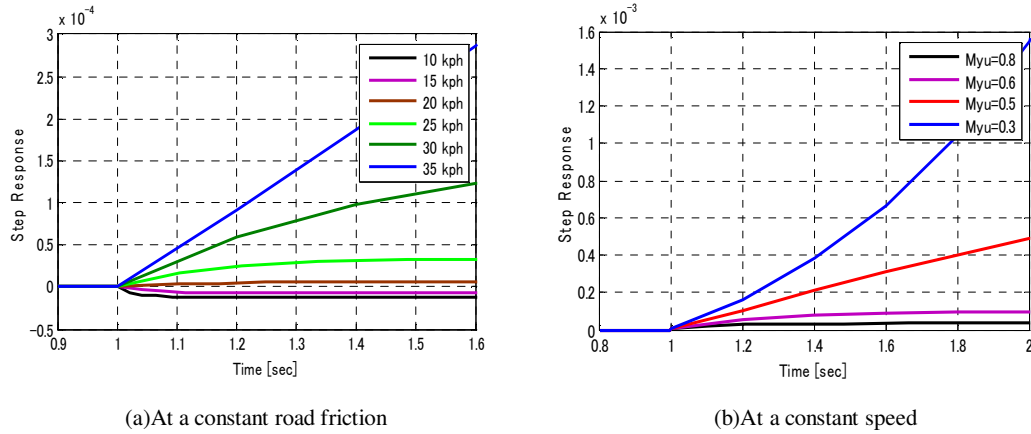
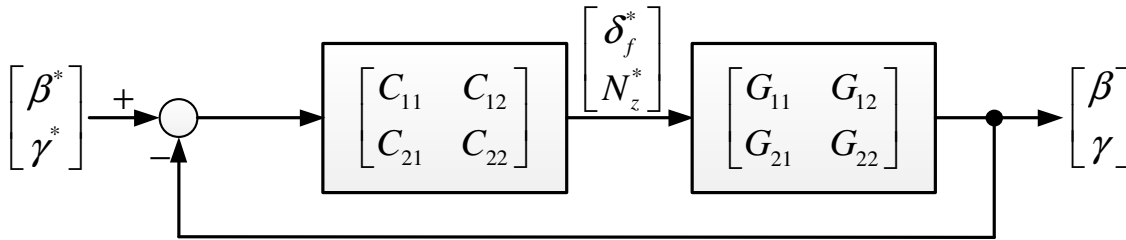

 Fig. 11 Step response of decoupling term  $D_{12}$ 


Fig. 12 Two-input two-output controller of vehicle stability system

In this section, a feedback TITO control configuration without any decoupling term is proposed. The desired model is expressed as the followings:

$$\begin{bmatrix} \beta \\ \gamma \end{bmatrix} = \begin{bmatrix} \frac{K}{s+K} & 0 \\ 0 & \frac{K}{s+K} \end{bmatrix} \begin{bmatrix} \beta^* \\ \gamma^* \end{bmatrix} \quad (33)$$

In the following calculation,  $G$  is the matrix of vehicle model and  $C$  is matrix of TITO controller. The matrix of controller must satisfy the following equation:

$$(I + GC)^{-1} GC = \begin{bmatrix} \frac{K}{s+K} & 0 \\ 0 & \frac{K}{s+K} \end{bmatrix} \Leftrightarrow C = G^{-1} \begin{bmatrix} \frac{K}{s+K} & 0 \\ 0 & \frac{K}{s+K} \end{bmatrix}^{-1} \left( I - \begin{bmatrix} \frac{K}{s+K} & 0 \\ 0 & \frac{K}{s+K} \end{bmatrix} \right)^{-1} \quad (34)$$

From (33) and (34), the controller  $C$  is designed as:

$$C = \begin{bmatrix} \frac{b_{22}s - b_{22}a_{11}}{b_{22}b_{11}} \frac{K}{s} & \frac{-b_{22}a_{12}}{b_{22}b_{11}} \frac{K}{s} \\ \frac{-b_{21}s - b_{11}a_{21} + b_{21}a_{11}}{b_{22}b_{11}} \frac{K}{s} & \frac{b_{11}s + b_{21}a_{12} - b_{11}a_{22}}{b_{22}b_{11}} \frac{K}{s} \end{bmatrix} = \begin{bmatrix} C_{11} & C_{12} \\ C_{21} & C_{22} \end{bmatrix} \quad (35)$$

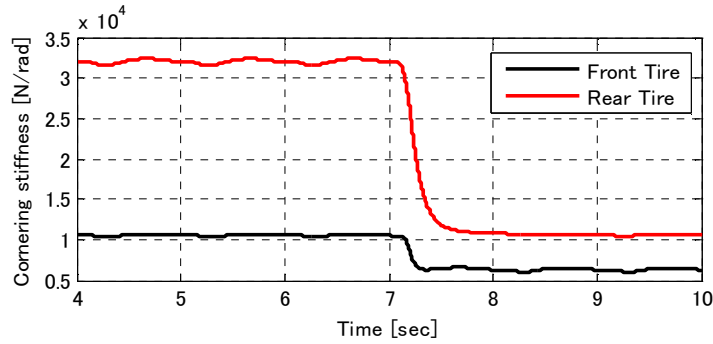
From (35), the proposed controller shown in Fig. 12 has the form of two-input two-output PI

controller. Vector state  $[\beta \ \gamma]^T$  is controlled by the vector input  $[\delta_f \ N_z]$ . In other words, the decoupling terms does not exist in the proposed configuration.

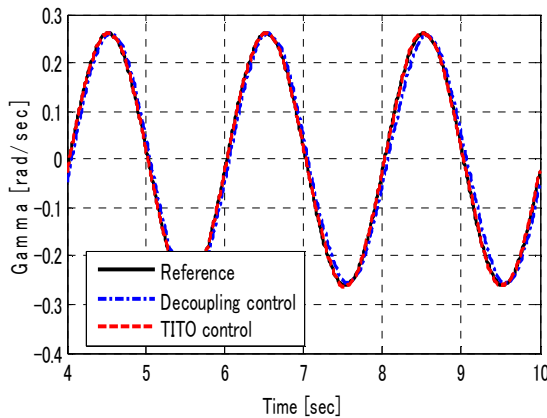
### 6.2 Simulation evaluation of two-input two-output control configuration

It is very important for the controller to be robust over the variation of road condition. Thus, the following simulation will be performed to test the vehicle running on sinusoidal trajectory and suddenly entering the low friction road from high friction road. Two methods are compared, decoupling control and proposed TITO controller. The cornering stiffness and vehicle velocity are time-varying parameters. The nominal values for designing the decoupling matrix and the TITO controller are  $C_{fn} = 10,000[N/rad]$ ,  $C_{rn} = 30,000[N/rad]$ ,  $V_n = 25kph$ .

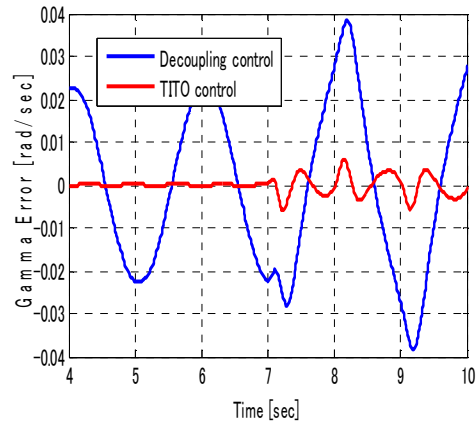
In order to test the robustness of the controller, simulation is conducted with parameter variation:  $C_f = C_{fn} + \Delta C_f$ ,  $C_r = C_{rn} + \Delta C_r$ ,  $V = V_n + \Delta V$ . The considerable change of cornering stiffness can be seen in Fig. 13 (a). Vehicle velocity is 35kph instead of the nominal value of 25kph. The results in Fig. 13 show that TITO control method provides better tracking with reference model over the variation of vehicle parameter. Even when suddenly entering the low friction road, TITO control has smaller tracking errors. This can be explained as the fixed decoupling matrix cannot adaptive to the nominal model and add the undesired signal to the control inputs.



(a) Cornering stiffness variation



(b) Yaw rate response



(c) Yaw rate tracking error

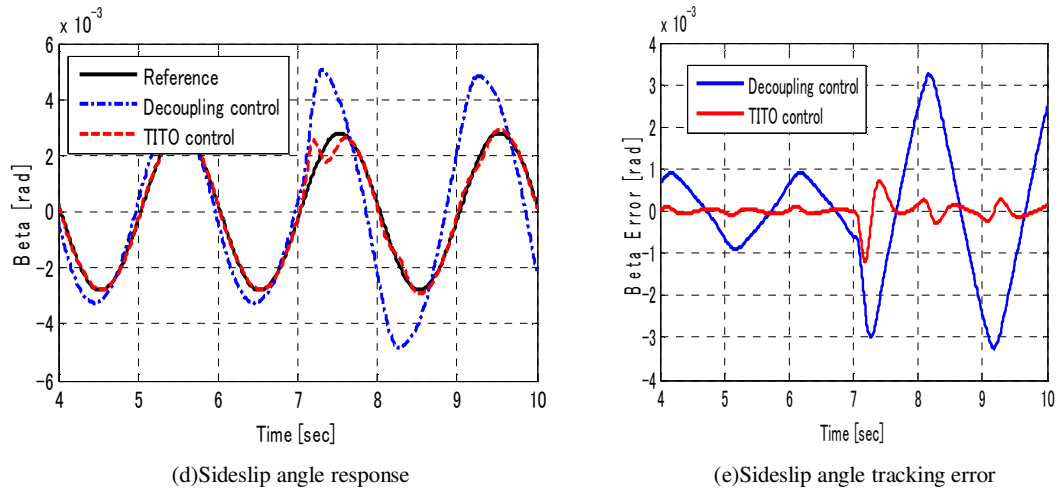


Fig. 13 Simulation results of vehicle stability by TITO control and decoupling control

## 7. Summary

In the special part, the application of lateral tire force sensor for vehicle stability control system is examined. By considering the difference between the left and right lateral tire forces, tire cornering stiffness can be identified without sideslip angle. This idea is also used for sideslip angle estimation without cornering stiffness. For accurate estimation, we consider the nonlinear part of tire lateral force as disturbance term to be simultaneously identified with sideslip angle. Experiments with electric vehicle Kanon and MSHubs are conducted to evaluate the proposed estimations. We also propose the TITO control design of vehicle stability control system. The high robustness of this method is verified by simulations.

## Chapter 5: Conclusions and future works

### 5.1 Achievements of the thesis

This thesis contributes to the stability control systems of electric vehicle in the following aspects:

#### 1. Parameter identifications

The online identification method of cornering stiffness without sideslip angle is proposed. This method is designed based on the difference between left and right side of lateral tire force sensors. The advantages of this method is confirmed by comparing with the with beta method.

#### 2. State estimation

Multi-rate Kalman filter is developed by two methods. The first is the prediction of measurement residual for inter-samples. The second is the integration of disturbance estimation with state estimation. All methods are easy for implementing in practical applications.

Multi-rate Kalman filter is successfully applied for sideslip angle estimation using GPS. We have proof by both simulations and experiments the advances the proposed methods in comparison with the previous researches on sideslip angle estimation using GPS. The inter-samples performance of multi-rate estimation is well enhanced. The proposal of multi-rate Kalman filter in this thesis is the novelty in the field of state estimation.

The research on sideslip angle estimation based on lateral tire force sensors had been done in the past. However, in this thesis, we develop the original method by considering the nonlinear part of tire lateral force as disturbance term to be estimated. We conduct experiments and compare this configuration with the conventional method which utilizes lateral accelerometers.

#### 3. Controller

Based on the sideslip angle estimation using GPS, we design the stability control system electric vehicle by LQR method. The system is implemented in electric vehicle COMS in which yaw moment generated by in-wheel motors is used for managing both yaw rate and sideslip angle.

We also propose the two-input two-output (TITO) controller for electric vehicle stability control system in which two control inputs are front steering angle and yaw moment. We show the higher robustness of the TITO control method in comparison with decoupling control method.

#### 4. GPS interface design

The GPS interface software is design and can be used for displaying the navigation information in real-time. It can also be used for capturing all the navigation data from GPS receiver for off-line analysis. Moreover, the software can send the measurements based on GPS to the controller of electric vehicle for estimation and control purposes (such as vehicle velocity, course angle, position...).

### 5.2 Limitations of the thesis

The works of this thesis has the following limitations:

### 1. Evaluation of the control system

Due to the limitation of experiment space and high requirement of safety, we just conduct the experiments at low speed. Hence, the critical situation of driving is not shown by experiment in this thesis. Therefore, we use simulation to confirm the control system under critical condition, such as driving at high speed on low friction road.

The general disturbance term is estimated by multi-rate Kalman filter. However, the feedback loop for rejecting the disturbance term is not analyzed and designed in this thesis.

The research on TITO controller is not actually finished so we cannot show the experiment results in this thesis.

### 2. Evaluation of GPS based estimation

The experiments of using GPS in this thesis are conducted under clear sky condition. By this way, we can receive the stable GPS signal and accurate measurement based GPS. The delay or reflection of GPS signal as well as the change of GPS accuracy are not examined in this thesis.

For Kalman filter design, we have not studied the tuning of process noise and measurement noise covariance matrixes. In fact, due to the change of GPS quality, the tuning of such covariance matrixes is desirable for adaptive estimation.

The dynamics of the general disturbance is assumed to be zero in this thesis. This assumption is acceptable for the simulation and experiment test in this thesis. However, thorough examination of the dynamics of general disturbance should be conducted for general study.

## 5.3 Future works

Based on the achievements and limitations of this thesis, the future works are proposed as the followings:

### 1. Theory of multi-rate Kalman filter:

In future, we will fulfill the theory of multi-rate Kalman filter with four points:

- a) The prediction of measurement residual for inter-samples estimation enhancement.
- b) The compensation of the effect of model error and external disturbance to multi-rate estimation accuracy by general disturbance estimation.
- c) The auto-tuning of process noise and measurement noise for multi-rate Kalman filter design.
- d) The consideration of measurement delay (such as the delay of GPS signal) for multi-rate Kalman filter.

### 2. Application of GPS and multi-rate theory in electric vehicle:

In this thesis, only sideslip angle estimation is studied. In future works, we will apply multi-rate Kalman filter for the full frameworks of vehicle state estimation and control by using GPS. The following states can be estimated: vehicle position, Euler angle (roll-pitch-yaw), sideslip angle, vehicle velocity (lateral and longitudinal).

### 3. Advanced motion control of personal electric vehicle for future society



As discussed in chapter 1, the future society requires electric vehicle as the means of transportation. Personal EVs will have an important position among variety types of EVs' family. The requirements of personal EVs are human-friendly, safe and comfortable driving. Such requirements can be achieved by advanced motion control of EVs which is proposed to be the combination of both dynamics control and autonomous navigation. Imagine that we just have to let the EVs know where we want to go. Then, the EVs will automatically find the route and bring us from departure till destination. The proposed configuration is shown in Fig 5.1.

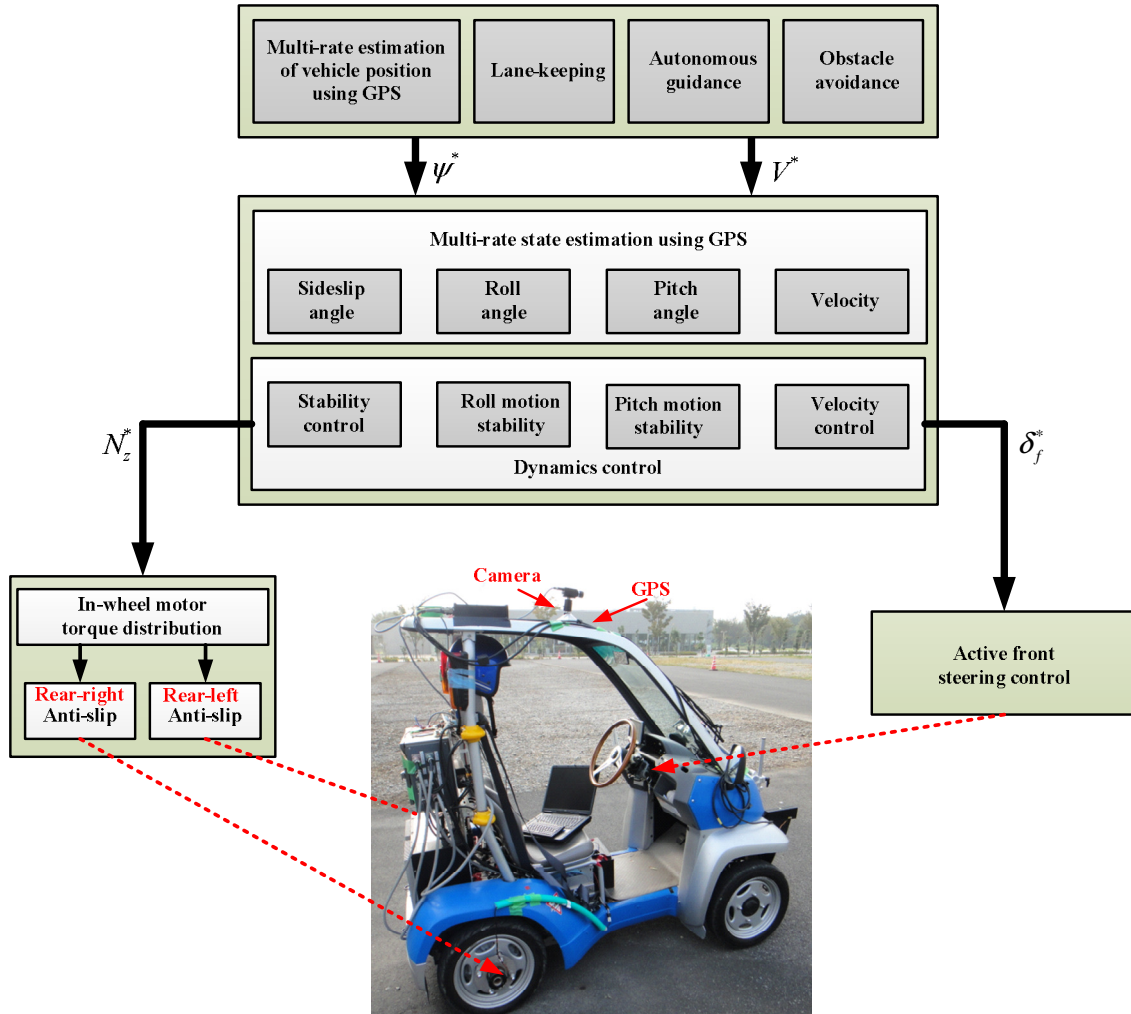


Fig 5.1 Framework of advanced motion control of personal electric vehicle

# Appendix 1: Feature of GPS receiver CCA-600

(Reference: Japan Radio Company's website: <http://www.jrc.co.jp>)

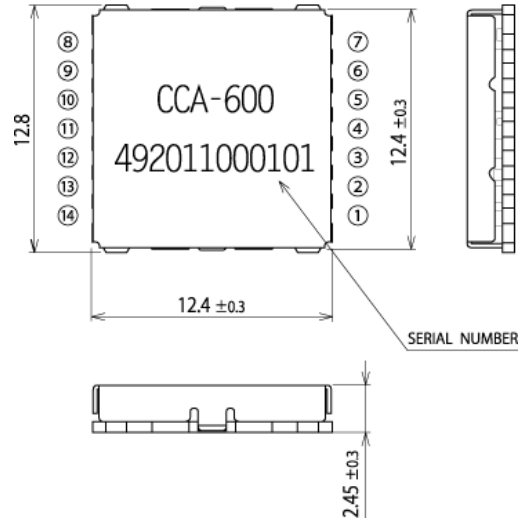


Fig 1 External dimensions of CCA-600

Table 1 Features of CCA-600

Receiving method	L1 Band (1575.42MHz) GPS (C/A)、SBAS
Receiving sensitivity	Acquisition level -147dBm Tracking level -163dBm
Positioning accuracy	2.5m CEP (6.0m 2DRMS)
TTF	Cold start 35sec. (Typ) Warm start 34sec. (Typ) Hot Start 3sec. (Typ)
Current consumption	36mA (typ., +3.3 V, acquisition ) 28mA (typ., +3.3 V, tracking)
Backup current	6μA (typ. +3.3V)
Data format	NMEA 0183
Operation temperature	-30~+70°C
Storage temperature	-40~+85°C
External dimensions	W 12.4mm× H 12.4mm× D 2.5mm
Mass	1.1 g

## Appendix 2: NMEA 0183 protocol for sending GPS data

(Reference in: The website of US's National Marine Electronics Association: [www.nmea.org](http://www.nmea.org))

NMEA 0183 is a combined electrical and data specification for communication between marine electronic devices such as echo sounder, sonar, anemometer, gyrocompass, autopilot, GPS receivers and many other types of instruments. It has been defined by, and is controlled by, the US -based National Marine Electronics Association.

The NMEA 0183 standard uses a simple ASCII, serial communications protocol that defines how data is transmitted in a "sentence" from one "talker" to multiple "listeners" at a time. Through the use of intermediate expanders, a talker can have a unidirectional conversation with a nearly unlimited number of listeners, and using multiplexers, multiple sensors can talk to a single computer port. A part of NMEA message received by GPS interface software is shown as the following:

```
$GPGSA,A,3,27,15,26,09,05,21,18,,,,,2.48,1.19,2.18*0D
$GPGSV,3,1,09,27,75,202,48,15,66,349,48,09,51,211,50,50,48,171,37*7F
$GPGSV,3,2,09,26,42,050,42,21,38,284,46,05,33,125,44,18,26,311,43*7E
$GPGSV,3,3,09,28,17,057,*4E
$GPRMC,202505.600,A,3554.0717,N,13956.1151,E,5.32,346.31,230711,,,D*66
$GPVTG,346.31,T,,M,5.32,N,9.85,K,D*3B
$GPGGA,202505.800,3554.0720,N,13956.1150,E,2,7,1.19,19.2,M,39.2,M,0000,0000*64
$GPGSA,A,3,27,15,26,09,05,21,18,,,,,2.49,1.19,2.18*0C
$GPGSV,3,1,09,27,75,202,47,15,66,349,48,09,51,211,51,50,48,171,36*70
```

The following is the details of an NMEA sentence sent by CCA-600 to GPS interface software:

```
[$GPRMC,161229.487,A,3723.2475,N,12158.3416,W,0.13,309.62,120598,,*10]
```

Table 2 RMC data format

Name	Example	Units	Description
Message ID	\$GPRMC		RMC protocol header
UTC position	161229.487		hhmmss.sss
Status	A		A=data valid or V data not valid
Latitude	3723.2475		ddmm.mmmm
N/S Indicator	N		N=north or S=south
Longitude	12158.3416		dddmm.mmmm
E/W	W		E=east or W=west
Speed Over Ground	0.13	knots	
Course Over Ground	309.62	degrees	True
Date	120598		ddmmyy
Magnetic Variation		degrees	E=east or W=west
Checksum	*10		
<CR><LF>			End of message termination

## Appendix 3: GPS coordinates to local coordinates

(Reference: S. V. Drake, "Converting GPS Coordinates to Navigation Coordinates," DSTO Electronics and Surveillance Research Laboratory, Edinburgh, South Australia, Australia 511, Published Date April 2002.)

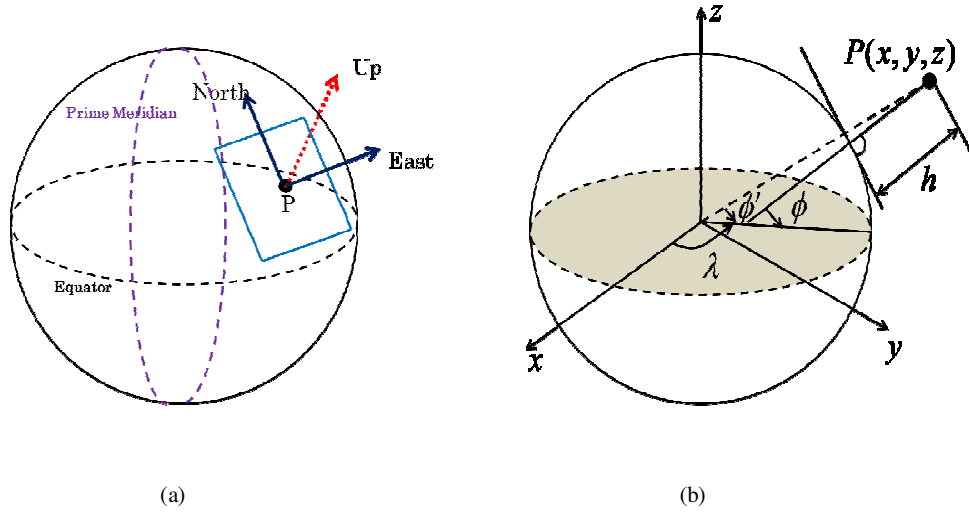


Fig 2 Earth and coordinates

From the GPS receiver, we get the position of the moving body including latitude, longitude, and height ( $\phi\lambda h$ ). In order to convert from GPS coordinates to ENU coordinates, firstly, we convert to the Earth centered earth fixed (ECEF) coordinates ( $xyz$ ). The transformation has 4 stages as following:

1. Determine latitude, longitude, and height of the moving body from NMEA sentences ( $\phi\lambda h$ ).
2. Convert from GPS coordinates to ECEF coordinates

$$x = \left( \frac{a}{\chi} + h \right) \cos \phi \cos \lambda \quad (1)$$

$$y = \left( \frac{a}{\chi} + h \right) \cos \phi \sin \lambda \quad (2)$$

$$z = \left( \frac{a(1-e^2)}{\chi} + h \right) \sin \phi \quad (3)$$

Where  $\chi = \sqrt{1 - e^2 \sin^2 \phi}$  and  $a$  and  $e^2$  are the semi-major axis and the numerical eccentricity of the Earth. In this report we used the WGS 84 ellipsoid.

$$e^2 = 1 - \left( \frac{b}{a} \right)^2, \quad a = 6378137[m], \quad b = 6356752.3142[m]$$

3. Express small change in position in ECEF coordinates

Considering a small change in position ( $\phi \rightarrow \phi + d\phi, \lambda \rightarrow \lambda + d\lambda, h \rightarrow h + dh$ ), by applying

Taylor formula to (1), (2), and (3), we have:

$$\begin{aligned}
dx = & \left( \frac{-a \cos \lambda \sin \phi (1 - e^2)}{\chi^3} - h \cos \lambda \sin \phi \right) d\phi - \left( \frac{a \sin \lambda \cos \phi}{\chi} + h \sin \lambda \cos \phi \right) d\lambda \\
& + \cos \phi \cos \lambda dh + \left[ \frac{1}{4} a \cos \phi \cos \lambda (-2 - 7e^2 + 9e^2 \cos \phi) - \frac{1}{2} h \cos \lambda \cos \phi \right] d\phi^2 \\
& + \left( \frac{a \sin \lambda \sin \phi (1 - e^2)}{\chi^3} + h \sin \lambda \sin \phi \right) d\phi d\lambda - \cos \lambda \sin \phi dh d\phi \\
& + \left( \frac{-a \cos \lambda \cos \phi}{2\chi} - \frac{1}{2} h \cos \lambda \cos \phi \right) d\lambda^2 - \sin \lambda \cos \phi dh d\lambda + \Theta(d\theta^3) + \Theta(dhd\theta^2)
\end{aligned} \tag{4}$$

$$\begin{aligned}
dy = & \left( \frac{-a \sin \lambda \sin \phi (1 - e^2)}{\chi^3} - h \sin \lambda \sin \phi \right) d\phi + \left( \frac{a \cos \lambda \cos \phi}{\chi} + h \cos \lambda \cos \phi \right) d\lambda \\
& + \sin \phi \cos \lambda dh + \left[ \frac{1}{4} a \cos \phi \sin \lambda (-2 - 7e^2 + 9e^2 \cos \phi) - \frac{1}{2} h \sin \lambda \cos \phi \right] d\phi^2 \\
& + \left( \frac{-a \cos \lambda \sin \phi (1 - e^2)}{\chi^3} - h \cos \lambda \sin \phi \right) d\phi d\lambda - \sin \lambda \sin \phi dh d\phi \\
& + \left( \frac{-a \sin \lambda \cos \phi}{2\chi} - \frac{1}{2} h \sin \lambda \cos \phi \right) d\lambda^2 + \cos \lambda \cos \phi dh d\lambda + \Theta(d\theta^3) + \Theta(dhd\theta^2)
\end{aligned} \tag{5}$$

$$\begin{aligned}
dz = & \left( \frac{a(1 - e^2) \cos \phi}{\chi^3} + h \cos \phi \right) d\phi + \sin \phi dh + \cos \phi dh d\phi \\
& + \left[ \frac{1}{4} a \sin \phi (-2 - e^2 + 9e^2 \cos^2 \phi) - \frac{1}{2} h \sin \phi \right] d\phi^2 + \Theta(dhd\theta^2)
\end{aligned} \tag{6}$$

Where  $\Theta(d\theta^3)$  and  $\Theta(dhd\theta^2)$  is higher order of either  $d\phi$  or  $d\lambda$ .

4. Convert the small change in position from ECEF coordinates to ENU coordinates by the following transform matrix

$$\begin{bmatrix} de \\ dn \\ du \end{bmatrix} = \begin{bmatrix} -\sin \lambda & \cos \lambda & 0 \\ -\sin \phi \cos \lambda & -\sin \phi \sin \lambda & \cos \phi \\ \cos \phi \cos \lambda & \cos \phi \sin \lambda & \sin \phi \end{bmatrix} \begin{bmatrix} dx \\ dy \\ dz \end{bmatrix} \tag{7}$$

From (4), (5), (6), and (7), and by neglecting the higher order terms, we get:

$$de = \left( \frac{a}{\chi} + h \right) \cos \phi d\lambda - \left[ \frac{a(1 - e^2)}{\chi^3} + h \right] \sin \phi d\phi d\lambda + \cos \phi d\lambda dh \tag{8}$$

$$dn = \left[ \frac{a(1 - e^2)}{\chi^3} + h \right] d\phi + \frac{3}{2} a \cos \phi \sin \phi e^2 d\phi^2 + dh d\phi + \frac{1}{2} \sin \phi \cos \phi \left( \frac{a}{\chi} + h \right) d\lambda^2 \tag{9}$$

$$du = dh - \frac{1}{2} a \left( 1 - \frac{3}{2} e^2 \cos \phi + \frac{1}{2} e^2 + \frac{h}{a} \right) d\phi^2 - \frac{1}{2} \left( \frac{a \cos^2 \phi}{\chi} - h \cos^2 \phi \right) d\lambda^2 \tag{10}$$

## References

- [1] Y. Hori: "Future Vehicle Driven By Electricity and Control-Research on 4 Wheel Motored UOT March II," IEEE Transactions on Industrial Electronics, Vol. 51, No. 5, pp. 954-962 (2004).
- [2] K. Furukawa and Y. Hori: "Recent Development of Road Condition Estimation Techniques for Electric Vehicle and Their Experimental Evaluation Using the Test EV UOT March I and II," 29<sup>th</sup> IEEE Annual Conference on Industrial Electronics, pp. 925-930 (2003).
- [3] H. Fujimoto, A. Tsumasaka, and T. Noguchi: "Direct Yaw Moment Control of Electric Vehicle Based on Cornering Stiffness Estimation," 31<sup>st</sup> IEEE Annual Conference on Industrial Electronics, pp. 2626-2631.
- [4] R. Rajamani: "Vehicle Dynamics and Control," Springer (2006).
- [5] J. Y. Wong: "Theory of Ground Vehicles," John Wiley & Sons, INC, Third Edition (2001).
- [6] Corrsys-Datron Optical Sensors, [Online], Available at:  
[http://www.corrsys-datron.com/optical\\_sensor.htm](http://www.corrsys-datron.com/optical_sensor.htm)
- [7] B. C. Chen and F. C. Hsieh: "Sideslip Angle Estimation Using Extended Kalman Filter," Vehicle System Dynamics, Vol. 46, No. 1, pp. 353-364 (2008).
- [8] U. Kiencke and A. Daib: "Observation of Lateral Vehicle Dynamics," Control Engineering Practice, Vol. 5, No. 8, pp. 1145-1150 (1997).
- [9] Y. Aoki, T. Inoue, and Y. Hori: "Robust Design of Gain Matrix of Body Slip Angle Observer for Electric Vehicles and Its Experimental Demonstration," 8<sup>th</sup> IEEE International Workshop on Advanced Motion Control, pp. 41-45 (2004).
- [10] C. Geng, L. Mostefai, M. Denai, and Y. Hori: "Direct Yaw Moment Control of an In Wheel Motored Electric Vehicle Based on Body Slip Angle Fuzzy Observer," IEEE Transactions on Industrial Electronics, Vol. 56, pp. 1411-1419 (2009).
- [11] L. Imsland, T. A. Johansen, T. I. Fossen, H. F. Grip, J. C. Kalkkuhl, and A. Suissa: "Vehicle Velocity Estimation Using Nonlinear Observers," Automatica, Vol. 42, No. 12, pp. 2091-2103 (2006).
- [12] M. Stria and M. C. Best: "State Estimation of Vehicle Handling Dynamics Using Non-linear Robust Extended Adaptive Kalman Filter," Vehicle System Dynamics, Vol. 41, pp. 103-112 (2004).
- [13] J. Stephant, A. Charara, and D. Mezei: "Evaluation of a Sliding Model Observer for Vehicle Sideslip Angle," Control Engineering Practice, Vol. 15, No. 7, pp. 803-812 (2007).
- [14] F. Cheli, E. Sabbioni, M. Pesce, and S. Mezei: "A Methodology for Vehicle Slip Angle Identification: Comparison with Experimental Data," Vehicle System Dynamics, Vol. 45, No. 6, pp. 549-563 (2010).
- [15] J. Kosecka, R. Blasi, C. J. Taylor, and J. Malik: "Vision Based Lateral Control of Vehicles," International IEEE Conference on Intelligent Transportation System, pp. 900-905 (1997).
- [16] J. Ryu: "State and Parameter Estimation for Vehicle Dynamics Control Using GPS," PhD

Dissertation, Stanford University (2004).

[17] R. Anderson: "Using GPS for Model Based Estimation of Critical Vehicle States and Parameters," Master Thesis, Auburn University (2004).

[18] Oxford Technical Solution: "RT3000 Inertia and Measurement System User Manual," (2004).

[19] B. Breuer, U. Eichhorn, and J. Roth: "Measurement of Tire Road Friction Ahead of the Car and Inside the Tire," 1<sup>st</sup> International Symposium on Advanced Vehicle Control (1992).

[20] A. J. Tuononen: "Optical Position Detection to Measure Tire Carcass Deflection," Vehicle System Dynamics, Vol. 46, No. 6, pp. 471-481 (2008).

[21] B. V. Leeuwen (SKF) and J. Zuurbier (TNO): "Vehicle State Estimation Based on Load Sensing," Vehicle Dynamics Expo (2007).

[22] A. J. Tuononen: "Vehicle Lateral State Estimation Based on Measured Tire Forces," Sensors, Vol. 9, pp. 8761-8775.

[23] M. Abe: "Vehicle Handling Dynamics," Published by Elsevier Ltd. (2009).

[24] E. Bakker, L. Nyborg, and H. B. Pacejka: "Tyre Modelling for Use in Vehicle Dynamics Studies," SAE Technical Paper, No. 870421 (1987).

[25] Elliot D. Kaplan and Christopher J. Hegarty: "Understanding GPS: Principles and Applications," Second Edition, Artech House, INC. (2006).

[26]<http://www.gpsworld.com/gnss-system/augmentation-assistance/news/michibiki-produces-3-centimeter-accuracy-10915>

[27] [http://qzss.jaxa.jp/is-qzss/index\\_e.html](http://qzss.jaxa.jp/is-qzss/index_e.html)

[28] A. M. Phillips and Masayoshi Tomizuka, "Multirate Estimation and Control Under Time-Varying Data Sampling with Application to Information Storage Device," Proceedings of American Control Conference, pp. 4151-4155 (1996).

[29] T. Hara and M. Tomizuka, "Performance enhancement of Multi-rate Controller for Hard Disk Drives," IEEE Transactions on Magnetics, Vol. 35, No. 2, pp. 898-903 (1999).

[30] H. Fujimoto, "General Framework of Multirate Sampling Control and Application to Motion Control Systems," Phd Dissertation, the University of Tokyo (2000).

[31] B. D. O. Anderson and J. B. Moore: *Optimal Filtering*, Dover Publications, INC. (2005).

[32] Frank L. Lewis, Vassillis L. Syrmos: "Optimal Control," Second Edition, John Wiley & Sons, INC. (1995).

[33] Y. Hori, Y. Toyoda, and Y. Tsuruoka: "Traction Control of Electric Vehicle: Basic Experimental Results Using the Test EV "UOT Electric March," IEEE Transactions on Industrial Applications, Vol. 34, No. 5 (1998).

[34] Y. Otawa and H. Fujimoto: "Estimation and Control of Sideslip Angle with Tire Lateral Force Sensor and Active Steering for Electric Vehicle," IEEJ Technical Report, No. IIC-10-103, pp. 35-40 (2010) (Japanese).

[35] W. Sienel: "Estimation for Tire Cornering Stiffness and its Application to Active Car Steering,"

- Proc. of 36<sup>th</sup> Conference on Decision & Control, pp. 4744–4749, USA (1997).
- [36] H. Fujimoto, N. Takahashi, and A. Tsumasaka: “Motion Control of Electric Vehicle Based on Cornering Stiffness Estimation with Yaw Moment Observer,” Proc. of IEEE International Workshop on Advanced Motion Control, pp.206–211 (2006).
- [37] H. Dugoff, P. S. Fancher, and L. Segel: “An Analysis of Tire Traction Properties and Their Influence on Vehicle Dynamics Performance,” SAE Paper, No. 700377 (1970).
- [38] P. Anderson: “Adaptive Forgetting in Recursive Identification through Multiple Models,” International Journal of Control, Vol. 42, No. 5, pp.1175–1193 (1985).
- [39] A. Vahidi, A. Stefanopoulou, and H. Peng: “Recursive Least Square with Forgetting for Online Estimator of Vehicle Mass and Road Grade: Theory and Experiments,” Vehicle System Dynamics, Vol. 41, No. 1, pp. 31-55 (2005).
- [40] Riccardo Marino and Fabio Cinili: “Input-Output Decoupling Control by Measurement Feedback in Four-Wheel-Steering Vehicles,” IEEE Transactions on Control Systems Technology, Vol. 17, No. 5 (2009).
- [41] R. E. Kalman: “A New Approach to Linear Filtering and Prediction Problems,” Transaction of the ASME-Journal of Basic Engineering, Vol. 82, Series D, pp. 35-45 (1960).
- [42] T. Umeno and Y. Hori: “Robust speed control of dc servomotors using two degrees-of-freedom controller design,” IEEE Transactions on Industrial Electronics, Vol. 38, No. 5, pp. 363–368 (1991).
- [43] C. Johnson: “Accommodation of External Disturbances in Linear Regulator and Servomechanism Problem,” IEEE Transaction on Automatic Control, Vol. 16, No. 6, pp. 535-644 (1971).
- [44] J. George, P. Singla, and J. L. Crassidis: “Adaptive Disturbance Accommodating Controller for Uncertain Stochastic Systems,” Proc. Of 2009 American Control Conference, pp. 2599-2605 (2009).



## **Publication list**

- [1] B. M. Nguyen, K. Nam, H. Fujimoto, Y. Hori, and C. M. Ta: "Modeling of Lateral Dynamics for Motion Control of Electric Vehicle," Proceeding of 5<sup>th</sup> Symposium of South East Asian Technical University Consortium, ISSN No. 1882-5796 (2011).
- [2] B. M. Nguyen, K. Nam, H. Fujimoto, and Y. Hori: "Proposal of Cornering Stiffness Estimation without Vehicle Sideslip Angle Using Lateral Force Sensor," IEEJ Technical Report, No. IIC-11-140 (2011).
- [3] B. M. Nguyen, Y. Wang, S. Oh, H. Fujimoto, and Y. Hori: "GPS Based Estimation of Vehicle Sideslip Angle Using Multi-rate Kalman Filter with Prediction of Course Angle Measurement Residual," FISITA 2012 World Automotive Congress (2012) (Submitted).
- [4] B. M. Nguyen, Y. Wang, H. Fujimoto, and Y. Hori: "Sideslip Angle Estimation Using Multi-rate Kalman Filter with Model Error and Disturbance Compensation for Electric Vehicle Stability Control," 8<sup>th</sup> IEEE Vehicle Power and Propulsion Conference (2012) (To be submitted).

### **Co-authored paper**

- [1] Y. Wang, B. M. Nguyen, P. Kotchapansompote, H. Fujimoto, and Y. Hori: "Vision-based Vehicle Body Slip Angle Estimation with Multi-rate Kalman Filter Considering Time Delay," 21<sup>st</sup> IEEE International Symposium on Industrial Electronics (2012) (Accepted).
- [2] Y. Wang, B. M. Nguyen, P. Kotchapansompote, H. Fujimoto, and Y. Hori: "Image Processing-Based State Estimation for Vehicle Lateral Control Using Multi-rate Kalman Filter," Journal of Recent patents on signal processing (2012) (Submitted).

## **Curriculum vitae**

Nguyen Binh Minh (阮平明) was born in Haiphong, Vietnam on February 23, 1984. He received B.S. Degree in Electrical Engineering from Hanoi University of Science and Technology in the autumn of 2007. In 2009, he received the scholarship from Panasonic Corporation to study in Japan. After one year as research student, in the spring of 2010, he entered the Graduate School of the University of Tokyo in pursuit of the Master's Degree in Electrical Engineering. His research interests include electrical drives and motion control of electric vehicles.